



universität  
wien

## DIPLOMARBEIT

Titel der Diplomarbeit:

Functional and structural studies on  
chlorite dismutase from *Nitrospira defluvii*

angestrebter akademischer Grad:

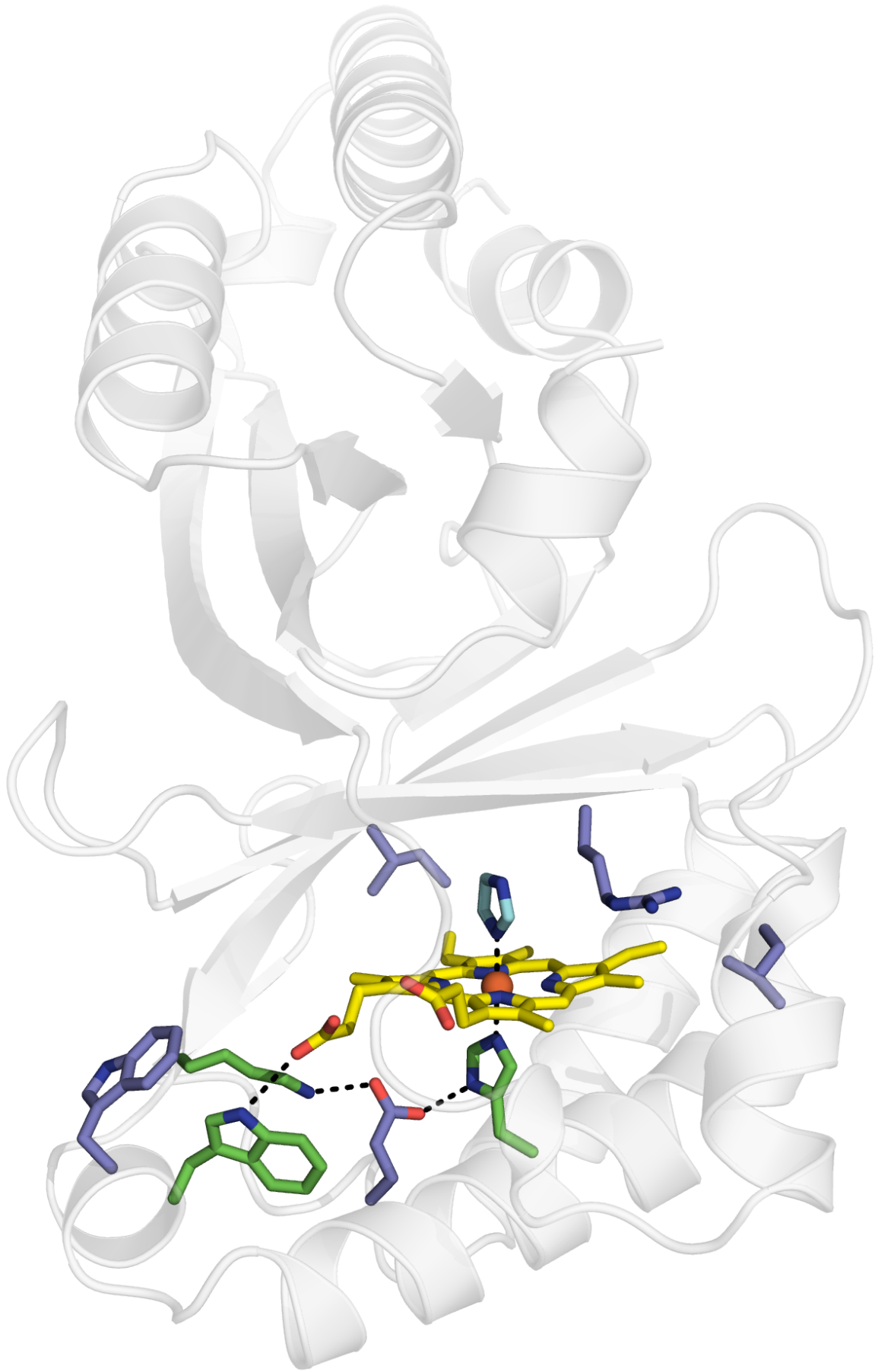
Magistra der Naturwissenschaften (Mag. rer. nat)

Wien, 2011

Verfasserin:  
Studienkennzahl lt. Studienblatt:  
Studienrichtung lt. Studienblatt:  
Betreuerin:

Kira Gysel  
A 0508468  
Diplomstudium Molekulare Biologie A 490  
Univ.-Prof. Dipl.-Ing. Dr. Kristina Djinović-Carugo





**Front:** Cartoon representation of the three-dimensional structure of the chlorite dismutase from the nitrifier *Candidatus Nitrospira defluvia* in complex with imidazole. Key residues in the active site of the enzyme are emphasized in stick representation, as well as the prosthetic group heme b. In this study, the reaction mechanism of chlorite dismutases was further elucidated by mutational, biochemical and structural studies.

# Contents

<b>Zusammenfassung</b>	<b>vii</b>
<b>Abstract</b>	<b>viii</b>
<b>1 Introduction</b>	<b>1</b>
1.1 Oxochlorates . . . . .	1
1.2 Microbial Perchlorate Respiration . . . . .	2
1.3 Diversity of Chlorite Dismutases . . . . .	4
1.4 Structure of Chlorite Dismutases . . . . .	7
1.5 Active Site . . . . .	11
1.6 Reaction Mechanism . . . . .	13
<b>2 Aim of this Thesis</b>	<b>17</b>
<b>3 Materials and Methods</b>	<b>19</b>
3.1 Antibiotics, Media and General Buffers . . . . .	19
3.2 Expression System and Expression Vectors . . . . .	20
3.3 Storage . . . . .	21
3.4 Molecular Cloning Techniques . . . . .	21
3.4.1 Site-Directed Mutagenesis . . . . .	22
3.4.2 Chemical Transformation of <i>E. coli</i> (Hanahan) . . . . .	26
3.4.3 Colony PCR . . . . .	26
3.4.4 Plasmid Preparation from <i>E. coli</i> Cells . . . . .	26
3.4.5 Subcloning . . . . .	27
3.4.6 List of Constructs . . . . .	28
3.5 Heterologous Protein Expression . . . . .	30
3.5.1 Cld from <i>Candidatus Nitrospira defluvia</i> (NdCld) - wild-type and mutants . . . . .	30
3.5.2 Cld from <i>Candidatus Nitrospira defluvia</i> without heme (apo-NdCld) . . . . .	30
3.5.3 Cld from <i>Nitrobacter winogradskyi</i> (NwCld) . . . . .	31
3.6 Protein Purification Techniques . . . . .	31
3.6.1 Purification of NdCld Mutants . . . . .	31
3.6.2 Purification of Apo-NdCld . . . . .	33
3.6.3 NdCld with Co-Protoporphyrine IX . . . . .	34
3.6.4 Purification of NwCld . . . . .	34
3.7 Analytical Size Exclusion Chromatography . . . . .	35
3.8 Crystallographic Techniques . . . . .	36
3.8.1 Crystallization of NdCld Mutants and Apo-NdCld . . . . .	36

## Contents

3.9	Structure Determination and Refinement Techniques . . . . .	37
3.9.1	Data Collection and Processing . . . . .	37
3.9.2	Molecular Replacement, Model Building and Refinement . . . . .	38
3.10	Enzymatic Activity Techniques . . . . .	38
3.10.1	Steady-state Kinetics . . . . .	38
3.11	Biophysical characterizations . . . . .	39
3.11.1	Static Light Scattering . . . . .	39
<b>4</b>	<b>Results</b>	<b>41</b>
4.1	Structural Studies of NdCld Mutants . . . . .	41
4.1.1	Structure of the W145V mutant in Complex with Imidazole . . . . .	46
4.1.2	Structure of the W146Y Mutant in Complex with Imidazole . . . . .	47
4.1.3	Structure of the R173E Mutant in Complex with Acetate . . . . .	47
4.1.4	Structure of the W146Y R173Q Double Mutant in Complex with Imidazole . . . . .	48
4.2	Steady-state Kinetics of NdCld, Mutants and Variants . . . . .	50
4.3	Structure of apo-NdCld . . . . .	55
4.4	Stability of the NwCld Dimer . . . . .	60
<b>5</b>	<b>Discussion</b>	<b>65</b>
5.1	Arginine 173 Mutations have Severe Effects on the Enzymatic Activity . . . . .	65
5.2	Investigation of Additional Signature Residues . . . . .	66
5.3	Mimicking the Active Site of Cld-like Proteins . . . . .	68
5.4	Exchanging Iron to Cobalt Leads to Decreased Substrate Binding . . . . .	71
5.5	The Structure of Apo-NdCld . . . . .	71
5.6	Mixed Nature of the NwCld Dimer Interface . . . . .	72
<b>6</b>	<b>Conclusions</b>	<b>73</b>
	<b>References</b>	<b>75</b>
	<b>List of Figures</b>	<b>80</b>
	<b>List of Tables</b>	<b>82</b>
	<b>Nomenclature</b>	<b>83</b>
	<b>Acknowledgements</b>	<b>85</b>
	<b>Curriculum Vitæ</b>	<b>87</b>

## Zusammenfassung

Das Enzym Chloritdismutase (Cld), eine Oxidoreduktase, katalysiert den Abbau von Chlorit zu Chlorid und molekularem Sauerstoff. Es ist hiermit eines von drei bekannten Enzymen, welches die Bildung einer molekularen Sauerstoffbindung als primäre Funktion durchführt. Ursprünglich waren Clds nur aus Perchlorat-respirierenden Bakterien (PCRB) bekannt, wo sie die Selbstvergiftung der Bakterien durch Abbau von cytotoxischem Chlorit, welches als Produkt der (Per)chloratreduktion entsteht, verhindern. Belastung des Trinkwassers durch anthropogenes (Per)chlorat wurde in den letzten 50 Jahren zu einer zunehmenden Bedrohung der öffentlichen Gesundheit in den Vereinigten Staaten. Bioremediation wäre ein geeignetes Mittel zur Entgiftung. Im Jahr 2008 wurden Cld - Homologe nicht nur in PCRBs, sondern in einer Vielzahl von Bakterien- und Archaeenstämmen entdeckt. Sie bilden nun die Chloritdismutase-Überfamilie, deren Mitglieder CFPs (Chlorite dismutase family proteins) genannt werden. Nur ein kleiner Anteil dieser katalysieren den Abbau von Chlorit; die Funktion der meisten ist noch unbekannt, auch wenn z.B. das CFP aus *L. monocytogenes* essentiell für das Pathogen ist und damit einen Ansatzpunkt für Medikamentenentwicklung bieten könnte. Um Chloritdismutaseaktivität in sequenzbasiert in CFPs vorhersagen zu können, wurden konservierte und teilweise konservierte Aminosäurereste identifiziert und als mögliche Signaturreste für Cld-Aktivität vorgeschlagen. In dieser Arbeit wurden diese Aminosäurereste in der Cld von *Candidatus Nitrospira defluvia*, eines wichtigen nitrifizierenden Klärbakteriums durch ortsspezifische Mutagenese ausgetauscht. Die Mutanten wurden durch biochemische Enzymaktivitätsmessungen und Röntgenkristallografie charakterisiert. Die wichtige Rolle des zuvor identifizierten Aminosäurerests Arginin 173 wurde nochmals bestätigt und erweitert. Für elf Mutanten und eine Cobalt Protoporphyrin IX Variante wurden Fließgleichgewichtskinetiken gemessen und die Struktur vierer Mutanten sowie der apo-Variante von NdCld wurde durch Röntgenkristallografie gelöst. Des Weiteren wurde die Relevanz elektostatischer bzw. hydrophober Interaktionen, welche zur Stabilität der dimeren Chloritdismutase von *Nitrobacter winogradskyi* beitragen, untersucht.

## Abstract

The enzyme chlorite dismutase (Cld), a heme b binding oxidoreductase, catalyzes the degradation of chlorite to chloride and molecular oxygen. It is therefore one of three known enzymes catalyzing the formation of a molecular O-O bond as its primary function. Clds were originally thought to be present in (per)chlorate respiring bacteria (PCRB), where they prevent self-toxication of the bacteria by degradation of cytotoxic chlorite, which is formed as a product of (per)chlorate reduction. Because freshwater pollution by anthropogenic perchlorate has become a serious public health threat in the United States, bioremediation would present an efficient method of detoxification. In 2008, many homologues to Cld were discovered not only in PCRBs, but in a large number of diverse bacterial and archaeal phylae. They comprise now a chlorite dismutase superfamily, whose members are called CFPs (Chlorite dismutase family proteins). Only a small subset of those were found to degrade chlorite, the function of the large moiety remains unknown, though e.g. the CFP from *L. monocytogenes* was shown to be essential for the organism, making the protein a suitable drug target. To predict chlorite dismutase activity in CFPs on a sequence basis, conserved and partially conserved residues were previously identified and suggested as possible signature residues for Cld activity. In this work, these residues in the active site of the Cld from *Candidatus Nitrospira defluvia* (NdCld), a key nitrifier in wastewater treatment, were exchanged by site-directed mutagenesis and the mutants characterized by biochemical enzyme activity assays (steady-state kinetics) and structurally by X-ray crystallography. The role of the previously identified catalytic residue arginine 173 was confirmed and steady-state kinetics measured for eleven mutants and a cobalt protoporphyrine IX variant of NdCld. The structure of four mutants and apo-NdCld was solved by X-ray crystallography. In addition, the respective contributions of electrostatic and hydrophobic interactions to the stability of the dimer interface in the chlorite dismutase from *Nitrobacter winogradskyi* were experimentally determined.



# 1 Introduction

## 1.1 Oxochlorates

Oxochlorates are the oxyanions derived from chlorine oxoacids, which are: i) perchloric acid ( $\text{HClO}_4$ , a strong acid), ii) chloric acid ( $\text{HClO}_3$ , also a strong acid), iii) chlorous acid ( $\text{HClO}_2$ , a weak acid) and iv) hypochlorous acid ( $\text{HClO}$ , a weak acid). Oxochlorate salts are strong oxidizers, a property which leads to their widespread use in industry.

Pollution with oxochlorates, especially perchlorate in drinking water has become a serious problem in the United States. This large scale oxochlorate contamination was found to be anthropogenic and potentially threatening to human health [7, 46, 49].

It was shown by Tonacchera et al. [45] that the affinity of the human sodium/iodide symporter (NIS) in the thyroid gland for  $\text{ClO}_4^-$  exceeds its affinity for  $\text{I}^-$  by thirty times, due to  $\text{ClO}_4^-$  having a similar size to  $\text{I}^-$  [49], making perchlorate a goitrogenic substance. This has been therapeutically used in cases of hyperthyroidism [51] in order to disrupt the production of the thyroid hormones thyroxine and triiodothyronine, but this therapy has also caused fatal bone marrow changes with doses of  $\text{ClO}_4^-$  as high as  $6 \frac{\text{mg}}{\text{kg} \cdot \text{day}}$  over a two-month period [48]. Chlorate and chlorite ( $\text{ClO}_2^-$ ) cause hemolytic anemia and have general cell-damaging effects [9, 47, 48]

Most perchlorate found on the planet is man-made and only entered the environment recently, the sole bigger natural source being found in mineral deposits in Chile, which contain up to 0.3 (w/w)% perchlorate [8, 31]. Perchlorate is industrially produced by electrolysis of the other oxochlorates and is highly used e.g. as anti-microbial agent, bleaching agent and  $\text{NH}_4\text{ClO}_4$  as an additive to rocket fuel [48, 49]. Chlorite ( $\text{ClO}_3^-$ ) is used as a herbicide and is formed as a by-product of bleaching in the paper industry [5].

The oxyanions of the chlorine oxoacids are very stable in environmental conditions, which, considering their threatening nature for human health, greatly increases the need for an effective way of degradation. Bioremediation using perchlorate-reducing microorganisms is a good way to tackle this problem [55], because physical and chemical technologies have proven to be difficult or failed [8].

## 1.2 Microbial Perchlorate Respiration

Oxochlorates possess a high reduction potential ( $\text{ClO}_4^-/\text{Cl}^-$   $E^0=1.287$  V;  $\text{ClO}_3^-/\text{Cl}^-$   $E^0=1.03$  V), which renders them on the one hand potentially dangerous substances (Section 1.1), but on the other hand they are suitable as electron acceptors for bacterial metabolism [8]. This is utilized by (per)chlorate reducing bacteria (PCRB), which are widely distributed in the proteobacterial phylum. PCRBs use this pathway for anaerobic respiration, with (per)chlorate being the terminal electron acceptor (Figure 1). Suitable electron donors include e.g. acetate, lactate, ethanol or  $\text{H}_2$  [8].

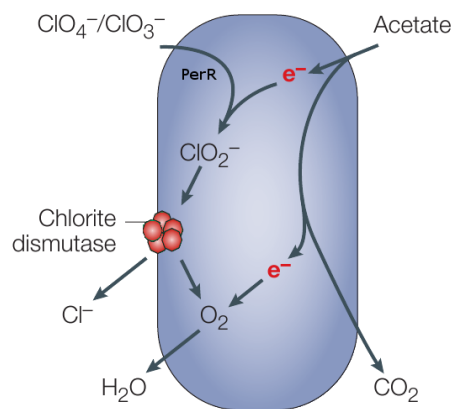


**Figure 1:** Overview of the perchlorate reduction pathway in PCRB. Emphasized is the role of chlorite dismutase, which detoxifies  $\text{ClO}_2^-$  produced by (per)chlorate reductase. Figure adapted from Coates and Achenbach [8].

The (per)chlorate reduction pathway consists mainly of two enzymes: i) (per) chlorate reductase (PerR) and ii) chlorite dismutase (Cld).

Perchlorate reductases catalyze the degradation of perchlorate and chlorate to chlorite. They are homologs to bacterial nitrate reductases, used by bacteria for nitrate respiration. It was speculated by Kengen et al. [28] that PerR evolved from nitrate reductases, Goblirsch et al. [17] propose that PerR evolved from DMSO reductase via gene duplication. PerR are promiscuous enzymes with many of them being able to reduce nitrate, iodate and bromate besides (per)chlorate. Some PCRB are capable of nitrate respiration as well[8].

Essential for the degradation of (per)chlorate to chloride is the enzyme **chlorite dismutase (Cld)**, which catalyzes the degradation of chlorite to chloride and molecular oxygen (see Figure 2) and thus prevents self-toxication of PCRB. Chlorite dismutase was first described by van Ginkel et al. [52] in the (per)chlorate-respiring strain

GR-1 (*Azospira oryzae*, DSM 11199). Most PCRB are facultatively anaerobic or microaerophilic organisms, so the molecular oxygen produced by the Cld is usually an intermediate and subsequently further converted to H<sub>2</sub>O [8].

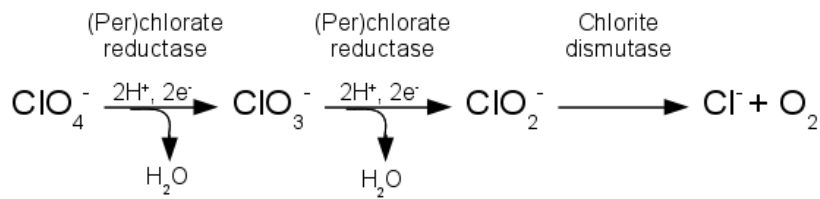


**Figure 2:** Schema of the microbial perchlorate-reducing pathway.

The catalyzed chlorite dismutase reaction is not a dismutation, but an intramolecular redox reaction. Therefore, the name *chlorite dismutase* is misleading and a more correct name besides the systematic identifier *chlorite:oxygen oxidoreductase* would be *chlorite-O<sub>2</sub>-lyase*<sup>1</sup> [20]. However, the term *chlorite dismutase* is still more prevalent in the literature and will be used throughout this thesis. Chlorite dismutase is a unique enzyme that does not share sequence similarities or obvious evolutionary relationships with other well-researched proteins. It is also very substrate specific and not promiscuous, unlike (per)chlorate reductase or nitrate reductase.

<sup>1</sup>EC 1.13.11.49 according to IUBMB

### 1.3 Diversity of Chlorite Dismutases

Chlorite dismutases were first found in PCRBs, where they are essential for the bacterial metabolism by detoxifying  $\text{ClO}_2^-$  to  $\text{Cl}_2$  and  $\text{O}_2$  and where they were used as markers for the ability of an organism to respire (per)chlorate [3].

Environmental genomics approaches revealed many homologs of chlorite dismutase genes in non-perchlorate reducing prokaryotes, distributed both in bacterial and archaeal phylae [32]. All these genes comprise now their own chlorite dismutase superfamily, and Goblirsch et al. [17] refer to them as *Cld family proteins* (CFPs). Phylogenetic trees comparing the Cld lineage to the 16SrRNA reveal hardly any lateral gene transfers (Figure 3), which indicates that Cld homologues were present in early common ancestors of *Archaea* and *Bacteria* [32]. Chlorite degradation has been observed in only a small subset of these proteins, the validated Clds, but the functions of the others remain still unknown. These CFPs were termed Cld-like proteins [34]. Several factors indicate that the capability to degrade chlorite was only recently acquired by this superfamily of proteins: i) perchlorate is a recent anthropogenic environmental pollutant, only a small, specialized number of the very diverse organisms with *cld* genes are associated with perchlorate respiration and an evolutionary pressure to detoxify chlorite. ii) the *cld* gene is localized in PCRBs in the PerR operon, which it entered by lateral gene transfer [8].

Functional and structural studies on validated chlorite dismutases and presumably non-functional CFPs lead to the suggestion of signature residues that could predict the catalytic activity of chlorite dismutases on a sequence basis [17, 29, 32, 34]. One important key residue is an arginine in the distal pocket of the active site (Details in Section 1.4), which was shown to have dramatic influence on the catalytic efficiency of Cld [29]. Figure 3 gives detailed information about the nature of this residue in Clds and Cld-like proteins.

In the phylogenetic tree (Figure 3) from Kostan et al. [29], validated active chlorite dismutases are clustered together and closely related; there are the chlorite dismutases from PCRBs. The Clds from *Azospira oryzae* (AoCld) and *Dechloromonas aromatica* (DaCld, not in Figure 3) have been structurally characterized [12, 18], the Cld from *Ideonella dechloratans* is also well-researched [40]. Active chlorite dismutases have also been found in non-PCRBs, with the best-researched being the chlorite dismutases from nitrite-oxidizing bacteria (NOB). The Cld from *Nitrospira defluvi* (NdCld) was the first Cld from a non-proteobacterial organism that was discovered and whose the structure was determined. The structure of the Cld from *Nitrobacter winogradskyi* (NwCld) was published shortly afterwards. Based on the phylogenetic analyses,

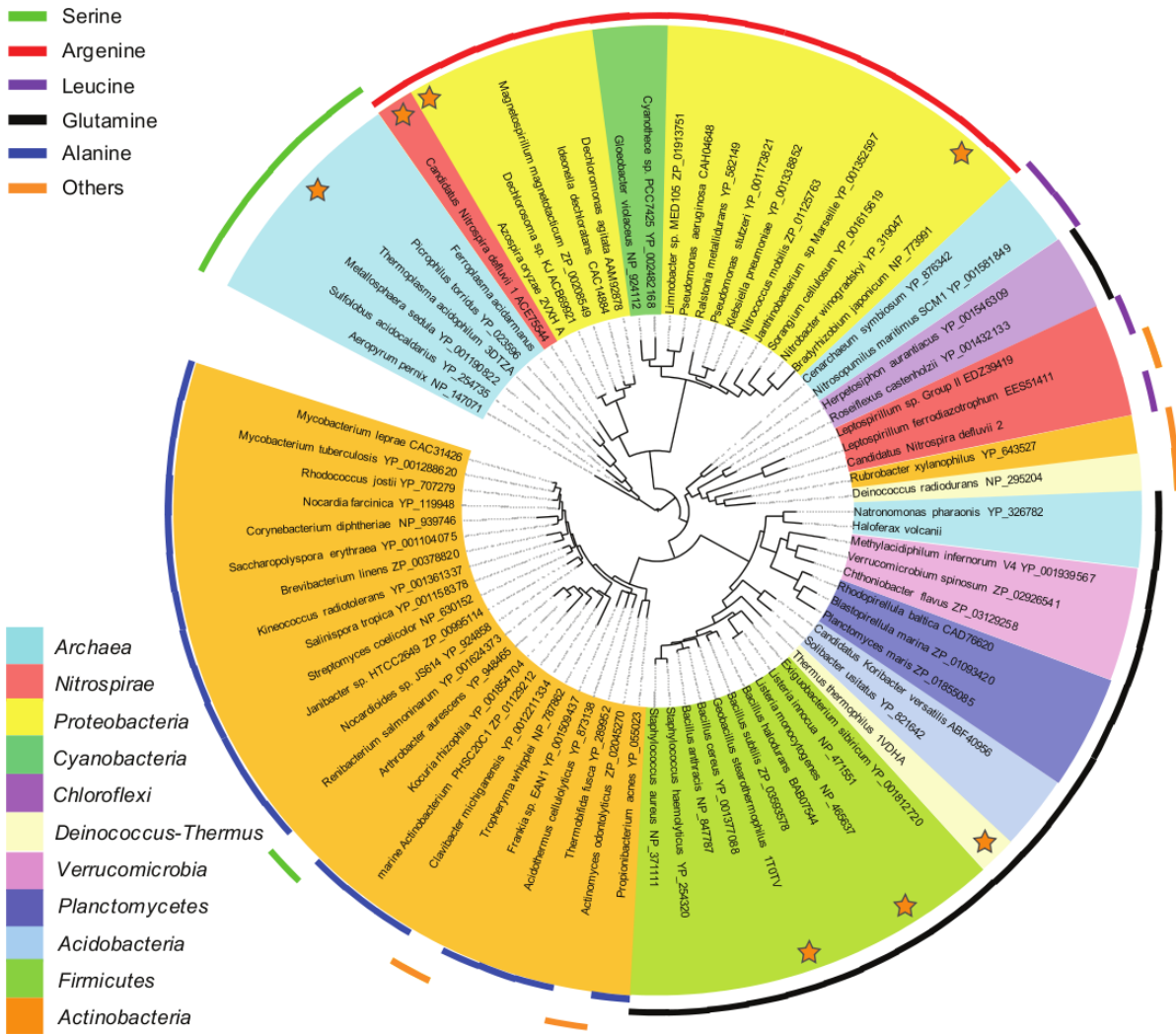


**Figure 3:** Phylogenetic tree of Clds and Cld-like proteins. The alignment is based on the amino acid sequence of the protein. Colours indicate different bacterial or archaeal phylae based on 16S rRNA. The coloured bars indicate the identity of the residue homologous to arginine 173 in NdCld, which was postulated to be a key residue for the chlorite dismutase reaction. Stars indicate proteins with determined structure (The CFP from *Dechloromonas aromatica* is missing in this tree). Figure adapted from Kostan et al. [29].

Mlynek et al. [34] suggested a classification of the validated and proposed active chlorite dismutases into two lineages; with Lineage I containing the canonical Clds, being mainly from PCRB - NdCld comprising the only non-proteobacterial member of this lineage and Lineage II, where NwCld and related proteins are located.

Apart from the cluster of validated and postulated active chlorite dismutases, where all proteins share the common catalytic arginine, there exists a multitude of CFPs with

## 1 Introduction

a different signature residue at the position corresponding to this catalytic residue (see Figure 3). A large cluster, containing mainly CFPs from *Firmicutes*, but also from *Deinococcus*, *Planctomycetes*, *Verrucomicrobia*, *Thermus* and even *Archaea* features a common glutamine residue instead of the arginine. In this “glutamine” cluster, many CFPs from human pathogens, e.g. *Listeria monocytogenes* and *Staphylococcus aureus* are located. The CFP from *Listeria monocytogenes* has a yet unknown function, no chlorite dismutase activity could be observed (and it does not match the proposed signature residues), but it was shown to be essential for this organism. (Füreder, unpublished data), which renders it a potential drug target. *Listeria* is a human facultative intracellular pathogen, causing potentially fatal listeriosis via the uptake of contaminated food. The other clusters in the phylogenetic tree, which are less well-characterized, contain proteins from *Actinobacteria*, with *Mycobacterium leprae* and *Mycobacterium tuberculosis* as human pathogens being the most prominent representatives. They feature mostly alanine instead of the signature arginine. A forth larger cluster, with the signature residue arginine replaced by a serine, is of archaeal origin. Other archaea exhibit leucine at this position.

CFPs comprise a manifold plethora of proteins distributed over many bacterial phylae that share a common, ancient fold and sequence similarities. The function of the majority of CFPs remains shrouded in mystery, despite being of great importance to e.g. *L. monocytogenes*, while validated or even canonical chlorite dismutase account only for a tiny subset of CFPs.

## 1.4 Structure of Chlorite Dismutases

Early Cld research determined the molecular mass of the protein, originating from the strain GR-1 (*Azospira oryzae*) and claimed it to be homotetrameric, based on its retention volume on a size exclusion chromatography column [52]. When the first X-ray diffraction structures of Clds and Cld-like proteins were determined, the structures revealed the enzymes to be pentameric or hexameric (but pentameric in solution) [12, 13, 18, 29]. All structurally characterized canonical Clds (and Cld-like proteins) share a common, characteristic fold.

The structure of a single subunit (Figure 4) reveals two sequential ferredoxin-like folds. The ferredoxin-like fold (Figure 5) is a  $\alpha+\beta$  fold with an  $\beta\alpha\beta\beta\alpha\beta$  signature secondary structure, with the  $\beta$ -strands arranged in the order  $4\downarrow 1\uparrow 3\downarrow 2\uparrow$ . The  $\beta$ -strands form an antiparallel  $\beta$ -sheet with the  $\alpha$ -helices packing against one side of the sheet.

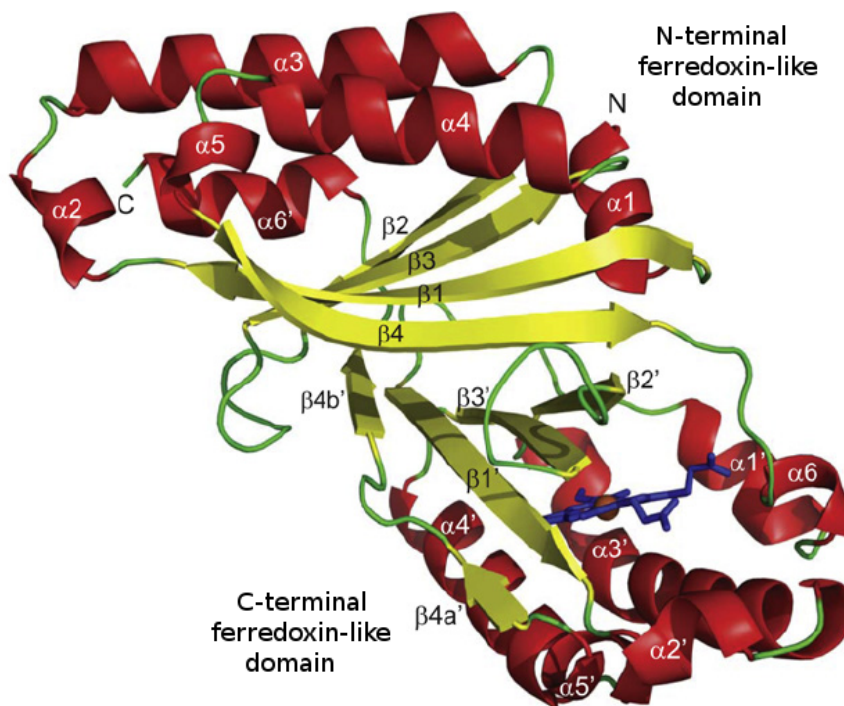


**Figure 4:** Subunit structure of chlorite dismutase from *Candidatus Nitrospira defluvii* with annotated secondary structure elements. The heme b group is shown as a stick model in the C-terminal domain. The structure of NdCld was solved by X-ray diffraction at  $1.8\text{\AA}$  and the protein was revealed to be a homopentamer. Figure adapted from Kostan et al. [29]

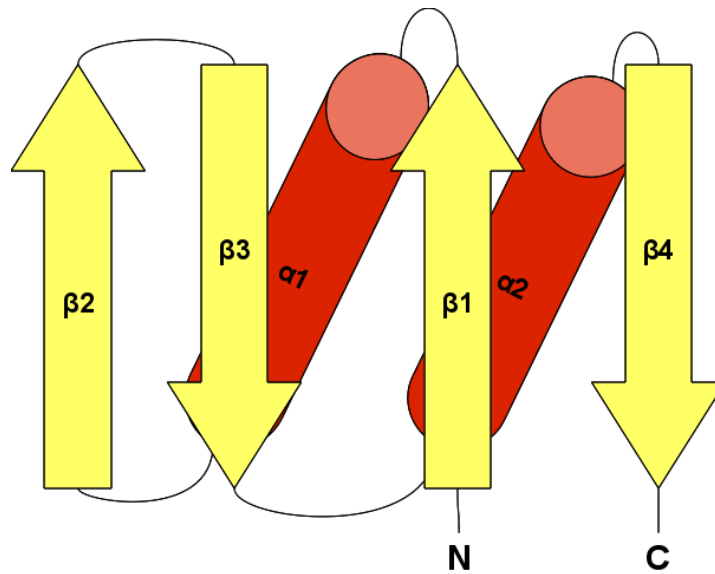


**Figure 5:** Topology of the ferredoxin-like fold. It is an  $\alpha + \beta$  fold with a signature secondary structure motif  $\beta\alpha\beta\alpha\beta$ . The  $\beta$ -strands form an antiparallel  $\beta$ -sheet with the helices packed on one side.

The central core of a Cld subunit is formed by the two antiparallel  $\beta$  sheets that stack top of each other at an angle of  $\approx 65^\circ$  to form a flattened  $\beta$ -barrel. They are surrounded by a variable number of flanking  $\alpha$ -helices. The Cld subunit consists thus of two structurally similar domains. The subunit fold is highly conserved, with the single subunits of other Clds and Cld-like proteins diverging only with an r.m.s.d. of  $1.72\text{\AA}$  (over 180  $C_\alpha$  atoms [29]).

An exception to the described tertiary and quaternary structure is the already mentioned chlorite dismutase from *Nitrobacter winogradskyi* (NwCld) [34], whose the amino acid sequence is about one-third smaller than of all other structurally characterized Cld and Cld-like proteins and misses the  $\alpha$ -helices of the N-terminal ferredoxin-like fold entirely. The N-terminal  $\beta$ -sheet and the C-terminal domain are preserved in NwCld. The shorter sequence takes its toll on the subunit interface; NwCld forms a dimer instead of a pentamer or a hexamer (see Figure 6). Mlynek et al. [34] suggest that the N-terminal part was lost during evolution. Nevertheless, NwCld is a highly active chlorite dismutase.

Four structures are known of CFPs that have no heme and have been observed to have no or only a very weak Cld activity. The structure of the already introduced LmCld was recently determined (Mlynek, unpublished data), with the heterologously expressed protein having no heme in its active site. Phylogenetically LmCld belongs to the previously described large group of CFPs, where the signature residue argi-



nine is replaced by a glutamine. Two more representatives of this group have been structurally characterized: The protein TT1485 from a thermophile, *Thermus thermophilus*[13]. The crystal structure of this protein did also not feature a heme; but *in silico* docking of a heme group was successful and the protein could be *in vitro* reconstituted with hemin; then exhibiting a very weak chlorite dismutase activity. Ebihara et al. [13] propose that TT1485 might bind heme c, which was proposed to be covalently bound via a single thioether bond. The other structure, from the thermophile firmicute *Geobacillus stearothermophilus* was solved by a structural genomics consortium (Gilski et al., [2004]). In addition, the structure of the CFP from *Thermoplasma acidophilum* was solved, also by means of structural genomics (Chang et al., [2008]). The CFP of *T. acidophilum* belongs to the archaeal “serine” cluster. No heme was found in its active site.

## 1 Introduction

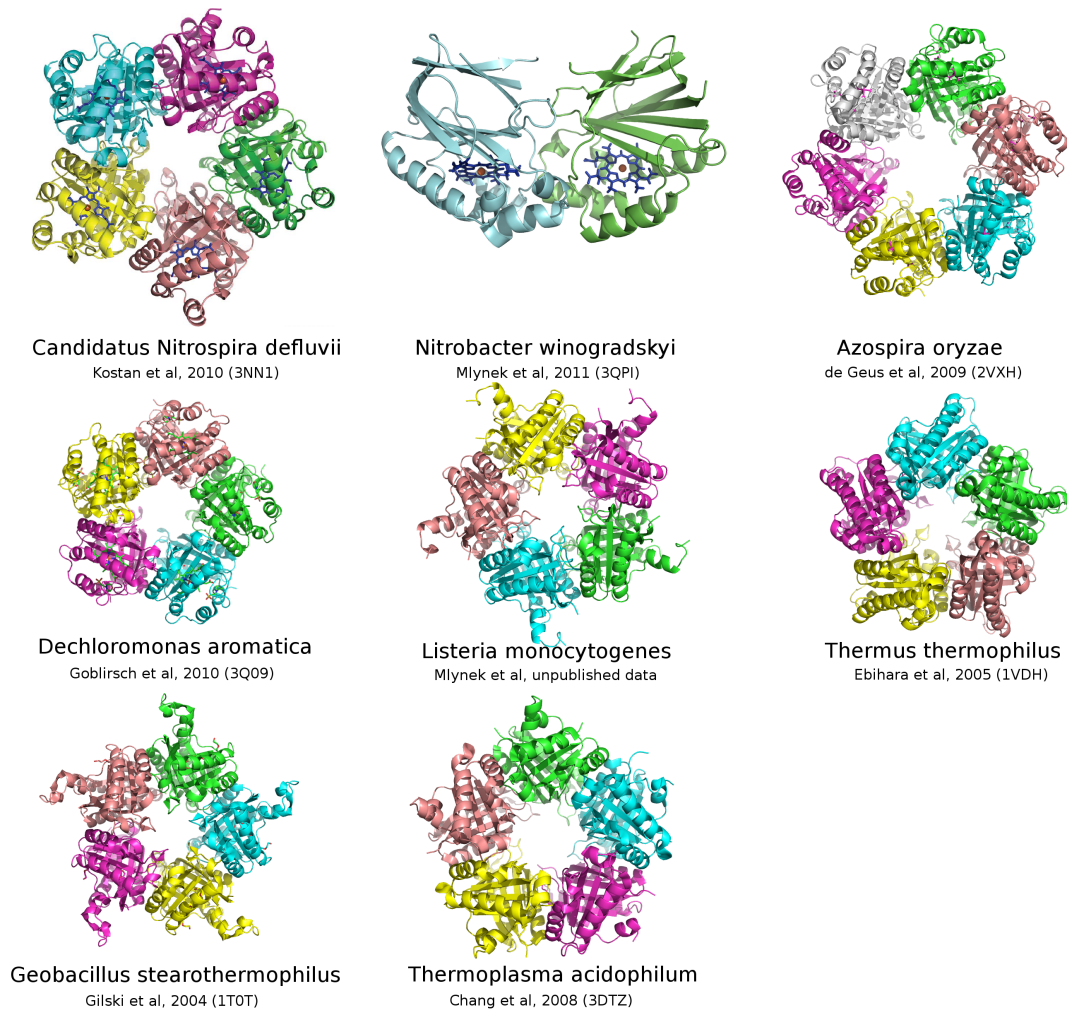


**Figure 6:** All hitherto known structures of Clds and Cld-like proteins. The confirmed Clds are from the following organisms: *Dechloromonas aromatica* and *Azospira oryzae* are confirmed PCRB, *Candidatus Nitrospira defluvi* and *Nitrobacter winogradskyi* are NOB. The rest are Cld-like proteins, not having a catalytical arginine and no or only very weak Cld activity: *Listeria monocytogenes* a firmicute and human pathogen *Thermus thermophilus*, a thermophile bacterium, *Geobacillus stearothermophilus*, a thermophile firmicute and *Thermoplasma acidophilum*, an thermophile archaeon.

## 1.5 Active Site

One chlorite dismutase subunit consists of two similar ferredoxin-like domains, but only one heme is bound in confirmed Clds in a cavity formed by the second, C-terminal  $\beta$  sheet and its flanking helices. It is enclosed by the central C-terminal  $\beta$ -sheet ( $\beta 1'$ ,  $\beta 2'$ ,  $\beta 3'$ ) and by helices  $\alpha 6$ ,  $\alpha 1'$  and  $\alpha 3'$ . Central to heme binding is the proximal histidine in  $\alpha 3'$ , which coordinates the iron as an axial ligand. The second ferredoxin-like fold lacks this histidine and is therefore unlikely to bind a heme. On the distal site of the heme is the proposed substrate binding site. The active site displayed in Figures 7 and 8 shows that the iron atom in the heme is hexacoordinated in a quadratic-bipyramidal (octahedral) way. The four nitrogen atoms of the pyrrol groups of the porphyrin ring comprise the equatorial ligands. The axial ligands are histidine on the proximal side and substrate/inhibitor/water on the distal side (Figure 7). Until now, there exists no Cld structure with substrate, product or an intermediate bound. Instead, either the inhibitors imidazole, cyanide [29], thiocyanate [12], nitrite [18] or simply water [34] have been observed to occupy the active site. The Cld-like protein from *Geobacillus stearothermophilus* crystallized with PEG 330 in the active site cavity in validated Clds (Gilski et al, [2004], PDB: 1T0T).

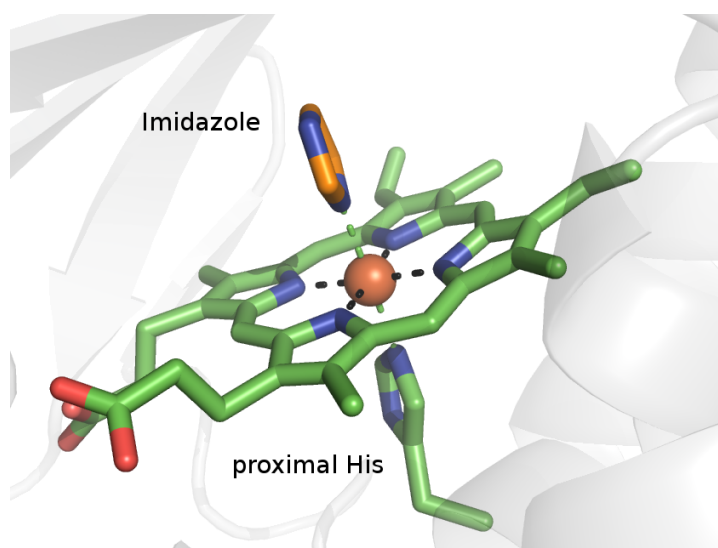


**Figure 7:** Octahedral coordination of the iron in the active site of the *Candidatus Nitrospira defluvii* chlorite dismutase. Four nitrogens from the pyrrol rings serve as equatorial ligands, the proximal histidine and the inhibitor imidazole as axial ligands.

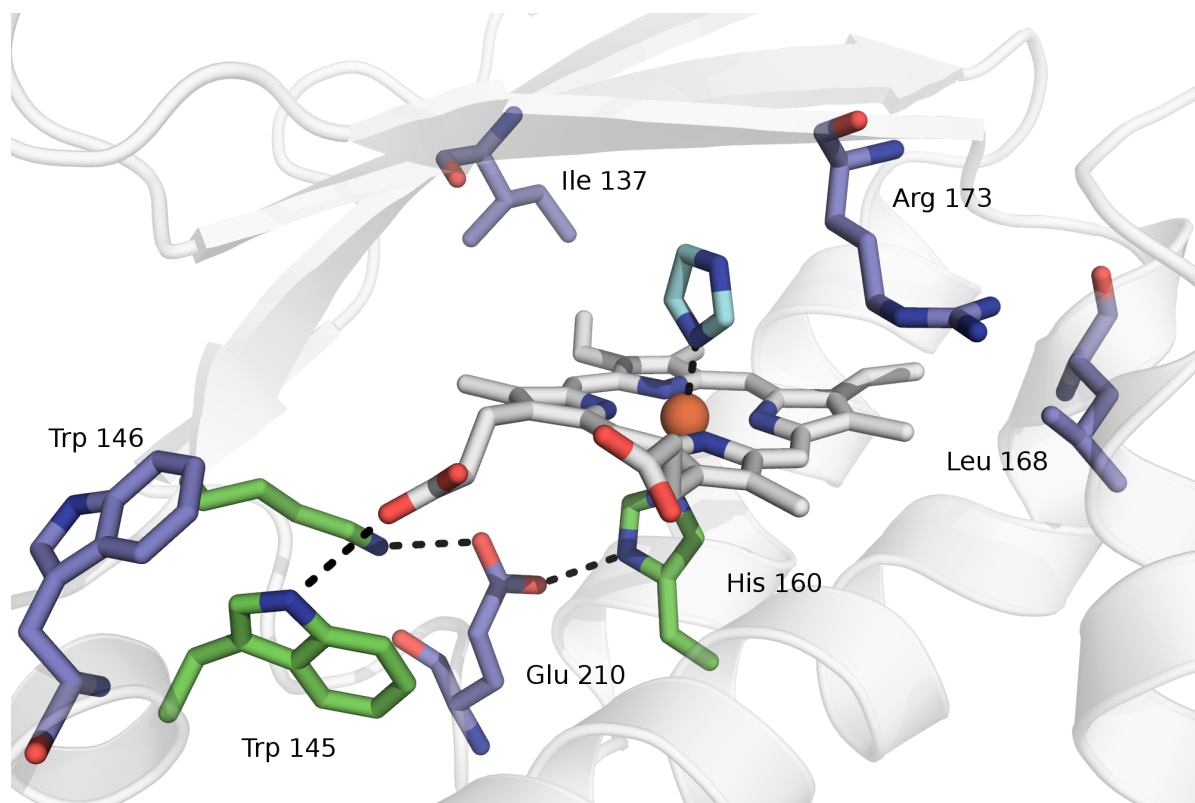
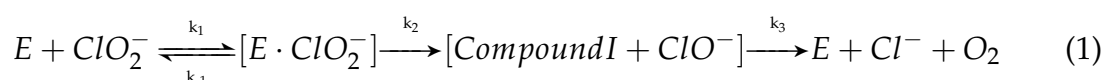


**Figure 8:** Overview of the active Site of chlorite dismutase from *Candidatus Nitrospira defluvia* in complex with imidazole as distal axial ligand. Chain A is visible in light grey in the background. Mauve residues are proposed signature residues for chlorite dismutase activity in CFPs, green residues are conserved throughout all CFPs. Residues 107-112 are not visible in the background cartoon structure.

## 1.6 Reaction Mechanism

Chlorite dismutase is remarkable from a biochemical point of view, as it is one of three known enzymes that catalyze the formation of a covalent O-O bond as their principal function, the other two being water:plastoquinone oxidoreductase (photosystem II) and a yet uncharacterized enzyme from an anaerobic methane-oxidizer [15, 36].

Lee et al. [31], Streit and DuBois [43] proposed a reaction mechanism similar to heme peroxidases and catalases (see Figures 9 and 10 as well as Equation 1), which was further explored by Kostan et al. [29], Mlynek et al. [34] and Goblirsch et al. [18].



The reaction cycle starts with a pentacoordinated iron in ferric (III) state. Initial  $ClO_2^-$  binding leads to hexacoordination and formation of the Michaels intermediate (Figure 9), which was proposed to occur in a simple, reversible collision complex model [43]. An oxoiron(IV) porphyrin  $\pi$ -cation radical complex (Compound I,  $Fe^{IV}=\text{O}$ ,  $\text{por}^{\cdot+}$ ), which is two oxidizing equivalents above the resting state, is then formed by heterolytic cleavage of a Cl-O bond. The rate of the conversion of the Michaelis intermediate to compound I +  $ClO^-$  ( $k_2$ ) was suggested to be the limiting step of the reaction [43]. Afterwards, a nucleophilic attack of the intermediate hypochlorite ( $ClO^-$ ) on Compound I leads to the formation of a rapidly decaying peroxychlorite anion, yielding the release of the products  $O_2$  and  $Cl^-$  from the active site and returning the iron to ferric state with a two-electron reduction that completes the cycle. An alternative pathway suggested by Goblirsch et al. [17] starts from homolytic cleavage of the Cl-O bond, resulting in a hypochloryl radical ( $\cdot O-Cl$ ) and the ferryl-porphyrin complex (Compound II,  $Fe^{IV}=\text{O}$ ,  $\text{por}$ ). The subsequent recombination of these leads also to product formation and release via the decay of the peroxychlorite anion.

A side path displayed in Figure 9 involves the formation of a tryptophanyl radical, which is also associated with formation of compound II [31, 43] and leads to degradation of the heme and therefore bleaching and inactivation of the enzyme. Both compound I and II have been detected spectroscopically (EPR, UV-VIS) in chlorite dismutases [31] and have even been trapped in a crystal structure in heme peroxidases [19], where compound II formation is part of the reaction cycle that reduces the enzyme back to its resting state via a two-step reduction[53]. Class I heme peroxidases use a Trp residue as site of the cation radical [39]. Figure 9 displays a compact overview.

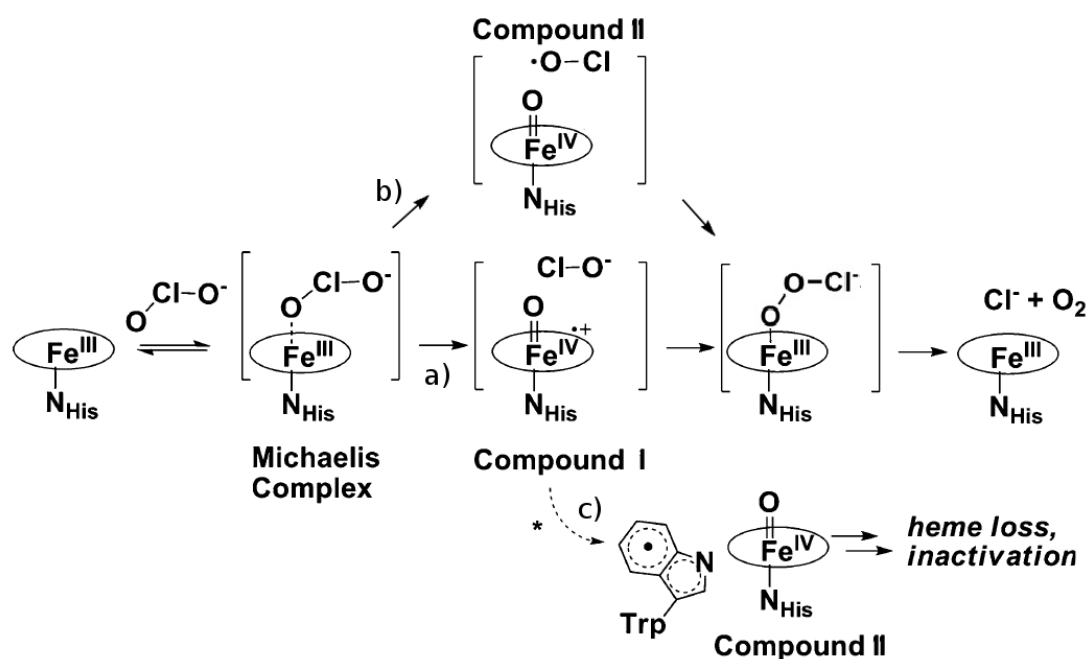


**Figure 9:** Possible reaction mechanisms for chlorite dismutases. a) Heterolytic cleavage of the Cl-O bond pathway yields compound I, b) Homolytic cleavage of the Cl-O bond yields compound II, c) Inactivation of Cld and heme degradation occurs via the off-pathway production of a tryptophanyl radical and compound II. Figure adapted from Goblirsch et al. [17, 18]

Figure 8 shows the active site of the chlorite dismutase from *N.defluvia* with its side chains closest to the heme, including the residues which were proposed to be signature residues for active chlorite dismutases [17, 34].

Central to heme binding is the proximal histidine, His 160, which contributes to iron coordination via its imidazole side chain, therefore serving as its axial ligand. This histidine is linked to several active site residues via an intricate hydrogen bonding network. Its imidazolic character is proposed to be enhanced by the neighboring Glu 210, to which it forms a hydrogen bond [29]. The residue Lys 141 donates a hydrogen bond to Glu 210.

The conserved arginine residue in the distal pocket (Arg 173) was shown to play a significant role in the reaction. If this residue is exchanged, the ability of Cld to bind and process its substrate is greatly reduced [29]. In the structure it points away from the active site with imidazole as the axial ligand. Its positive charge is supposed to position and stabilize the substrate and intermediates [34]. Figure 10 shows the proposed compound I path of the proposed reaction mechanism with emphasis on the role of arginine [34].

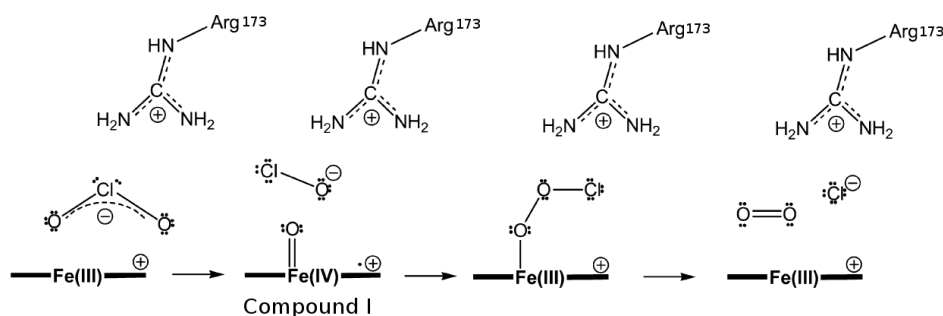


**Figure 10:** Proposed reaction mechanism of chlorite dismutation emphasizing the role of arginine in the distal pocket. Figure adapted from Mlynek et al. [34]

Ile 137 and Leu 168 are two hydrophobic residues that were also suggested to be signature residues for chlorite dismutase activity [34], comprising a favourable environment to the binding of heme, that does not lead to clashes.

**Table 1:** Signature residues (according to Mlynek et al. [34]) in the active site for active chlorite dismutases and other conserved residues for CFPs. All residues are numbered according to the *N. defluvii* numbering. His 214 and Trp 217 are only conserved throughout PCRB, in *N. defluvii* they are changed to an asparagine and a phenylalanine, respectively

Residue	Conservation status	proposed function
Ile 137	signature residue	heme stability, ligand cavity size
Lys 141	all CFPs	proximal H-bonding network
Trp 145	all CFPs	radical pathway
Trp 146	signature residue	radical pathway
His 160	all CFPs	proximal axial ligand for heme
Leu 168	signature residue	heme stability, ligand cavity size
Arg 173	signature residue	catalytic function
Gln 210	signature residue	proximal H-bonding network
His 214	PCRBs	radical pathway
Trp 217	PCRBs	radical pathway

The Trp residue required for the off-reaction formation of compound II and subsequent bleaching should be located near the active site and close to the propionate groups of the heme for electron transfer [25]. All ClDs and ClD-like proteins have at least one conserved Trp in the vicinity of the active site, validated ones always bear two neighboring Trp residues [29], which are oriented orthogonally to each other (see Figure 8, residues Trp 145 and Trp 146) [43]. A third Trp and a His residue (Trp 224 and His 227 in DaClD numbering, corresponding to Asn 214 and Phe 217 in NdClD)

## *1 Introduction*

neighboring the juxtaposed pair of Trp residues are conserved throughout ClDs from PCRBs and could be additionally involved in radical formation, comprising a continuous path for the electron [17].



## 2 Aim of this Thesis

The aim of this thesis was to elucidate reaction mechanism details of chlorite degradation by the enzyme chlorite dismutase via a comprehensive structural, biochemical and genetic approach.

Section 4.1 and 4.2 describe the mutational studies on the proposed chlorite dismutase “fingerprint” residues in combination with biochemical enzyme activity assays that were conducted to confirm the relevance of these amino acids for the chlorite dismutase reaction. Also, structural studies were performed on these mutants to see effects of the mutations in the active site. One goal was to generate a NdCld variant suitable for gaining structural insights into the chlorite dismutase reaction, i.e. trapping substrate bound states or reaction intermediates in a crystal structure. While this was not achieved, the generated mutants provide insights about the reaction mechanism and important residues and will be utilized for further biochemical and structural studies.

In section 4.3 the successful preparation and crystal structure of the *N. defluvii* chlorite dismutase without heme b is presented. Apo-NdCld was used as an intermediate for the production of NdCld with a different prosthetic group, cobalt protoporphyrine IX, contributing to the mutational studies summarized before. The structure of apo-NdCld was determined to gain insights into the heme environment and for comparison with CFPs where no heme binding has been observed.

The study described in Section 4.4 emerged from the *Nitrobacter winogradskyi* chlorite dismutase project. Here, the stability of the subunit interactions in NwCld was experimentally determined. Therefore, the contributions of electrostatic and hydrophobic forces that account for the formation of the dimer, which are different from the subunit contacts in pentameric chlorite dismutase were elucidated.



## 3 Materials and Methods

### 3.1 Antibiotics, Media and General Buffers

Composition of all general buffers, stock solutions, media and antibiotics is described in Tables 2 and 3.

**Table 2:** Stock solutions and used concentrations of antibiotics. All stock solutions were sterile filtered ( $\varnothing$  0.22  $\mu\text{m}$ ) before freezing. All antibiotics were purchased from Sigma.

Antibiotic	Preparation
Ampicilin	100 $\frac{\text{mg}}{\text{ml}}$ in $\text{H}_2\text{O}$ , stored at $-20^\circ\text{C}$ . Used 1:1000.
Kanamycin	100 $\frac{\text{mg}}{\text{ml}}$ in $\text{H}_2\text{O}$ , stored at $-20^\circ\text{C}$ . Used 1:1000.
Chloramphenicol	34 $\frac{\text{mg}}{\text{ml}}$ in ethanol, stored at $-20^\circ\text{C}$ . Used 1:1000.

**Table 3:** Preparation of general buffers, media and stock solutions.

Solution	Preparation
LB-medium	10 g tryptone, 5 g yeast extract, 10 g NaCl, adjusted to pH 7.0 with NaOH (ready-made, Sigma, 30 g for 1000 ml $\text{H}_2\text{O}$ ); autoclaved.
LB agar	15 g agar dissolved in 1000 ml LB medium
PBS	137 mM NaCl, 2.7 mM KCl, 8.1 mM $\text{Na}_2\text{HPO}_4 \cdot 2\text{H}_2\text{O}$ , 1.7 mM $\text{KH}_2\text{PO}_4$ , pH 7.4. Used as PBS buffer tablets (Sigma). One tablet is dissolved in 200 ml dd $\text{H}_2\text{O}$ .
50x TAE buffer	2 M Tris-HCl pH 8, 1 M acetic acid, 50 mM $\text{Na}_2\text{-EDTA}$ , pH 8.0. Used for preparation of agarose gels.
TE buffer	10 mM Tris-HCl pH 8.0, 1 mM EDTA
10x SDS running buffer	0.25 M Tris-HCl pH 8.3, 2 M glycine, 1% (w/v) SDS
Destaining Solution	250 ml ethanol, 50 ml acetic acid, filled to 1000 ml with $\text{H}_2\text{O}$
Staining Solution	250 ml ethanol, 80 ml acetic acid, 2.5 g Coomassie brilliant blue, filled to 1000 ml with $\text{H}_2\text{O}$ .
Hemin	50 $\frac{\text{mg}}{\text{ml}}$ in 0.1 N NaOH, used 1:1000, unless stated otherwise. Always freshly prepared, short-term storage at $4^\circ\text{C}$ . Purchased from Fluka.
Cobalt protoporphyrine IX	Powder stored at $4^\circ\text{C}$ , stock solution of 5-10 $\frac{\text{mg}}{\text{ml}}$ in 0.1 N NaOH. Freshly prepared, short-term storage at $4^\circ\text{C}$ . Purchased from Fluka.

### 3.2 Expression System and Expression Vectors

Several laboratory strains of the bacterium *Escherichia coli* were used as system for genetic manipulation (subcloning and mutagenesis) as well as heterologous protein expression system throughout this thesis. The strains are summarized in Table 4.

The expression vectors all carry a copy of the *lacI* gene for the lac-repressor and thus are all inducible by addition of lactose or the artificial inducer Isopropyl-beta-D-thiogalactopyranoside (IPTG).

**Table 4:** *Escherichia coli* host strains used for cloning and expression.

Host strains	Genotype	Usage
DH5 $\alpha$	F <sup>-</sup> , $\phi$ 80 $\Delta$ lacZ $\Delta$ M15 $\Delta$ (lacZYA-argF)U169 deoR recA1 endA1 hsdR17(rk-mk+) phoA supE44 thi-1 gyr A96 relA1	Cloning
XL1-Blue	recA1 endA1 gyrA96 thi-1 hsdR17 supE44 relA1 lac [F' proAB lacIqZ $\Delta$ M15 Tn10 (Tet <sup>r</sup> )]	Cloning
Tuner (DE3) (Novagen)	F <sup>-</sup> ompT hsdS <sub>B</sub> (r <sub>B</sub> <sup>-</sup> m <sub>B</sub> <sup>-</sup> ) gal dcm lacY1 (DE3)	Expression
Rosetta <sup>TM</sup> 2 (Novagen)	F <sup>-</sup> ompT hsdS <sub>B</sub> (r <sub>B</sub> <sup>-</sup> m <sub>B</sub> <sup>-</sup> ) gal dcm pRARE2 (Cam <sup>R</sup> )	Expression

### 3.3 Storage

**Proteins** Short-term storage of proteins was either done on ice or at 4°C, e.g. during purification. For long-term storage, protein samples were aliquoted to 100 µl in thin-walled 500 µl reaction tubes, flash-frozen in LN<sub>2</sub> and stored at -80°C.

**DNA** DNA samples in 1xTE buffer were stored on 4°C for short term (1-3 days) and frozen at -20°C for long-term storage.

**Glycerol Stocks** All constructs (see the construct list 10) were transformed into a cloning strain (DH5α, XL-1 blue) and an expression strain (Tuner (DE3) or Rosetta™2). The glycerol stock was created by pelleting 50 ml of a dense culture grown in selective LB medium and resuspending the cell pellet in sterile 15% (v/v) glycerol, aliquoting to 500-1000 µl into 1 ml cryotubes (Nunc) and flash-freezing in LN<sub>2</sub>. Stocks were stored at -80°C.

**Buffers and Stock Solutions** Sterile filtered buffers and stock solutions were stored at room temperature. Buffers and solutions used for protein purification or protein crystallization at 4°C were cooled down before usage. PEG stocks were stored protected from light.

### 3.4 Molecular Cloning Techniques

Molecular cloning techniques were mainly used to introduce specific mutations into the *cld* gene from *Candidatus Nitrospira defluvii* and to change expression vectors from pETM-11 to the custom StrepTEVpET21 expression vector.

DNA concentration was determined spectroscopically with a NanoDrop 2000c (ThermoFisher Scientific), unless stated otherwise. All restriction enzymes and T4 ligase were purchased from Fermentas, as well as the appropriate buffers.

All oligonucleotides were ordered at Sigma-Aldrich on a synthesis scale of 0.2 µmol, purified by desalting. Upon arrival, the dry oligos were dissolved in 1xTE in an appropriate volume to reach a concentration of 100 µM.

### 3 Materials and Methods

#### 3.4.1 Site-Directed Mutagenesis

To introduce the desired mutations of specific residues in the active site of NdCld, site-directed mutagenesis via polymerase chain reaction (PCR) was employed. This enables the targeted exchange of one or more base pairs in a DNA sequence with designed primers. The mutagenesis primers containing the desired mutation were designed as the reverse primer being the reverse complement of the forward and thus complementary to opposite strands of the template vector. A complete primer list is found in Table 5. Template vector was either the wild-type plasmid, pJK23 (see Table 10) for single mutants or the appropriate single mutant construct for double mutants.

Two different PCR setups were used for site-directed mutagenesis, the first utilizing Pfu DNA polymerase from *Pyrococcus furiosus* (Fermentas), the second using the 2x PhusionFlash MasterMix (Finnzymes). The latter was used prevalently because of the easier handling and the faster polymerase (Pfu:  $1 \frac{kb}{min}$ ; PhusionFlash:  $4 \frac{kb}{min}$ ). The PCRs were carried out on an Eppendorf Mastercycler gradient PCR machine. After the PCR reaction, the PCR reaction mix was treated with the DNA restriction enzyme *DpnI* at  $37^\circ$  for 1 hour. *DpnI* (recognition sequence: 5'-G<sup>me</sup>A'TC-3') digests the methylated wild-type DNA and leaves only the mutated plasmid generated by the mutagenesis PCR. This mixture, containing the nicked mutated vector DNA, was subsequently transformed into DH5 $\alpha$  chemically competent *E.coli* cells.

**Table 5:** Primers (Sigma-Aldrich) used for site-directed mutagenesis of NdCld (top, with the mutated triplet indicated in green) or for specific amplification of a Cld insert (bottom). All primers were ordered dry and dissolved in the appropriate amount of 1xTE buffer to a concentration of 100  $\mu$ M upon arrival. Primers for NwCld and LmCld are used to amplify the respective gene and fit it with NcoI/XhoI restriction sites for use with appropriate expression vectors, e.g. StrepTEVpET21 or pETM-11. The melting temperature was calculated as the salt-adjusted  $T_M$  with the Promega BioMath Calculator.

Name	Primer sequence	$T_M$ ( $^{\circ}$ C)
W145V fwd	5'-GAAGGACGCGGAA <b>GTG</b> TGGGCACTGGACCAGG-3'	66
W145V rev	5'-CCTGGTCCAGTGCCCA <b>CAC</b> TTCCGCGTCCTTC-3'	66
W145F fwd	5'-TCCCTATCAAGAAGGACGCGGAA <b>TTT</b> TGGGCACTG-3'	62
W145F rev	5'-CAGTGCCCA <b>AAA</b> TTCCGCGTCCTTCTTGATAGGGA-3'	67
W146Y fwd	5'-GAAGGACGCGGAATGG <b>TAC</b> GCACTGGACCAGG- 3'	64
W146Y rev	5'-CCTGGTCCAGTGCGTACCATTCCGCGTCCTTC-3'	64
VY fwd	5'-GAAGGACGCGGAA <b>GTG</b> GCACTGGACCAGG-3'	63
VY rev	5'-CCTGGTCCAGTGCGTACACTTCCGCGTCCTTC-3'	64
R173E fwd	5'-CCTATCTGAAGACGGTGAAA <b>GAA</b> AAACTGTATCATTTCGACGGG-3'	62
R173E rev	5'-CCCGTCGAATGATACAGTTTT <b>TTCTTT</b> CACCGTCTTCAGATAGG-3'	62
R173Q fwd	5'-CTGAAGACGGTGAAA <b>CAA</b> AAACTGTATCATTTCG-3'	56
R173Q rev	5'-CGAATGATACAGTTTT <b>TTG</b> TTTCACCGTCTTCAG-3'	56
E210A fwd	5'-CTGCAGCAGGTGAAG <b>GCA</b> TTCCGCCACAATCGAC-3'	64
E210A rev	5'-GTCGATTGTGGCGGAAT <b>TGC</b> CTTCACCTGCTGCAG-3'	64
NwCld fwd	5'-GCTGAGCCATGGGGACGTTACAGTCTTCACC-3'	63
NwCld rev	5'-AGTTTCCTCGAGTCATATCGCGCGGCCAATCGAAT-3'	63
LmCld fwd	5'-GCTGAGCCATGGGGATGAGCGATTACGACATCCC-3'	64
LmCld rev	5'-CCCCTCCTCGAGCTAAATAGTAAA TAATTTAGAAAGTTG-3'	57
NdCld fwd	5'-GGAGATATACCCATGGCCGATC-3'	55
NdCld rev	5'-TTCGGATCCTACTGTGCGAACT-3'	55

### 3 Materials and Methods

**Table 6:** PCR setups I and II for site-directed mutagenesis using Pfu DNA polymerase and PhusionFlash DNA polymerase, respectively.

<b>Component</b>	<b>Concentration</b>	<b>Volume</b>	<b>Stock</b>
<b>PCR setup I</b>			
Forward primer	0.2 $\mu\text{M}$	1 $\mu\text{l}$	10 $\mu\text{M}$
Reverse primer	0.2 $\mu\text{M}$	1 $\mu\text{l}$	10 $\mu\text{M}$
Template	15 $\frac{\text{ng}}{50\mu\text{L}}$	1 $\mu\text{l}$	15 $\frac{\text{ng}}{\mu\text{L}}$
10x Pfu buffer + MgSO <sub>4</sub>	1x	5 $\mu\text{l}$	10x
dNTPs	0.3 mM	6 $\mu\text{l}$	2.5 mM
Pfu		1 $\mu\text{l}$	2.5 $\frac{\text{U}}{\mu\text{L}}$
dd H <sub>2</sub> O sterile		ad 50 $\mu\text{l}$	
<b>PCR setup II</b>			
Forward primer	0.2 $\mu\text{M}$	1 $\mu\text{l}$	10 $\mu\text{M}$
Reverse primer	0.2 $\mu\text{M}$	1 $\mu\text{l}$	10 $\mu\text{M}$
Template	15 $\frac{\text{ng}}{50\mu\text{L}}$	1 $\mu\text{l}$	15 $\frac{\text{ng}}{\mu\text{L}}$
2x PhusionFlash MasterMix		25 $\mu\text{l}$	
dd H <sub>2</sub> O sterile		ad 50 $\mu\text{l}$	



**Table 7:** PCR settings for site-directed mutagenesis for PCR setups (Table 6). Annealing temperatures were calculated with the Promega BioMath calculators.

<b>Process</b>	<b>Temperature (°C)</b>	<b>Duration (sec)</b>
<b>Mutagenesis PCR for PCR setup I</b>		
Initial denaturation	95 °C	300
Denaturation	95 °C	30
Primer annealing	x °C	45
Extension step	72 °C	360
Cycles	30	
Final extension	72 °C	600
Cooling	4 °C	hold
<b>Mutagenesis PCR for PCR setup II</b>		
Initial denaturation	95 °C	300
Denaturation	95 °C	30
Primer annealing	x °C	45
Extension step	72 °C	120
Cycles	30	
Final extension	72 °	300
Cooling	4 °C	hold

### 3 Materials and Methods

#### 3.4.2 Chemical Transformation of *E. coli* (Hanahan)

100  $\mu$ l of chemically competent cells [23] (stored at  $-80^{\circ}\text{C}$ ) were thawed on ice, transformed with 5-20 ng DNA (unless stated otherwise; 6  $\mu$ l of *DpnI*-treated PCR product after site-directed mutagenesis) and incubated on ice for 20 minutes. After a 60 s heat shock ( $42^{\circ}\text{C}$ ), the cells were incubated again for 3 minutes on ice. Subsequently, 900  $\mu$ l nonselective LB medium was added and the cells put into recovery at  $37^{\circ}\text{C}$  and 800 rpm for one hour. Afterwards, the cells were plated onto a selective agar plate and grown in an incubator overnight at  $37^{\circ}\text{C}$ .

#### 3.4.3 Colony PCR

Presence of a specific insert was verified by performing PCR on colonies grown on petri dishes before a small-scale DNA preparation for sequencing. For colony PCR, single colonies were picked and resuspended each in a PCR tube in 5  $\mu$ l sterile ddH<sub>2</sub>O. 2  $\mu$ l of the cell suspension were subsequently dropped on a selective agar plate with a grid to identify correct clones later on. A PCR mix was set up as described in Table 8, using generic primers for the respective gene (see Table 5). The PCR products were analyzed on a 1 % agarose gel for the presence of a band at the corresponding size. Clones containing the desired insert were used for inoculation of a small-scale culture (see section 3.4.4).

**Table 8:** PCR setup for colony PCR.

<b>Component</b>	<b>Concentration</b>	<b>Volume</b>	<b>Stock</b>
Cell suspension	-	3 $\mu$ l	-
2x PhusionFlash MasterMix	1x	12.5 $\mu$ l	2x
Primer fwd	0.8 $\mu$ M	1 $\mu$ l	10 $\mu$ M
Primer rev	0.8 $\mu$ M	1 $\mu$ l	10 $\mu$ M
dd H <sub>2</sub> O sterile	ad 25 $\mu$ l		

#### 3.4.4 Plasmid Preparation from *E. coli* Cells

Two different commercial kits were used for plasmid preparation from *E. coli* DH5 $\alpha$  or XL1-blue cells, depending on the needed plasmid yield. For identification of correct clones and subsequent sequencing, small-scale minipreps were performed using the

**Table 9:** PCR program used for colony PCR.

Process	Temperature (°C)	Time (sec)
Cell lysis	98 °C	600
Initial denaturation	95 °C	120
Denaturation	95 °C	30
Annealing	x°C	54
Elongation	72 °C	60
Cycles	30	
Final elongation	72 °	180
Cooling	4 °C	Hold

Plasmid Mini Kit from Fermentas. To produce a larger, stable DNA stock of a confirmed construct in transformation quality, medium-scale plasmid purifications were done with the NucleoBond® Xtra Midi Kit from Macherey-Nagel.

**Small-scale (“Miniprep”)** For a miniprep, 5 ml of selective LB medium was inoculated with a single colony and the culture grown shaking at 37°C overnight in an incubator. The dense cell culture was harvested by centrifugation next day (15 minutes at 4000 rpm) and the plasmids purified according to the manufacturer’s instructions, which utilizes the alkaline lysis method. The DNA was eluted from the spin columns with 50 µl TE buffer.

**Medium-scale (“Midiprep”)** For larger amounts of plasmid DNA, 50-100 ml of selective LB medium was inoculated with a single colony and the culture grown overnight at 37° shaking. The cells were harvested by centrifugation (4000 rpm, 25 minutes) and the plasmids purified according to the manufacturer’s instructions. The plasmid DNA pellet was resuspended in 100-150 µl TE.

### 3.4.5 Subcloning

The expression vector was changed from pETM-11 to a modified version of pET21(+) with an N-terminal Strep-Tag II, cleavable by TEV protease. This vector will be referred to as StrepTEVpET21(+) throughout this thesis. The cld insert was cut out from pJK29, pJK30, pJK32, pJK53, pJK54, pJK55, pKG1, pKG2, pKG3 and pKG5 (see Table 10) with the restriction endonucleases *NcoI* (5'-C'CATGG-3') and *XhoI* (5'-C'TCGAG-3'). The StrepTEVpET21 vector was treated with the same enzymes. The reaction mix

### 3 Materials and Methods

consisted of 1  $\mu\text{g}$  vector DNA, 5  $\mu\text{l}$  10x buffer R (Fermentas), 1  $\mu\text{l}$  XhoI, 1  $\mu\text{l}$  NcoI (both Fermentas, 10  $\frac{\text{U}}{\mu\text{L}}$ ). Sterile ddH<sub>2</sub>O was added to a total volume of 50 $\mu\text{l}$  and the reaction mix was incubated at 37°C for 1 hour.

The digested DNA was purified with an 1% (w/v) agarose gel containing either 0.5  $\frac{\mu\text{g}}{\text{ml}}$  ethidium bromide or SYBR® Safe DNA gel stain (Invitrogen, at a ratio of 1:10000) for UV visualization of the DNA. The appropriate bands were cut out from the gel, extracted with the GeneJET Gel extraction kit (Fermentas) and subsequently eluted from the spin column in 20-30  $\mu\text{l}$  TE.

The DNA yield was determined spectroscopically to set up the ligation reaction, which consisted of 1  $\mu\text{l}$  10x T4 ligation buffer, digested vector and insert at a molar ratio of 1:4 with approx. 20 ng of vector, 0.5  $\mu\text{l}$  T4 ligase and was adjusted with sterile ddH<sub>2</sub>O to a total volume of 10  $\mu\text{l}$ . The ligation reaction was incubated at 16°C overnight and the whole ligation mix subsequently transformed to either DH5 $\alpha$  or XL-1 blue.

An overview over all constructs is presented in Table 10.

#### 3.4.6 List of Constructs

This table represents a comprehensive list of all the constructs used and created during this thesis.

For the heterologous expression of the chlorite dismutase from *N.defluvii* (accession no. ACE75544), Kostan et al. [29] used a truncated version of the gene which lacked the first 26 N-terminal amino acids, which were predicted to be a signal peptide for periplasmic localization, because the full-length protein was not functional. This truncated gene in the pETM-11 (EMBL) vector, construct pJK23, provided by Kostan et al. [29], was used as the starting point of this work.

The chlorite dismutase gene from *N.winogradskyi* (NwCld, accession no. YP\_319047) was provided as the full-length version by Stephanie Füreder and cloned into pET21b(+) (Novagen), as well as the Cld-like genes from *L.monocytogenes* (*lmo2113*, accession no. NC003210) and *S.solfataricus* (accession no. ACX92972.1).

**Table 10:** List of all constructs that were used and/or created during this thesis. See the text for details.

<b>Construct</b>	<b>Vector</b>	<b>Insert</b>	<b>Tag</b>
pJK23	pETM-11	NdCld	N-term 6x His
pJK29	pETM-11	LmCld	N-term 6x His
pJK53	pETM-11	NdCld W146Y	N-term 6x His
pJK53s	StrepTEVpET21	NdCld W146Y	N-term Strep-Tag II
pJK54	pETM-11	NdCld W145Y	N-term 6x His
pJK54s	StrepTEVpET21	NdCld W145Y	N-term Strep-Tag II
pJK55	pETM-11	NdCld W145V W146Y	N-term 6x His
pJK55s	StrepTEVpET21	NdCld W145V W146Y	N-term Strep-Tag II
pKG1	pETM-11	NdCld R173Q	N-term 6x His
pKG1s	StrepTEVpET21	NdCld R173Q	N-term Strep-Tag II
pKG2	pETM-11	NdCld E210A	N-term 6x His
pKG2s	StrepTEVpET21	NdCld E210A	N-term Strep-Tag II
pKG3	pETM-11	NdCld W146Y R173Q	N-term 6x His
pKG3s	StrepTEVpET21	NdCld W146Y R173Q	N-term Strep-Tag II
pKG4	StrepTEVpET21	LmCld	N-term Strep-Tag II
pKG5	pETM-11	NdCld E210A	N-term 6x His
pKG5s	StrepTEVpET21	NdCld E210A	N-term Strep-Tag II
pKG6	StrepTEVpET21	NdCld R173Q E210A	N-term Strep-Tag II
pKG8	StrepTEVpET21	NdCld W145F	N-term Strep-Tag II
pKG9	StrepTEVpET21	NdCld W145V R173E	N-term Strep-Tag II
pKG10	StrepTEVpET21	SsCld	N-term Strep-Tag II
pSF22	pET21b(+)	LmCld	C-term 6x His
pSF29	pET21b(+)	NwCld	C-term 6x His

### 3.5 Heterologous Protein Expression

All proteins were expressed recombinant in *E.coli* expression strains, listed in Table 4. Starter cultures were grown from a glycerol stock stored at  $-80^{\circ}$  by scratching the surface of a frozen stock with a pipette tip and were inoculated in 50 ml LB medium.

Protein expression at  $18^{\circ}\text{C}$  and  $24^{\circ}\text{C}$  was carried out in a coolable incubator shaker (New Brunswick Scientific), at  $37^{\circ}\text{C}$  in a non-coolable incubator shaker (New Brunswick Scientific). The cells were always harvested by centrifugation in 1 L centrifuge tubes using an SLC-4000 rotor at  $4^{\circ}\text{C}$  for 20 minutes at 4000 rpm in a coolable centrifuge (Sorvall Evolution RC Superspeed Centrifuge). The resulting pellet was resuspended in 10 ml of the supernatant medium, transferred to a 50 ml Falcon tube and the cells pelleted again at 4000 g for 20 minutes at  $4^{\circ}\text{C}$  in an Eppendorf benchtop centrifuge.

#### 3.5.1 Cld from *Candidatus Nitrospira defluvii* (NdCld) - wild-type and mutants

*E.coli* BL21 (DE3) Tuner cells or Rosetta2 cells carrying an expression vector for a NdCld mutant (see Table 10) were grown in 50 ml selective LB medium (pETM-11: Kanamycin; StrepTEVpET21: Ampicilin; Rosetta2 cells: additional chloramphenicol) at  $37^{\circ}$  shaking overnight.

An aliquot of the dense starter culture was then used to inoculate the desired amount of selective LB in baffled shaker flasks to a starting  $\text{OD}_{600} \approx 0.05$ . The expression cultures were grown shaking at  $37^{\circ}\text{C}$  to a  $\text{OD}_{600} \approx 0.8$ , when the temperature was reduced to  $24^{\circ}\text{C}$ , heme was added at a concentration of  $50 \frac{\text{mg}}{\text{ml}}$  (1:1000, see 3) and the expression of Cld induced with 0.5 mM IPTG. Cld was expressed 6-8 hours and the cells afterwards harvested by centrifugation, frozen in  $\text{LN}_2$  and stored at  $-80^{\circ}\text{C}$ .

#### 3.5.2 Cld from *Candidatus Nitrospira defluvii* without heme (apo-NdCld)

*E.coli* BL21 (DE3) Tuner cells carrying the pJK23 plasmid (NdCld wild-type) were grown in 50 ml LB-medium supplemented with kanamycin ( $100 \frac{\mu\text{g}}{\text{ml}}$ ) at  $37^{\circ}\text{C}$  overnight. This starter culture was used for inoculation and added to LB-Kan to a starting  $\text{OD}_{600} \approx 0.05$ . The cells were grown at  $37^{\circ}\text{C}$  under 180 rpm agitation to an  $\text{OD}_{600} \approx 0.8$ . The protein expression was then induced with 0.5 mM IPTG and protein was expressed for 4 hours at  $37^{\circ}$ . This yields the maximum amount of protein, while keeping the heme content as low as possible. The cells were harvested by centrifugation, the cell pellets flash-frozen in  $\text{LN}_2$  and stored at  $-80^{\circ}\text{C}$  until further use.

### 3.5.3 Cld from *Nitrobacter winogradskyi* (NwCld)

*E.coli* BL21 (DE3) cells carrying the pSF29 plasmid were grown in 50 ml LB-medium supplemented with ampicillin ( $100 \frac{\mu\text{g}}{\text{ml}}$ ) at 37° overnight. 10 ml of this overnight culture were used to inoculate the expression culture consisting of LB-Amp ( $100 \frac{\mu\text{g}}{\text{ml}}$ ) in baffled shaker flasks to a starting  $\text{OD}_{600} \approx 0.05$ . The culture was grown at 37 °C in a shaker to an  $\text{OD}_{600} \approx 0.8$ . The temperature was lowered to 18°C, heme added to a final concentration of  $50 \frac{\text{mg}}{\text{L}}$  and protein expression induced with a final IPTG concentration of 0.5 mM.

The protein was expressed overnight ( 16 h) at a low temperature to facilitate correct protein folding to yield as high amounts of soluble protein as possible. A large part of NwCld was expressed insolubly as inclusion bodies, as presumably heme is required for the protein to fold correctly and is the bottleneck. Supplementing heme and slow expression helps to express the protein soluble, but still a large part of the protein was found mis- or unfolded in inclusion bodies.

The cells were harvested by centrifugation, pellets flash-frozen in LN<sub>2</sub> and stored at -80°C until lysis and purification.

## 3.6 Protein Purification Techniques

All purification steps were carried out on ÄKTA PURIFIER systems (GE Healthcare) at 4°C. All columns were purchased from GE Healthcare, unless stated otherwise. Progress of the purification was monitored by measuring absorption at  $\lambda_1 = 280 \text{ nm}$ ,  $\lambda_2 = 410 \text{ nm}$ , which corresponds to the soret peak of bound heme and  $\lambda_3 = 360 \text{ nm}$ , corresponding to the soret peak of free heme. Extinction coefficients for  $A_{280}$ , according to Mlynek et al. [34] and Kostan et al. [29]:

- NdCld:  $\epsilon=37930 \text{ M}^{-1}\text{cm}^{-1}$ ; E 0.1% (=  $1 \frac{\text{g}}{\text{l}}$ ) = 1.382
- NwCld:  $\epsilon=40450 \text{ M}^{-1}\text{cm}^{-1}$ ; E 0.1% (=  $1 \frac{\text{g}}{\text{l}}$ ) = 1.984

### 3.6.1 Purification of NdCld Mutants

- Lysis buffer: 50 mM HEPES-NaOH pH 7.4, 5% (v/v) Glycerol, 0.5% (v/v) Triton X-100
- Ni-NTA Binding buffer: 20 mM HEPES-NaOH pH 7.4, 2% (v/v) Glycerol, 20 mM Imidazole

### 3 Materials and Methods

- Ni-NTA Elution buffer: 20 mM HEPES-NaOH pH 7.4, 2% (v/v) Glycerol, 500 mM Imidazole
- StrepTrap Elution buffer: 20 mM HEPES-NaOH pH 7.4 2% (v/v) Glycerol, 2.5 mM Desthiobiotin
- StrepTrap Binding/Dialysis/SEC buffer: 20 mM HEPES-NaOH pH 7.4, 2% (v/v) Glycerol

Cell pellets stored on  $-80^{\circ}\text{C}$  were thawed and resuspended in 35 ml Lysis buffer per L culture. Cells were broken either by sonication (3 x 5 minutes, 3 cycles, 60% power) or on a french press and the lysate subsequently cleared by centrifugation (SS34 rotor) at  $4^{\circ}\text{C}$ , 38'000 g for 25 minutes.

**Ni-NTA Affinity Purification** The protein was expressed with an N-terminal 6xHis-tag, imidazole was added to the supernatant to a final concentration of 20 mM and the supernatant subsequently loaded on a HisTrap Crude FF 5 ml or HisTrap FF 5ml column equilibrated with Ni-NTA Binding buffer. After a 5 CV washing step with the Ni-NTA Binding buffer, red coloured Cld was eluted with a linear imidazole gradient over 10 CV to 500 mM imidazole. The fractions were collected, analyzed by SDS-PAGE and pooled together.

**Strep-Tactin Affinity** The protein was expressed with an N-terminal Strep-Tag II, the clear supernatant was loaded on a clean StrepTrap HP column previously equilibrated with StrepTrap Binding buffer and subsequently eluted with a step gradient of 2.5 mM Desthiobiotin in the StrepTrap Elution buffer. After analysis by SDS-PAGE, the fractions containing Cld were pooled together.

Tags of the affinity-purified proteins were afterwards cleaved with TEV protease. The pooled fractions were transferred to a dialysis bag with a molecular weight cutoff of 12'000-14'000 Da, TEV protease added at a 1:30 - 1:50 mass ratio and dialyzed overnight at  $4^{\circ}\text{C}$  against 1-2 l of dialysis buffer. Uncleaved protein was then removed by another Ni-NTA or Strep-Tactin affinity purification step, respectively. Cleavage of the tag was again verified by SDS-PAGE. In order to get the protein fully loaded with heme, hemin (freshly prepared in 0.1 N NaOH, see Table 3) was added to the protein solution at a molar ratio of 2:1 hemin:protein, incubated for 1-3 hour(s) on ice. Insoluble heme was then removed by centrifugation for 30 minutes at 18000 rpm at  $4^{\circ}\text{C}$ .



The protein solutions were concentrated in an Amicon Ultra centrifugal filter unit (Milipore) with a molecular weight cutoff of 30'000 to a volume of maximum 5 ml, (which also removes most of the remaining TEV protease in case of the Strep-Tactin based purification) and loaded on an equilibrated Superdex 200 16/60 size exclusion column.

Pure NdCld was further concentrated in an Amicon Ultra centrifugal filter unit to 5-10  $\frac{mg}{ml}$ , divided to 100  $\mu$ l aliquots, flash-frozen in LN<sub>2</sub> and stored at -80°C.

#### 3.6.2 Purification of Apo-NdCld

##### Buffers

- Lysis buffer: 50 mM HEPES-NaOH pH 7.4, 5% (v/v) Glycerol, 0.5% (v/v) Triton X-100, 20 mM Imidazole
- Ni-NTA Binding buffer: 20 mM HEPES-NaOH pH 7.4, 2% (v/v) Glycerol, 20 mM Imidazole
- Ni-NTA Elution buffer: 20 mM HEPES-NaOH pH 7.4, 2% (v/v) Glycerol, 500 mM Imidazole
- AEX Buffer 1: 20 mM HEPES-NaOH pH 7.4, 2% (v/v) Glycerol
- AEX Buffer 2: 20 mM HEPES-NaOH pH 7.4, 2% (v/v) Glycerol, 2 M NaCl
- Dialysis/SEC buffer: 20 mM HEPES-NaOH pH 7.4, 2% (v/v) Glycerol

Frozen cell pellets were thawed and resuspended in 35 ml Lysis buffer per 1 L cell culture. The cells were broken with a french press and the lysate subsequently cleared by centrifugation at 38'000 g for 25 minutes at 4°C. The supernatant was subjected to Ni-NTA affinity chromatography using a HisTrap Crude FF 5 ml or HisTrap FF 5 ml column with a washing step of 5 CV with the Ni-NTA Binding buffer and elution with a 10 CV linear gradient of the Ni-NTA Elution buffer to a imidazole concentration of 500 mM. The purification was inspected on a gel and the fractions containing Cld were pooled together.

In order to cleave the His-Tag, TEV protease was added at a mass ratio of 1:40 (TEV:protein) to the protein solution and dialyzed overnight at 4 °C in a 12'000-14'000 Da dialysis bag against 1-2 l of dialysis buffer. The protein solution was then subjected to another Ni-NTA purification step to remove uncleaved protein and TEV protease.

Apo-NdCld and fully or partially loaded NdCld were subsequently separated from each other by AEX chromatography. Previous experiments had shown that NdCld

### 3 Materials and Methods

elutes from an AEX column in two peaks containing different  $A_{Soret}:A_{280}$  ratios. The cleaved NdCld was loaded on a 6ml ResourceQ anion exchange column equilibrated with AEX Buffer 1 (containing no NaCl). Afterwards, a subsequent washing step with 5% AEX Buffer 2 (=100 mM NaCl) was applied to remove fully and partially heme-loaded NdCld at a conductivity of usually  $\approx 11.5 \frac{mS}{cm}$ . A slow linear salt gradient ascending over 15 CV to 20% Buffer 2 (=400 mM NaCl) was then applied to elute apo-NdCld, usually at  $\approx 16 \frac{mS}{cm}$ .

The fractions containing apo-NdCld ( $\frac{A_{Soret}}{A_{280}} \approx \frac{1}{10}$ ) were concentrated to a volume of maximum 10 ml in an Amicon cell with 30'000 Da cutoff and loaded on a equilibrated Superdex 200 26/60 column via an appropriately sized loop. apo-Cld was then eluted with 1.5 CV SEC buffer.

Pure apo-Cld was concentrated to 5-10  $\frac{mg}{ml}$ , flash-frozen in LN<sub>2</sub> and stored at -80°C.

#### 3.6.3 NdCld with Co-Protoporphyrine IX

Protoporphyrine IX containing cobalt instead of iron as a center atom was used to exchange the metal of NdCld by reconstituting apo-NdCld.

A solution of apo-NdCld (see 3.6.2) was incubated with a 2× molar excess of cobalt protoporphyrine IX overnight at 4°. Precipitated Co-protoporphyrine IX was subsequently removed by centrifugation at 18000 rpm for 30 minutes at 4° in a coolable microcentrifuge (Eppendorf) and the supernatant concentrated in a Amicon Ultra centrifugal filter unit (10'000 Da) to a volume of 250 µl.

The supernatant was loaded on a Superdex 200 10/300 GL analytical size exclusion column previously equilibrated with 20 mM HEPES pH 7.4, 2% Glycerol and the pink-coloured main peak retrieved, pooled, concentrated to 3  $\frac{mg}{ml}$  and frozen in LN<sub>2</sub>. The enzyme's Soret peak shifts with bound Co-protoporphyrine IX to  $\lambda_{max}=425$  nm compared to  $\lambda_{max}=413$  nm in wild-type NdCld with heme b bound. Incorporation of the cobalt protoporphyrine IX was also confirmed by measuring X-ray fluorescence on a non-diffracting crystal (data not shown).

#### 3.6.4 Purification of NwCld

##### Buffers

- Lysis buffer: 50 mM Tris-HCl pH 8.5, 150 mM NaCl, 5% (v/v) Glycerol, 0.5 % (v/v) Triton X-100, 20 mM Imidazole

- Ni-NTA Binding buffer: 50 mM Tris-HCl pH 8.5, 150 mM NaCl, 2% Glycerol, 20 mM Imidazole
- Ni-NTA Elution buffer: 50 mM Tris-HCl pH 8.5 150 mM NaCl 2% Glycerol, 500 mM Imidazole
- Dialysis / SEC buffer: 50 mM Tris-HCl pH 8.5, 150 mM NaCl, 2% Glycerol

Frozen cell pellets were thawed and resuspended in 35 ml Lysis buffer per L cell culture. Cells were broken on a french press and the lysate cleared by centrifugation at 38'000 g for 25 minutes. The cleared lysate was loaded onto an equilibrated HisTrap Crude FF 5 ml Ni-NTA column (GE Healthcare). NwCld was eluted with a linear gradient with the Ni-NTA Elution buffer, the fractions collected and inspected with SDS-PAGE. The fractions containing NwCld were pooled and dialyzed overnight at 4 ° against the dialysis buffer in a dialysis bag with a 12'000-14'000 Da molecular mass cutoff. The dialyzed protein solution was concentrated in an Amicon Ultra centrifugal filter unit to a volume of 5 ml and subsequently loaded onto an equilibrated Superdex 75 16/60 column (GE Healthcare) via a 5ml loop and eluted with 1.5 CV in a single peak. Fractions were analyzed on a gel, pooled and concentrated to  $3 \frac{mg}{ml}$ . Aliquots of 100  $\mu$ l volume were made, flash-frozen in LN<sub>2</sub> and stored at -80°C.

### 3.7 Analytical Size Exclusion Chromatography

Pure NwCld was used for analytical size-exclusion chromatography to assay the dimer stability with increasing ionic strength.

A frozen sample of NwCld ( $3 \frac{mg}{ml}$ ) was thawed (see 3.6.4), diluted 1:10 with either Buffer 1 (0.1 M NaCl), Buffer 2 (0.25 M NaCl), Buffer 3 (1 M NaCl) or Buffer 4 (2 M NaCl). The samples were incubated on ice for at least 3 hours. In the meantime, a Superdex 75 10/300 GL analytical size exclusion column (GE Healthcare) was equilibrated with 2 CV of the corresponding buffer. 250  $\mu$ l of sample were loaded onto the column with an adequate sample loop (250  $\mu$ l) and eluted for 1.5 CV. The experiments were carried out on an ÄKTA PURIFIER system (GE Healthcare) at 4 °C.

- Buffer 1: 50 mM Tris-HCl pH 8.5, 0.15 M NaCl, 2% Glycerol
- Buffer 2: 50 mM Tris-HCl pH 8.5, 0.25 M NaCl, 2% Glycerol
- Buffer 3: 50 mM Tris-HCl pH 8.5, 1 M NaCl, 2% Glycerol
- Buffer 4: 50 mM Tris-HCl pH 8.5, 2 M NaCl, 2% Glycerol

### 3 Materials and Methods

The column was then calibrated with different molecular mass standards: RNase A (13.7 kDa), Carbonic Anhydrase (29 kDa) and Conalbumin (75 kDa) using the different NaCl concentrations. A solution containing the three reference proteins in concentrations of 3-5  $\frac{mg}{ml}$  was prepared and as described above, diluted with the corresponding buffer and incubated for 30 minutes on ice before being loaded on the column.

$$K_{av} = \frac{V_e - V_o}{V_c - V_o} \quad (2)$$

$K_{av}$  was calculated for every molecular mass standard using equation 2.  $K_{av}$  values were plotted against the logarithm of the standard's respective molecular mass and fitted to a linear equation  $y = ax + c$ . The molecular mass of the protein of interest was then determined by calculating  $K_{av}$  and solving the linear equation.

## 3.8 Crystallographic Techniques

**Robotics and Materials** For the setup and monitoring of crystallization trials, following robotics were employed: i) an Alchemist II liquid handling robot (Rigaku) for pipetting of non-commercial optimization screens and 24-well Linbro format hanging drop plates, ii) a Phoenix liquid handling system (Art Robbins Instruments) for setting up 96-well crystallization trials, iii) a Minstrel DT imaging system (Rigaku) equipped with the Atlantis software for automatic imaging. Images were inspected using the CrystalTrak software (Rigaku).

For commercial screens and optimizations in 96-well format pipetted by the Phoenix liquid handling system, 3-well IntelliPlates (Art Robbins instruments) were used. 24-well optimizations, which were set up by hand, were performed in 24-well Linbro format plates, pregreased (Crystalgen).

Crystals were stored in a crystallization room at either 22 °C or 4 °C.

### 3.8.1 Crystallization of NdCld Mutants and Apo-NdCld

NdCld mutants W145V, W146Y and W146YR173Q, concentrated and stored in their respective SEC buffer, were crystallized in conditions with high ammonium sulfate and low pH ranges from 3.5 - 4.5 (derived from condition 13 of JCSG+ commercial screen, Qiagen), which is similar to the crystallization conditions of the wild-type [29]. For cryo protection, the crystal was soaked stepwise in the mother liquor plus increasing concentrations (10%) of ethylene glykol, up to final 50% (v/v). If directly

put into the final cryoprotecting solution, the crystals crack and dissolve. These three mutants were purified using Ni-NTA affinity (see Section 3.6.1). The cryoprotectants were freshly prepared, with the final solutions containing exactly the mother liquor and the final concentration of cryoprotecting agent. The R173E mutant was crystallized in 0.1 M sodium acetate, pH 4 and 40% (v/v) ethylene glykol (Condition 2 from the CryoI+II screen, Emerald Biosciences), which already served as cryoprotectant. The protein was purified using Strep-Tactin affinity.

Apo-NdCld crystallizes in half of the conditions of the PACT I+II screen (Qiagen), for the best condition see Table 11.

**Table 11:** Crystallization conditions of the different NdCld mutants. Drop ratio specifies the ratio of protein:precipitant solution in absolute volumes in  $\mu\text{l}$ .

Mutant	Condition	Drop [ $\mu\text{l}$ ]	Cryoprotectant
W145V	10 $\frac{\text{mg}}{\text{ml}}$ protein, 0.1 M citric acid pH 4.0, 1 M $(\text{NH}_4)_2\text{SO}_4$ , 22°C	2:1, hanging	50% (v/v) ethylene glycol
W146Y	10-11 $\frac{\text{mg}}{\text{ml}}$ protein, 0.1 M citric acid pH 4.0, 0.8 M $(\text{NH}_4)_2\text{SO}_4$ , 22°C	2:1, hanging	50% (v/v) ethylene glycol
W146Y R173Q	10 $\frac{\text{mg}}{\text{ml}}$ protein, 0.1 M citric acid pH 3.5, 0.8 M $(\text{NH}_4)_2\text{SO}_4$ , 22°C	1:1, hanging	50% (v/v) ethylene glycol
R173E	0.1 M NaAc pH 4.5, 40% (v/v) ethylene glycol, 4°C	0.3:0.1, sitting	None
Apo	10 $\frac{\text{mg}}{\text{ml}}$ protein, 0.1 M bis-tris propane pH 6.5, 20% (w/v) PEG 3350, 0.2 M NaAc, 22°C	0.3:0.1, sitting	35% (w/v) PEG 3350

## 3.9 Structure Determination and Refinement Techniques

### 3.9.1 Data Collection and Processing

Diffraction data were collected either in-house on a Bruker Microstar (Bruker AXS Inc.) rotating anode at 1.54 Å wavelength or at several ESRF beamlines (ID14.4, ID23, ID29, BM14U). Details are presented in Tables 12, 13, 16. Integration and scaling was

### 3 Materials and Methods

done with XDS and XSCALE [27], except for the data collected in-house, which was processed with the software Proteum2 (Bruker AXS Inc.).

Valid for all following tables and data collection statistics, unless stated otherwise:

$$R_{meas} = \frac{\sum_{hkl} \left[ \frac{N}{N-1} \right]^{\frac{1}{2}} \sum_i |I_i(hkl) - \langle I(hkl) \rangle|}{\sum_{hkl} \sum_i I_i(hkl)} \quad (3)$$

$$R_{merge} = \frac{\sum_{hkl} \sum_i |I_{hkl} - \langle I(hkl) \rangle|}{\sum_{hkl} \sum_i I_i(hkl)} \quad (4)$$

Where in equations 3 and 4  $I_i(hkl)$  and  $\langle I(hkl) \rangle$  are the  $i^{th}$  and the mean measurements of the intensity of reflection  $hkl$  and  $N$  is the redundancy.

#### 3.9.2 Molecular Replacement, Model Building and Refinement

All structures were solved by molecular replacement using the program MOLREP [50] with chain A from the wild-type NdCld structure (3NN1, [29]). Subsequent refinement was performed with phenix.refine from the PHENIX suite [1] and coot [14]. The overall structure quality was judged with the web server Molprobity [11]. NCS, secondary structure and ramachandran restraints were utilized during refinement, as well as a stepwise adjustment of X-ray/geometry (wxc\_scale) and X-ray/ADP (wxu\_scale) weight scale factors.

Valid for all following refinement statistics:

$$R_{work} = \frac{\sum |F_o - F_c|}{\sum F_o} \quad (5)$$

$R_{free}$  is the cross-validation  $R_{factor}$  computed for the test set of reflections (5%) which are omitted in the refinement process.

Visualizations of molecular models were generated in PyMOL (<http://www.pymol.org>).

## 3.10 Enzymatic Activity Techniques

### 3.10.1 Steady-state Kinetics

The activity of NdCld mutants was determined by quantifying the release of oxygen when the enzyme is processing its substrate,  $\text{ClO}_2^-$ . This was measured with a Clark-type electrode (Oxygraph System, Hansatech Instruments, Norfolk, UK) in a stirred

water bath at a constant temperature of 30°C. Measurements were done in 100 mM phosphate buffer, pH 7.0. The electrode was equilibrated to 100% O<sub>2</sub> saturation by bubbling O<sub>2</sub> to a blank reaction mixture for 10 minutes and with 0% O<sub>2</sub> by bubbling with N<sub>2</sub> for another 10 minutes, thus purging all oxygen.

For activity measurements the substrate was added to the cell in increasing concentrations of 25-1000 μM ClO<sub>2</sub><sup>-</sup>. The buffer-substrate solution (total volume of 1.95 ml) was purged from all oxygen by bubbling the solution with N<sub>2</sub> until a stable baseline was reached. Subsequently the reaction was initiated by injecting 50 μl of a 2 μM NdCl<sub>3</sub> solution into the cell with a hamilton syringe to a final concentration of 100 nM.

Only the initial linear rate was used to calculate the reaction rate. Molecular oxygen production rates (μM O<sub>2</sub>s<sup>-1</sup>) were determined and plotted against chlorite concentrations in SigmaPlot (Systat Software Inc., v12). The Michaelis-Menten equation was utilized for fitting and calculating the values of the kinetic constants of the enzyme: K<sub>M</sub>, the Michaelis constant -  $K_M = \frac{V_{max}}{2}$  (μM); k<sub>cat</sub>, the turnover number (s<sup>-1</sup>) and  $\frac{k_{cat}}{K_M}$ , the catalytic efficiency of the enzyme.

### 3.11 Biophysical characterizations

#### 3.11.1 Static Light Scattering

The biophysical technique of static light scattering can be used experimentally determine the molecular mass (M<sub>w</sub>), radius of gyration of the molecule, and second virial coefficient (A<sub>2</sub>) [35]. Here it was used to assay the molecular mass of different chlorite dismutases in solution, thus yielding information about their oligomeric state.

A miniDawn Treos (Wyatt) light scattering detection system connected to an RI-101 refractometer (MD Scientific) and an Agilent 1260 Infinity HPLC with a Superdex 200 10/300 GL analytical size exclusion column (GE Healthcare) was equilibrated overnight with the respective protein SEC buffer, unless stated otherwise, until a stable baseline was reached. The protein solution was either dialyzed overnight against this buffer or the protein buffer exchanged against this buffer on a spin column (Bio-Rad) immediately before the experiment. 100 μl of a 1  $\frac{mg}{ml}$  protein solution were loaded to the system described above with the autosampler. The protein peak was identified with A<sub>280</sub> and correlated to the molecular mass determined by static light scattering at the given retention volume.

### *3 Materials and Methods*



## 4 Results

### 4.1 Structural Studies of NdCld Mutants

The NdCld mutants W145V (pJK54), W146Y (pJK53), W146Y R173Q (pKG3) and R173E (pKG5s) were crystallized (see Figure 11, 12 and 13) and their three-dimensional structure determined by X-ray diffraction. The proteins were expressed and purified using the methods described in 3.5.1 and 3.6.1. Crystallization procedures and conditions are described in 3.9. Interestingly, the achieved resolution did never exceed 2.8 Å, despite testing different crystal types. Similarly, the structure of two other mutant versions of NdCld (R173A and R173K) was determined to the resolution of 2.8 Å, while the wild-type NdCld structure was solved at a resolution of 1.8 Å. Therefore, it can be assumed that the introduced active site point mutations give a number of residues in the active site additional flexibility, leading to less ordered crystals and consequently to diffraction to lower resolution.

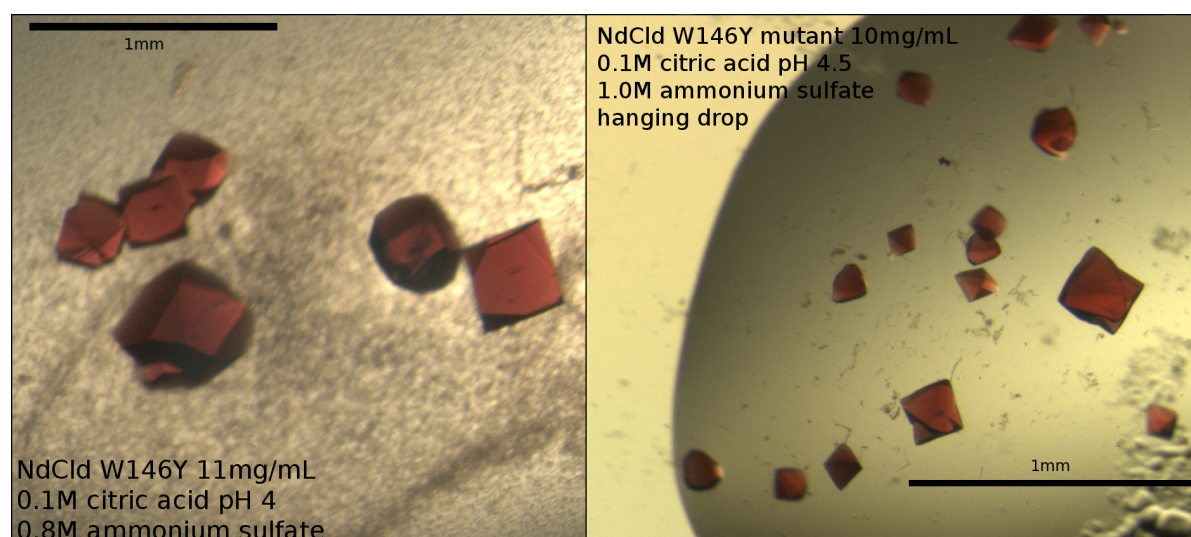


**Figure 11:** Crystals of NdCld mutant W146Y. The scalebar indicates a size of 1 mm.

While the proteins purified by Ni-NTA affinity (mutants W145V, W146Y, W146Y R173Q) crystallized in conditions similar to the wild-type, the R173E mutant instead crystallized in the very different condition 2 of the CryoI+II screen (0.1 M sodium acetate pH 4.5, 40% (v/v) ethylene glycol, 4°C). Most likely the different protein purification approaches without an inhibitor affect the crystallization behaviour of NdCld. Nevertheless, crystallization of R173E was successful at a pH of 4.5, the low pH being a common factor for all crystallization conditions.

## 4 Results

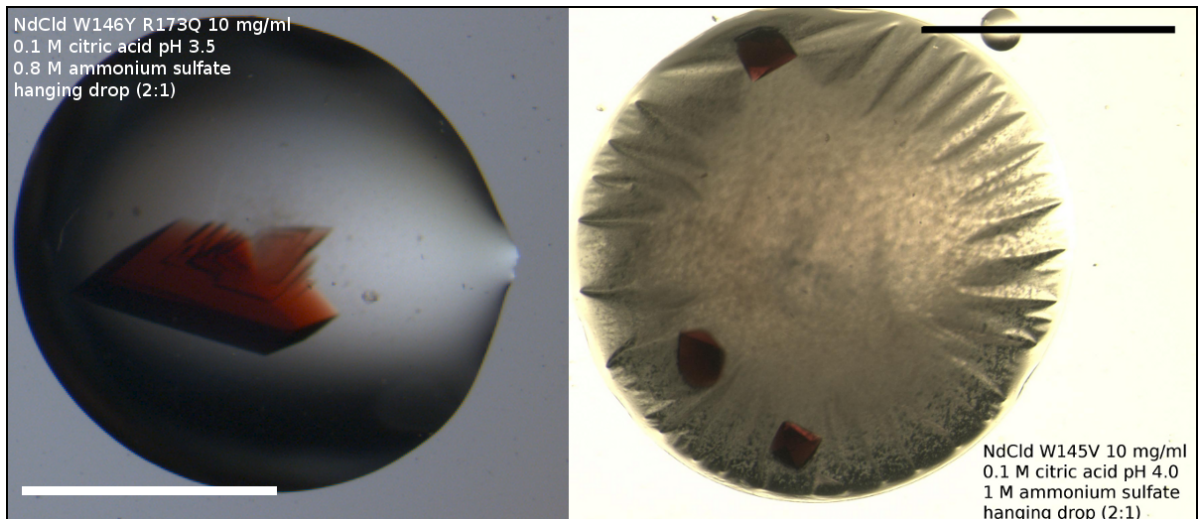


**Figure 12:** Crystals of NdCld mutants W146Y R173Q (left) and W145V (right). The scalebars indicate a size of 1 mm.

Data collection and refinement statistics are displayed in Tables 12 and 13. Interestingly, while wild-type and mutants where R173 is not changed to another amino acid, always crystallize in the primitive hexagonal spacegroup  $P3_221$ . As soon as the residue Arg 173 is mutated, or the heme is missing (see section 21), the crystal packing changes and with it the spacegroup to the base-centered orthorhombic spacegroup  $C2$ . This was already noticed by Kostan et al. [29] and further confirmed here. Despite the mutant structures being highly similar to the wild-type (the maximum r.m.s.d. is  $0.8 \text{ \AA}$ , for details see the respective section), the change of one single residue is sufficient to change crystal packing completely.

**Table 12:** Data collection and refinement statistics for NdCld mutants W145V and W146Y.

Mutant	W145V	W146Y
Source	home source	home source
Wavelength (Å)	1.54	1.54
Spacegroup	P3 <sub>2</sub> 21	P3 <sub>2</sub> 21
Unit cell	a=145.83, b=145.83, c=137.22	a=145.89, b=145.89, c=135.38
Temperature (K)	100	100
Molecules a.u.	5	5
Unique reflections	41972(4187)	39319(3837)
Resolution	66.80-2.80(2.90-2.80)	73.93-2.85(2.95-2.85)
Completeness	99.1(99.9)	100.0 (100.0)
Redundancy	35.4(21.74)	38.3(27.60)
I/ $\sigma$ (I)	23.3(2.10)	32.2(4.80)
R <sub>merge</sub>	0.16(0.72)	0.12 (0.47)
R <sub>work</sub>	0.248	0.232
R <sub>free</sub>	0.309	0.282
RMSD, bonds (Å)	0.016	0.013
RMSD, angles (°)	0.682	1.508
Avg. B-factor (Å <sup>2</sup> )	80.7	61.02
Residues modeled	1195	1195
Waters	159	122

## 4 Results

**Table 13:** Data collection and refinement statistics for NdCld mutants R173E and W146Y R173Q

<b>Mutant</b>	<b>R173E</b>	<b>W146Y R173Q</b>
Source	BM14-U	ID23-1
Wavelength (Å)	0.976	0.667
Spacegroup	C <sub>2</sub>	C <sub>2</sub>
Unit cell	a=138.26 b=111.95 c=120.29 $\beta$ =118.6	a=138.22 b=114.93 c=118.90 $\beta$ =118.1
Temperature (K)	100	100
Molecules a.u.	5	5
Unique reflections	37433(2768)	35640(2627)
Resolution	(2.92-2.85)	44.39-2.90(2.98-2.90)
Completeness	99.6(99.1)	98.9(98.6)
Redundancy	4.01(6.07)	3.7(6.03)
I/ $\sigma$ (I)	8.52(1.93)	9.3(2.28)
R <sub>merge</sub>	0.179(0.958)	0.145(0.853)
R <sub>meas</sub>	0.206(1.047)	0.168(0.934)
R <sub>work</sub>	0.217	0.230
R <sub>free</sub>	0.282	0.290
RMSD, bonds (Å)	0.006	0.006
RMSD, angles (°)	0.965	1.051
Avg. B-factor (Å <sup>2</sup> )	72.9	80.7
Residues modeled	1195	1195
Waters	165	15



**Figure 13:** Crystal of NdCld mutant R173E in a nylon loop mounted on ESRF beamline BM14U. The scalebars indicate a size of 0.1 mm.

## 4 Results

### 4.1.1 Structure of the W145V mutant in Complex with Imidazole

The W145V mutant was designed with the rationale to assay the side pathway described in section 1.6 involving the formation of a tryptophanyl radical, proposed to lead ultimately to heme bleaching. Its structure was solved at a resolution of 2.80 Å. Data collection and refinement statistics are listed in Table 12. It is highly similar to the wild-type, with a r.m.s.d. over all subunits of 0.55 Å over 1185 C $\alpha$ -atoms (out of 1190) and an r.m.s.d. of 0.40 Å over 238 out of 238 C $\alpha$ -atoms. Figure 14 displays the active site structure of the mutant (Panel A) and superimposed with the wild-type structure of NdCld (Panel B). Trp 145 is conserved throughout all CFPs (see Table 1). Replacement of the large aromatic tryptophan side chain with a valine yields a cavity, which is filled with a sulfate with variable occupancy in the 5 subunits. The juxtaposed Trp 146, oriented orthogonally to Trp 145 in the wild-type structure tilts, with its  $\chi$ -angle differing by 20° compared to the wild-type structure. The other active site residues retain their conformations with the exception of the proximal H-bonding network triad, which seems to be destabilized because of the missing Trp 145 and the presence of SO $_2^-$ . Lys 141 seems to form H-bonds with a water molecule, as could Glu 210. Either of these interactions is likely to have a destabilizing effect on the proximal triad. Furthermore, the position of the tetrahedral ion (PO $_4^{3-}$  in the wild-type, SO $_4^{2-}$  in W145V, both originating from the respective precipitant solution) moves to the cavity opened by the missing aromatic side chain, possibly also influencing the orientation of Glu 210.

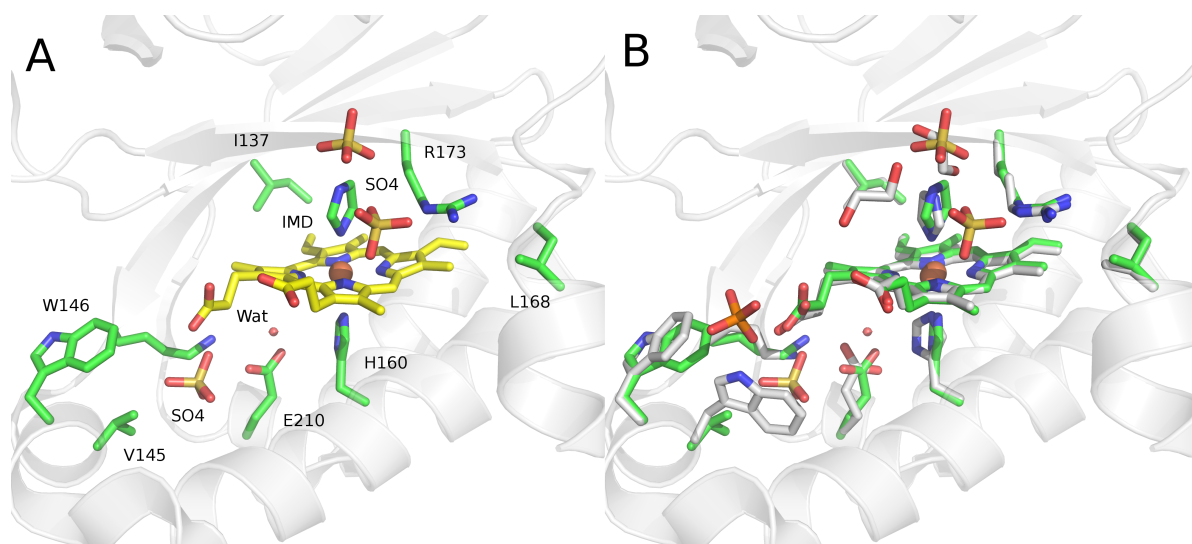


**Figure 14:** Active site structure of NdCld single mutant W145V (Panel A), overlay with active site structure of wild-type NdCld (Panel B).

#### 4.1.2 Structure of the W146Y Mutant in Complex with Imidazole

The second of the juxtaposed orthogonal tryptophans, Trp 146 was changed to a tyrosine residue due to its status as a proposed signature residue (see Table 1). In many Cld-like CFPs, e.g. LmCld, the corresponding residue to Trp 146 is a tyrosine. The active site structure of this mutant and the overlay with the wild-type are depicted in Figure 15. The r.m.s.d. between the mutant pentamer and the wild-type is 0.50 Å over 1183 C $\alpha$ -atoms (out of 1190), single subunits overlay with an r.m.s.d. of 0.30 Å over 238 C $\alpha$ -atoms (out of 238), the mutant structure therefore being only marginally different from the wild-type structure. The active site structure of this mutant in the reveals no further effect on the other signature residues except the obvious replacement of tryptophan with a tyrosine residue. The position of the tetrahedral ion located between residue 146 and the propionate group of the heme is also well-preserved here. Instead of two cryoprotecting ethylene glycol molecules in the vicinity of the heme, another SO $_4^{2-}$  ion is present in the W146Y mutant.

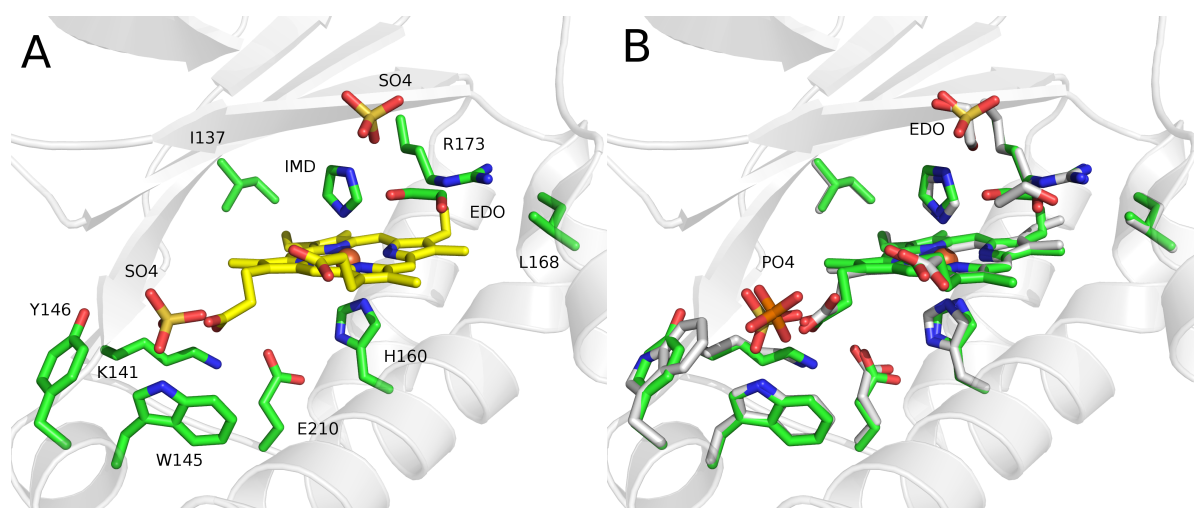


**Figure 15:** Active site structures of NdCld single mutant W146Y (Panel A), overlay with active site structure of wild-type NdCld (Panel B).

#### 4.1.3 Structure of the R173E Mutant in Complex with Acetate

Arg 173 was already shown to be a crucial residue for the mechanism of chlorite degradation [29], the structures of two Arg 173 mutants, R173A and R173K were already solved previously. Figure 16 shows the active site structure of the R173E mutant which was designed to see the effect of a switched charge on the reaction and the structure. Also in this mutant, the overall fold is well-preserved with an r.m.s.d. of 0.40 Å over 1033 c $\alpha$ -atoms (out of 1190) and an r.m.s.d. of 0.41 Å over 234 out of 238

## 4 Results

residues when superposing the single subunits. A distal axial ligand of iron, which is too large for water is found in the electron density. Because the protein was purified and crystallized without the use of imidazole, this ligand is most likely acetate, being present in the crystallization solution. The glutamate side chain is smaller than the arginine, but its charge is similarly oriented away from the active site. Leu 168 shifts towards Glu 173, filling the cavity occupied in the wild-type by the guanidinium group of Arg 173.

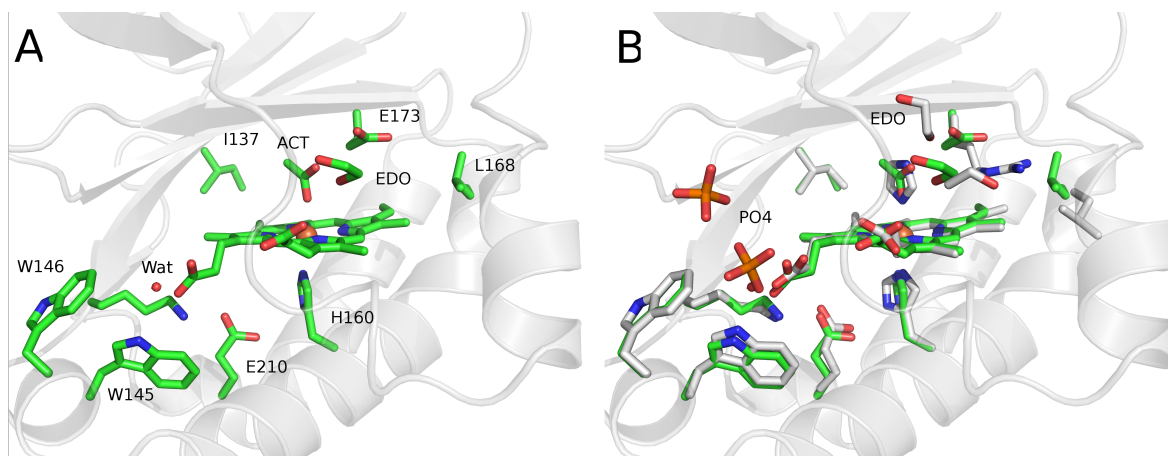


**Figure 16:** Active site structure of NdCld mutant R173E (Panel A) in complex with acetate, Overlay with active site structure of wild-type NdCld (Panel B) in complex with imidazole.

### 4.1.4 Structure of the W146Y R173Q Double Mutant in Complex with Imidazole

The double mutant W146Y R173Q was designed to mimick the active site of Cld-like CFPs, e.g. LmCld. As in the W146Y single mutant, the electron density for a tyrosine side chain is recognizable, but apart from that there are no structural effects on the rest of the active site (Figure 17) Gln 173 is shorter than Arg, but has the same orientation, facing away from the active site. The small cavity formed by the absence of the guanidinium group leads here to a slight change of position of the adjacent Leu 168, pointing now slightly more towards the heme inside the cavity, resembling the R173E mutant (see Figure 16) The structure of a single subunit of the double mutant is also highly similar to the wild-type with an r.m.s.d. of 0.32 Å over 218 C $\alpha$ -atoms (out of 238), the pentamers superpose with an r.m.s.d. of 0.80 Å over 1183 residues (out of 1190).



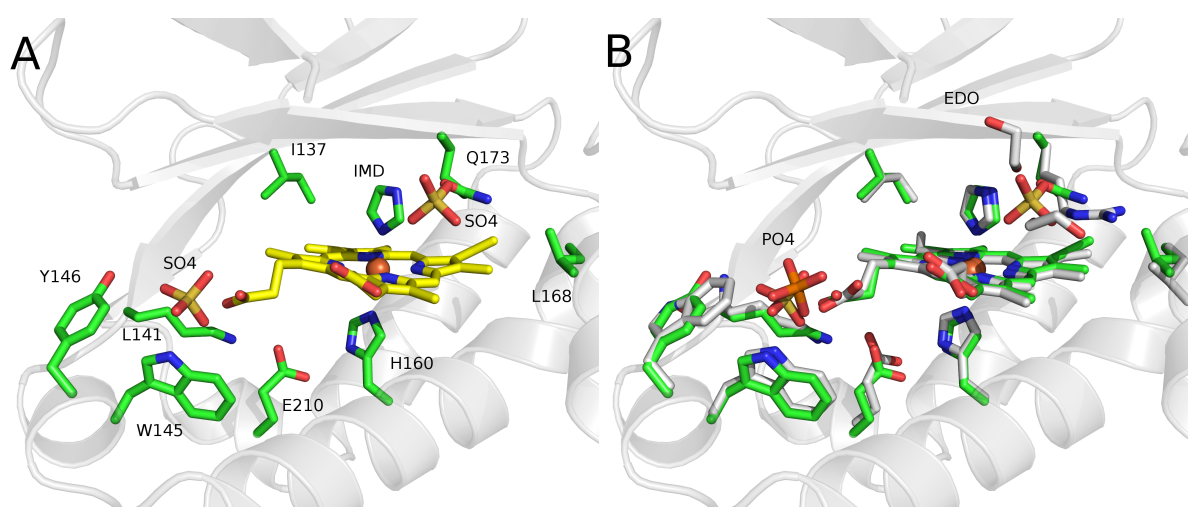


**Figure 17:** Active site structure of NdCld double mutant W146Y R173Q (Panel A) in complex with imidazole. Overlay with active site structure of wild-type NdCld (Panel B), also in complex with imidazole.

## 4.2 Steady-state Kinetics of NdCld, Mutants and Variants

Steady-state kinetics were measured for NdCld wild-type, single and double mutants of described signature residues and of the cobalt protoporphyrin IX - binding variant. As imidazole is a known weak inhibitor of heme binding proteins [29, 39], and we also see imidazole in the active site as distal axial ligand of the iron in crystal structures of NdCld purified by Ni-NTA affinity purification. Additionally, imidazole binding to the heme iron was also observed by UV-VIS spectroscopy, as displayed in Figure 18. Upon addition of imidazole, the soret band of the wild-type NdCld shifts from  $\lambda_{max}=408$  nm to the right, with  $\lambda_{max}=413$  nm. For comparison, binding of the irreversible inhibitor  $CN^-$  shifts the soret band to  $\lambda_{max}=425$  nm. Data in Figure 18 is shown for the wild-type NdCld, each mutant has a different  $\lambda_{max}$ , which are displayed in Table 14.

**Table 14:** UV-VIS spectral characterization of NdCld wild-type and mutants. The proteins were expressed without imidazole. The column on the far right is  $\frac{A_{Soret}}{A_{280}}$ , the *Reinheitszahl* (RZ) of the protein. The low RZ of W145V is surprising, as the crystal structure exhibited a completely occupied molecule.

Protein	Soret [nm]	$\frac{A_{Soret}}{A_{280}}$
wildtype	408	2.1
K141E	410	2.9
W145V	412	1.3
W146Y	413	2.1
R173A	412	0.5
R173K	412	1.2
R173E	411	1.8
R173Q	406	1.4
E210A	412	1.8
W145V W146Y	408	2.5
W146Y R173Q	409	1.8
R173Q E210A	405	0.9

Therefore, Ni-NTA affinity purification, which relies on the displacement of a poly-histidine tag from a  $Ni^+$ -charged resin with high concentrations of imidazole, was avoided for isolation of proteins required for measurements of steady-state kinetics. Instead, the purified proteins utilized for kinetic measurements were expressed as fusion proteins with a cleavable N-terminal Strep-Tag II, which was removed by TEV protease during purification. Strep-Tag based affinity purification relies on elution with desthiobiotin [37], thus allowing purification of NdCld without imidazole.

**Table 15:** Steady-state kinetics for molecular oxygen evolution of NdCld wild-type, mutants and variants. Values for  $K_m$  and  $k_{cat}$  were determined by measuring the initial linear rates of oxygen evolution with a Clark-type electrode from 25  $\mu\text{M}$  to 1 mM substrate concentration and fitting the Michaelis-Menten equation. All mutated residues are located in the enzyme's active site, compare Figure 8. Values from Kostan et al. [29] and van Ginkel et al. [52] are listed for direct comparison with a) the previous work on NdCld and b) a Cld from a PCRB.

Protein	$K_M$ [ $\mu\text{M}$ ]	$K_{cat}$ [ $\text{s}^{-1}$ ]	$\frac{K_{cat}}{K_M}$ [ $\text{M}^{-1} \text{s}^{-1}$ ]	Notes
NdCld (wt)	58 $\pm$ 37	35	6.0 $\times$ 10 <sup>5</sup>	Kostan et al. [29], + imidazole
NdCld (wt)	52 $\pm$ 7	42	8.1 $\times$ 10 <sup>5</sup>	
NdCld K141E	60 $\pm$ 11	1.8	3.0 $\times$ 10 <sup>4</sup>	
NdCld W145V	103 $\pm$ 11	14	1.4 $\times$ 10 <sup>5</sup>	
NdCld W146Y	87 $\pm$ 8	36	4.1 $\times$ 10 <sup>5</sup>	
NdCld R173A	107 $\pm$ 54	7.1	6.6 $\times$ 10 <sup>4</sup>	Kostan et al. [29], + imidazole
NdCld R173A	90 $\pm$ 9	2.8	3.1 $\times$ 10 <sup>4</sup>	
NdCld R173K	818 $\pm$ 250	21	2.5 $\times$ 10 <sup>4</sup>	Kostan et al. [29], + imidazole
NdCld R173K	898 $\pm$ 250	14	1.5 $\times$ 10 <sup>4</sup>	
NdCld R173E	82 $\pm$ 4	3	3.6 $\times$ 10 <sup>4</sup>	
NdCld R173Q	130 $\pm$ 7	2.3	1.8 $\times$ 10 <sup>4</sup>	
NdCld E210A	128 $\pm$ 15	36	4.1 $\times$ 10 <sup>5</sup>	
NdCld W145VW146Y	76 $\pm$ 7	2.9	3.8 $\times$ 10 <sup>4</sup>	
NdCld W146YR173Q	205 $\pm$ 18	4.1	2.0 $\times$ 10 <sup>4</sup>	
NdCld E210AR173Q	184 $\pm$ 36	0.85	4.6 $\times$ 10 <sup>3</sup>	
Cobalt-NdCld	763 $\pm$ 109	11.3	1.4 $\times$ 10 <sup>4</sup>	
<i>Azospira oryzae</i>	170	1200	7.1 $\times$ 10 <sup>6</sup>	van Ginkel et al. [52], Strain GR-1

## 4 Results

Table 15 shows a summary of the kinetics with the measured kinetic parameters, which are  $K_M$ ,  $k_{cat}$  and  $\frac{k_{cat}}{K_M}$ . Comparable to the wild-type and the previously measured mutants of NdCld and the NwCld wild-type [29, 34], the steady-state data could be fitted best with a double rectangular hyperbola equation. Enzyme kinetics were only measured up to a  $\text{ClO}_2^-$  concentration  $< 1\text{mM}$ , which corresponds to natural conditions.

In principle, all mutations, single and double, were detrimental for the activity of NdCld, with  $K_M$  concentrations increasing and  $k_{cat}$  rates decreasing, leading to an overall reduced catalytic efficiency  $\frac{k_{cat}}{K_M}$ . The contributions of  $K_M$  and  $k_{cat}$  to the catalytic efficiency vary, though.

An overview is displayed in Figure 19, which presents an overall evaluation of the respective ability of the mutants to bind and process substrate. In order to analyze the effect of a mutation of an active site residue it is necessary to evaluate  $K_M$  and  $k_{cat}$  separately. Mutants with a higher  $K_M$  than the wild-type are deficient in formation of the Michaelis complex ES, mutants with lower  $k_{cat}$  are deficient in catalyzing the reaction, metabolizing less substrate in the same timespan. Figure 20 displays both values separately, thus enabling evaluation of the contribution of each residue to substrate binding or to the turnover rate, respectively.

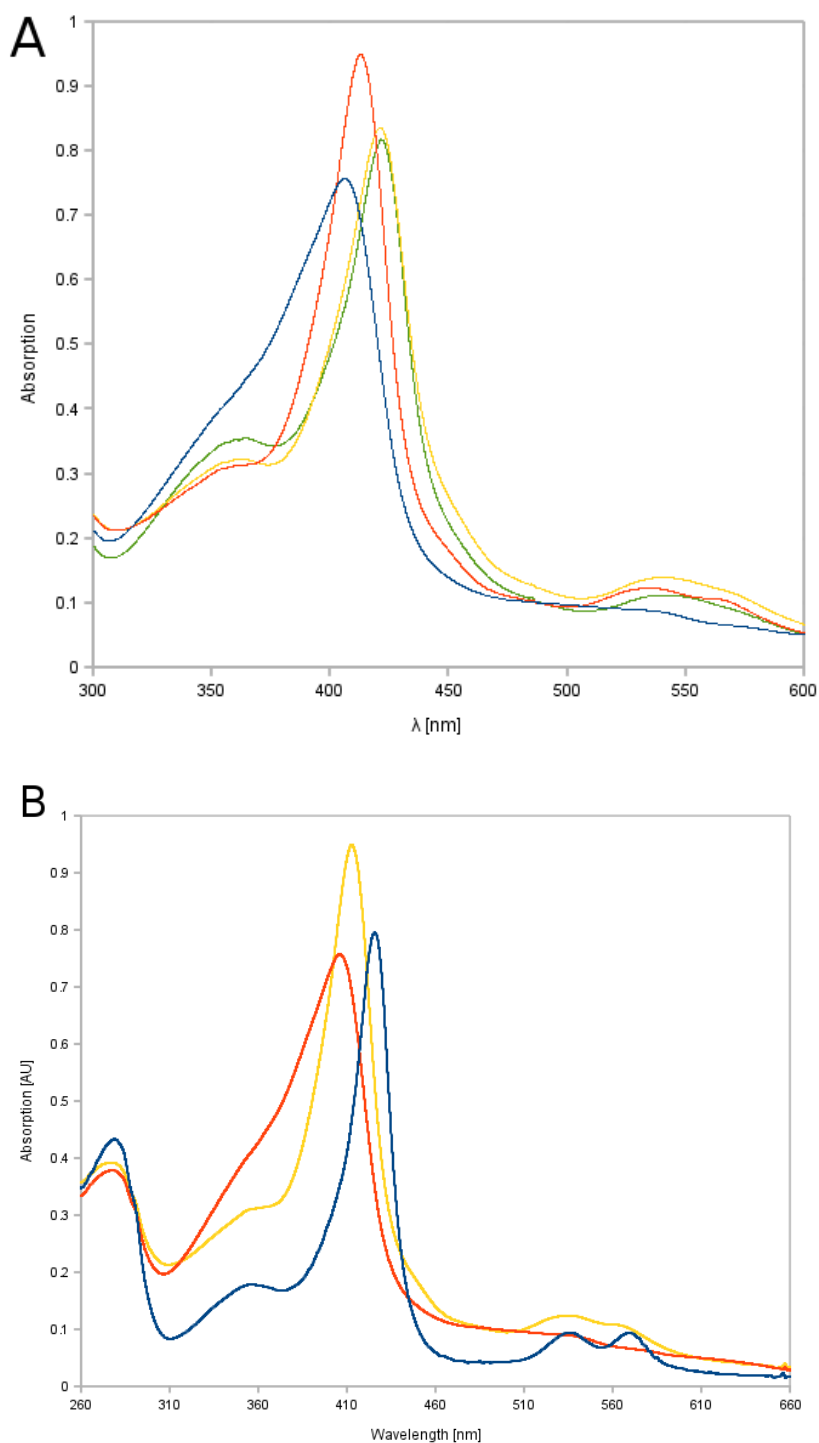


**Figure 18:** Panel A: Comparison of NdCl<sub>3</sub> UV-VIS spectra upon addition of inhibitors. Blue:  $0.3 \frac{\text{mg}}{\text{ml}}$  NdCl<sub>3</sub> without imidazole.  $\lambda_{\text{max}} = 408$  nm. Red: NdCl<sub>3</sub> + 2 mM imidazole.  $\lambda_{\text{max}} = 413$  nm. Yellow: NdCl<sub>3</sub> with 2 mM CN<sup>-</sup> and 2 mM imidazole.  $\lambda_{\text{max}} = 421$  nm. Green: NdCl<sub>3</sub> with 2 mM CN<sup>-</sup>.  $\lambda_{\text{max}} = 421$  nm. Panel B: UV-VIS spectra of NdCl<sub>3</sub> variants. Red:  $0.3 \frac{\text{mg}}{\text{ml}}$  Fe-NdCl<sub>3</sub> without imidazole.  $\lambda_{\text{max}} = 408$  nm. Yellow:  $0.3 \frac{\text{mg}}{\text{ml}}$  NdCl<sub>3</sub> + 2 mM imidazole.  $\lambda_{\text{max}} = 413$  nm. Blue:  $0.3 \frac{\text{mg}}{\text{ml}}$  Cobalt-NdCl<sub>3</sub>.  $\lambda_{\text{max}} = 425$  nm.

## 4 Results

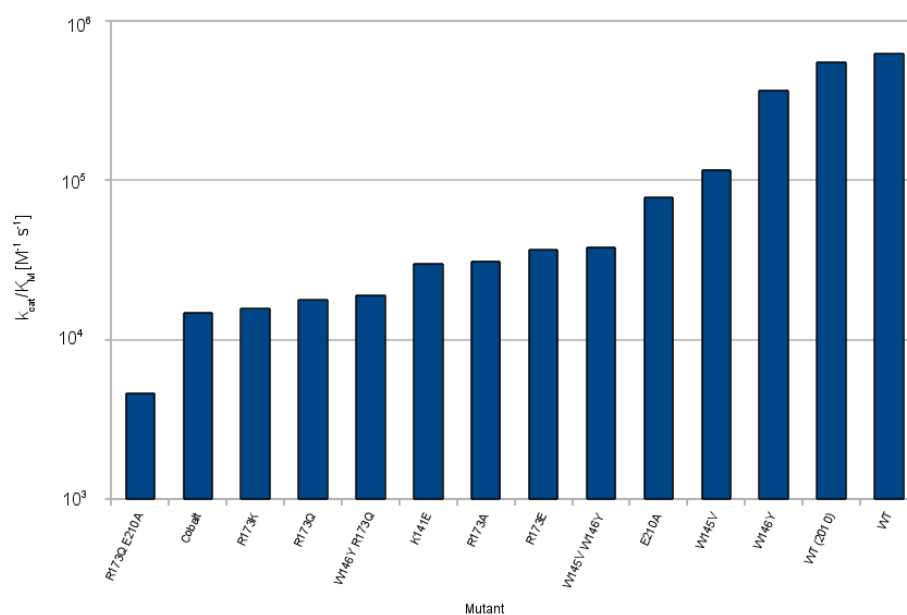


**Figure 19:** The catalytic efficiency  $\frac{k_{cat}}{K_M}$  of NdCld mutants plotted on a logarithmic scale. WT(2010) represents the value published by Kostan et al. [29] for comparison.

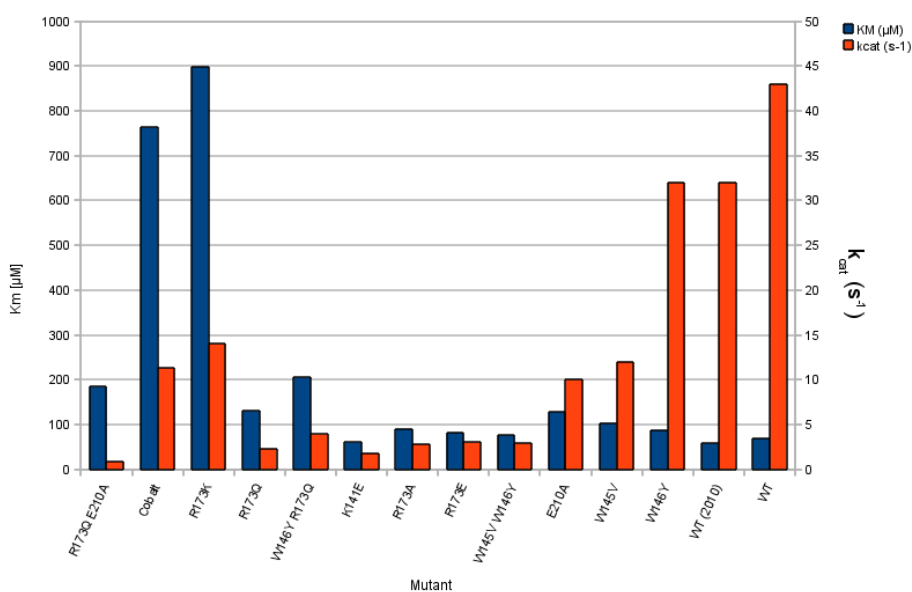


**Figure 20:**  $K_M$  and  $k_{cat}$  values of NdCld mutants compared. WT(2010) represents the value published by Kostan et al. [29] for comparison.

### 4.3 Structure of apo-NdCld

Apo-NdCld was crystallized in 0.2 M sodium acetate, 20% (w/v) PEG 3350, 0.1 M bis-tris propane pH 6.5, which is condition 67 from the PACT I+II commercial screen (Qiagen). Crystals were found in over 50% of the condition of the PACT I+II screen, but this condition yielded large single crystals (Figure 21), which diffracted best. Similarly to the structures of the NdCld mutants, the dataset was collected to 2.9 Å, indicating that increased flexibility of residues binding to heme in the holo-form of the enzyme affects the diffraction ability of the crystals. Unlike the holo-enzyme, which crystallized in the hexagonal primitive spacegroup P3<sub>2</sub>21, apo-NdCld crystallized in the monoclinic base-centered spacegroup C2, similar to all Arg 173 mutants. The data collection and refinement statistics are displayed in Table 16.

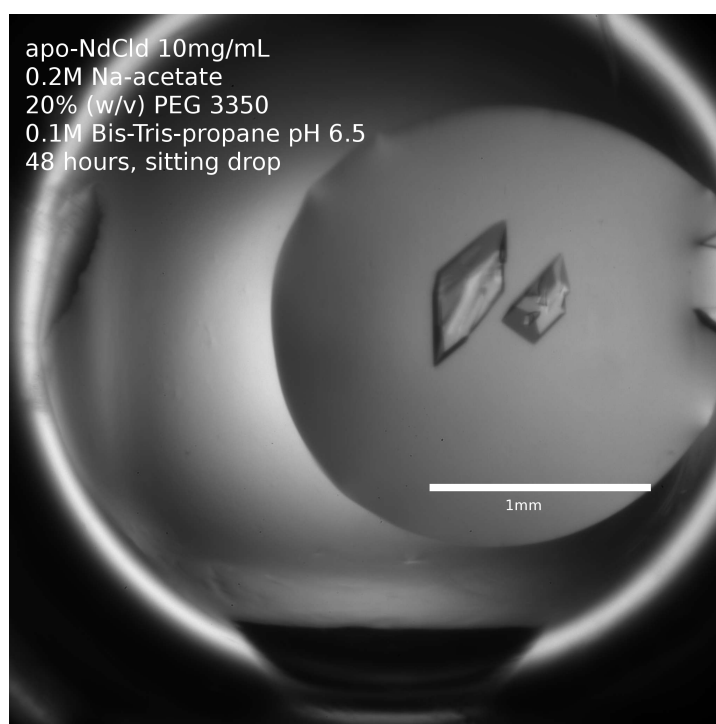


**Figure 21:** Crystals of apo-NdCld after 2 days. The scalebar indicates a size of 1 mm.

Surprisingly, the oligomeric state of apo-NdCld in the crystal was found to be hexameric, not pentameric as seen in the wild-type (Figure 22). The molecular mass of apo-NdCld was determined in solution with static light scattering and was found to be a pentamer, having roughly the same size as the fully loaded active form. Therefore the hexameric structure is a crystallographic artifact, maybe originating from the slight conformational changes that differentiate holo-NdCld and apo-NdCld. Figure 24 shows the SLS data. Analysis of the hexameric X-ray structure by PISA [30] suggests that the hexamer has no specific or too weak interactions which could result in

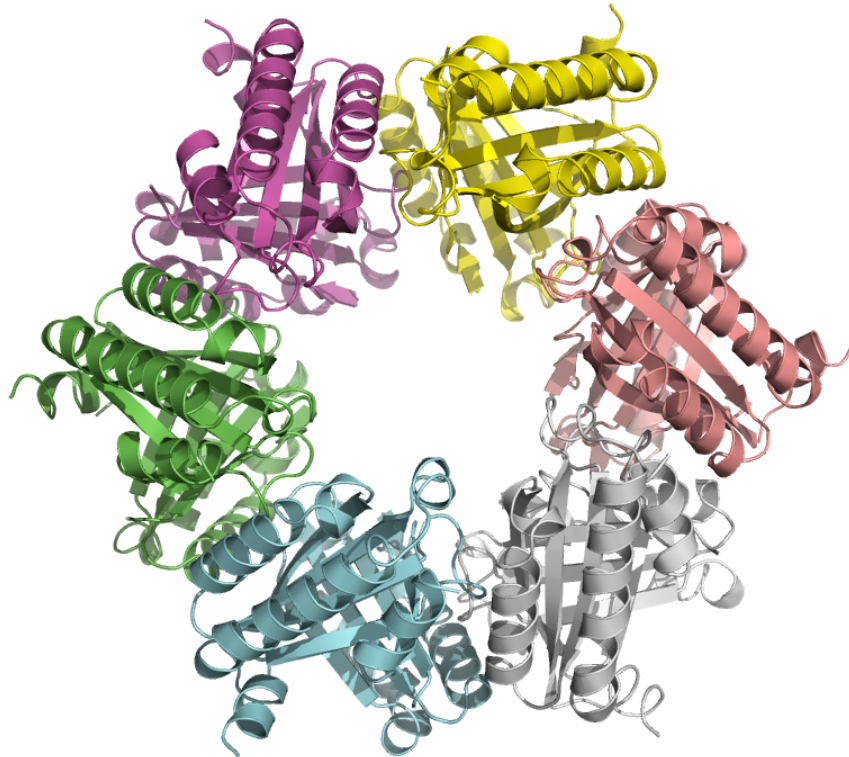


**Figure 22:** Top view of the structure of hexameric apo-NdCld in cartoon representation.

the formation of a stable quarternary structure in solution.

The structures of one subunit of apo-NdCld and holo-NdCld are very similar, with a root mean square deviation of 0.490 Å over 196 C $\alpha$  atoms (out of 216) (see Figure 23). An exception is the region over the heme-binding cavity that is formed by the residues 107 - 130 (comprising  $\alpha$ 6 of the N-terminal and  $\alpha$ 1' of the C-terminal domain), which is disordered in all six monomers in the crystal structure of apo-NdCld and is likely to be flexible in solution as well. Therefore, in apo-NdCld, 216 instead of 238 residues (holo-NdCld) could be modeled (see Figure 23).

After incubation of apo-NdCld with hemin, binding of heme was observed that restored the enzyme to an active state (see 3.6.2), resulting in the stabilization of this region. In the structure of the holo-enzyme and the mutant versions with bound heme, there is visible electron density for the region from residue 107-130. In the structure of the Cld-like homolog from *Listeria monocytogenes*, where no heme density is visible, the structurally similar part of this protein is as well flexible, having no interpretable electron density (Mlynek et al, unpublished data).

As  $\alpha$ 6 and  $\alpha$ 1' are directly interacting with the heme in NdCld, it is likely for this part of the protein to become disordered in the absence of heme. The rest of the C-terminal



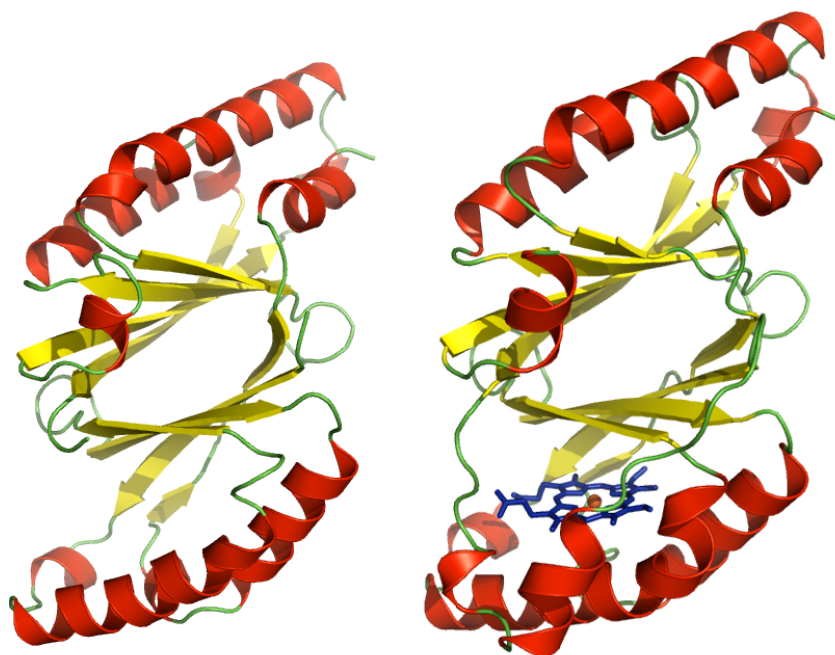


**Figure 23:** Comparison of apo-NdCld (left) and holo-NdCld with coloured secondary structure elements:  $\alpha$ -helices in red,  $\beta$ -strands in yellow and loops in green. The region from residue 107-130 is disordered in apo-NdCld and could not be modeled.

ferredoxin fold is rather well-ordered, with the exception for helix  $\alpha 3'$ , which is also directly involved in heme binding.  $\alpha 3'$  is still visible and tracable in the electron density, but less defined than the rest of the molecule.

Some differences are in side chains of the active site residues; Figure 25 shows an overlay of the important active site residues in stereo view. The role of Leu 168 in heme stabilization and determining the size of the heme cavity, as suggested by Mlynek et al. [34], is emphasized by the side chain becoming flexible, the visible density pointing into the cavity of protein without heme present. The conformation of Ile 138, which is the other residue that restrains the cavity, is not affected whether heme is present or not. When lacking the hydrogen bond to the heme's propionate group, Trp 145 becomes destabilized. In 4 of 6 subunits Trp 145 flips and takes the conformation visible in Figure 25. Density of Arg 173 is not very clear, especially the guanidinium group lacking clear density. Nevertheless it can be seen, that the side chain seems to point in direction of His 160 and not to the side as in the holo-form, indicating possible hydrogen bonding with His 160.

## 4 Results

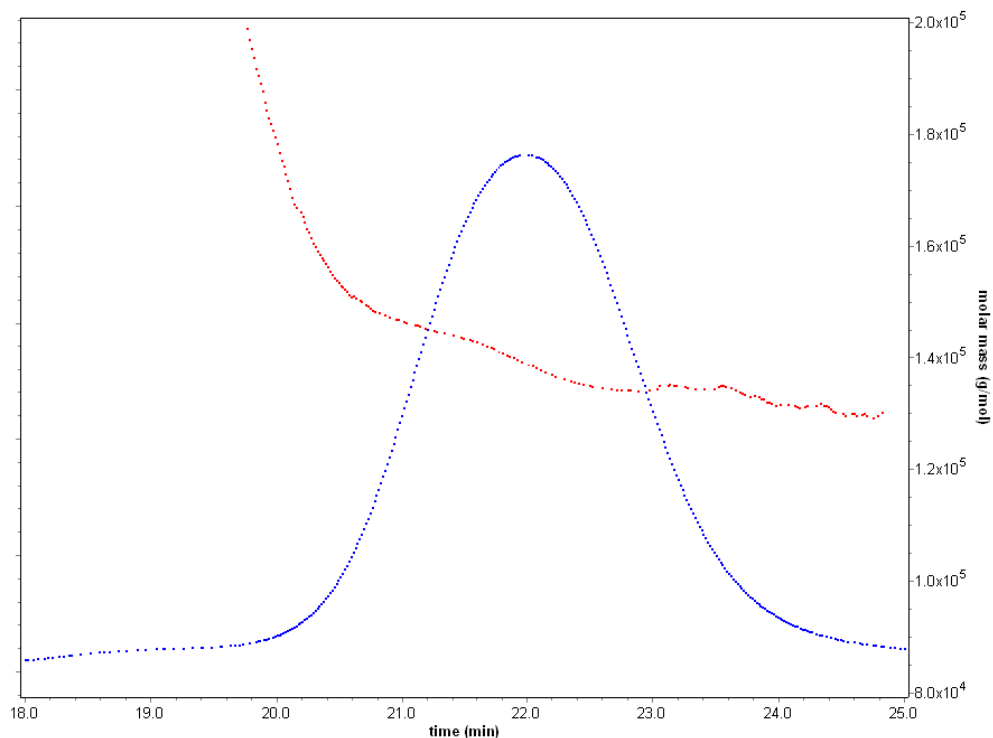


**Figure 24:** SLS experiment with apo-NdCld. The molecular mass at the peak was determined to be 135 kDa, corresponding to 5.0 monomers of apo-NdCld.

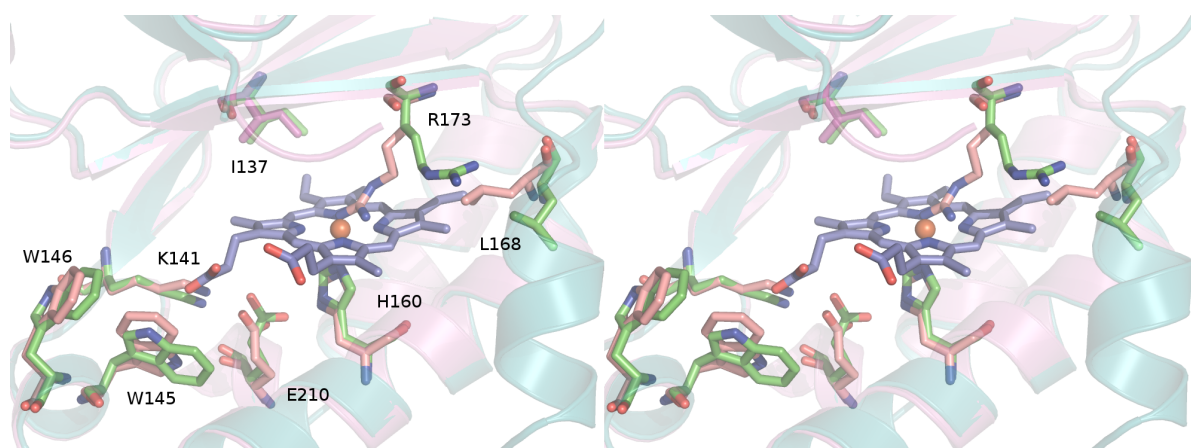


**Figure 25:** Stereo view of the holo-NdCld and the apo-NdCld active site. Differences in side chain positioning are clearly visible. Leu 168 becomes more flexible without bound heme, Arg 173 becomes flexible and seems in some subunits to hydrogen bond to His 160. Lacking the hydrogen bond to the heme's propionate group, Trp 145 is lacks stability and flips in half of the subunits. Residues 107-112 are omitted from the cartoon representation.

**Table 16:** Data collection and refinement statistics of apo-NdCl<sub>4</sub>.  
**apo-NdCl<sub>4</sub> Statistics**

Data collection statistics	
Source	ID14-4 (ESRF)
Wavelength (Å)	0.939
Spacegroup	C <sub>2</sub>
Unit cell (Å, °)	a=115.84 b=118.96 c=114.94 β=109.9
Temperature (K)	100
Molecules a.u.	6
Unique Reflections	63699(10172)
Resolution (Å)	41.18-2.90 (2.98-2.90)
Completeness	99.5 (99.8)
Multiplicity	2.09 (2.1)
I/σ(I)	14.38 (2.56)
R <sub>merge</sub>	0.044 (0.437)
R <sub>meas</sub>	0.060 (0.584)
R <sub>work</sub>	0.187
R <sub>free</sub>	0.256
RMSD, bonds (Å)	0.004
RMSD, angles (°)	0.900
Avg. B-factor (Å <sup>2</sup> )	81.1
Residues modeled	1300
Waters	5

#### 4.4 Stability of the NwCld Dimer

The stability of the NwCld dimer was assayed by analytical size exclusion chromatography as described in 3.7 in function of increasing ionic strength ranging from 0.1 M NaCl to 2 M NaCl. The primary sequence of NwCld is about 30% shorter than the confirmed Clds, with the large  $\alpha$ -helical part of the N-terminal region ( $\alpha 1$ - $\alpha 5$ ,  $\alpha 6'$ ) missing. The C-terminal domain with the heme-binding active site is highly similar to the canonical Clds.

The interface between the two subunits in NwCld was predicted by the PISA server [30] to be mostly of electrostatic and to a less extent of hydrophobic nature [34]. Subjecting the protein to increasing ionic strength was assumed to break these interaction and to yield a monomeric protein population. Figure 26 shows the elution profiles of NwCld under increasing salt conditions, traced by OD<sub>280</sub>, Table 17 shows the corresponding data. Interestingly, the protein seems continues to be stable up to the highest salt concentrations used (2 M NaCl). Furthermore, no protein was eluted at the void volume, an indication of aggregation. Instead, NwCld elutes as a single peak at all salt concentrations. Additionally, a static light scattering experiment was performed as described in Section 3.11.1 in a 20 mM HEPES, 2% glycerol buffer, containing no additional salts contributing to ionic strength. Here, the protein was also shown to be a dimer, having a molecular mass of approx. 45 kDa.

These results were published in Mlynek et al. [34].

**Table 17:** Analytical SEC experiments with increasing ionic strength. The calculated molecular mass of the NwCld protein is shown.

<b>Protein</b>	<b>Mw [kDa]</b>	<b>log MW</b>	<b>Kav</b>	<b>Retention volume [ml]</b>
<b>0.1 M NaCl</b>				
Conalbumin	75	1.88	0.21	11.33
Carbonic Anhydrase	29	1.46	0.38	13.89
RNase A	13.7	1.14	0.49	15.61
NwCld (experimental)	45.58	1.66	0.26	11.98
<b>0.25 M NaCl</b>				
Conalbumin	75	1.88	0.22	11.33
Carbonic Anhydrase	29	1.46	0.39	13.89
RNase A	13.7	1.14	0.50	15.61
NwCld (experimental)	44.80	1.66	0.31	12.21
<b>1 M NaCl</b>				
Conalbumin	75	1.88	0.22	11.46
Carbonic Anhydrase	29	1.46	0.39	14.00
RNase A	13.7	1.14	0.50	15.85
NdCld (experimental)	48.05	1.68	0.31	12.56
<b>2 M NaCl</b>				
Conalbumin	75	1.88	0.22	11.42
Carbonic Anhydrase	29	1.46	0.38	13.97
RNase A	13.7	1.14	0.51	16.02
NwCld (experimental)	47.72	1.68	0.31	12.74

## 4 Results

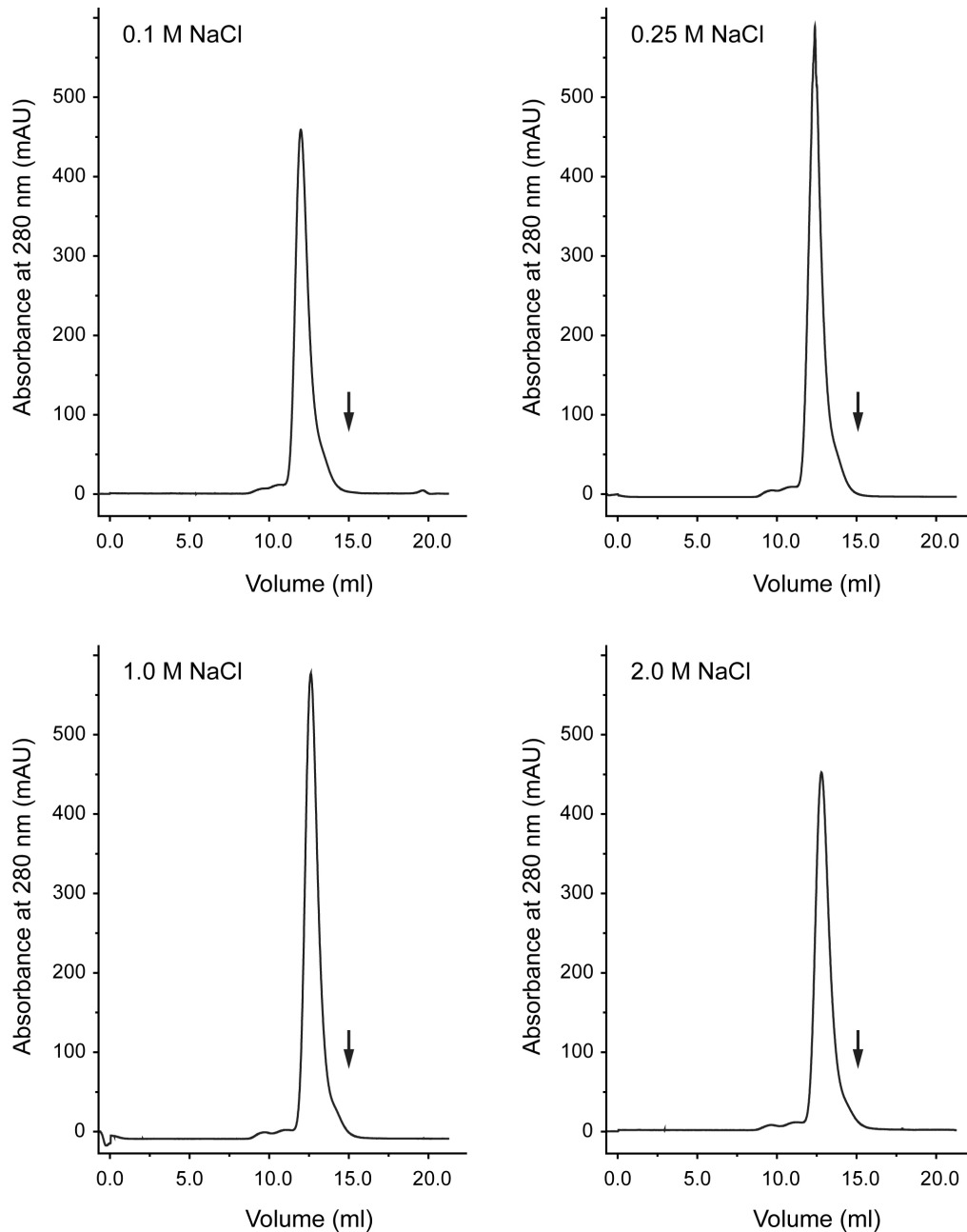


**Figure 26:** Elution profile ( $A_{280}$ ) of NwCld subjected to increasing ionic strength. The arrows indicate the elution of the hypothetical NwCld monomer. 250  $\mu$ l sample were applied via a 250  $\mu$ l sample loop onto a Superdex 75 10/300 GL analytical size exclusion column (GE Healthcare) on an ÄKTA PURIFIER system with a flowrate of 0.8  $\frac{ml}{min}$ . The main and only peak shows always the dimeric NwCld, also there is no peak visible in the void volume, which would indicate denaturation and subsequent aggregation of the protein upon high ionic strengths.

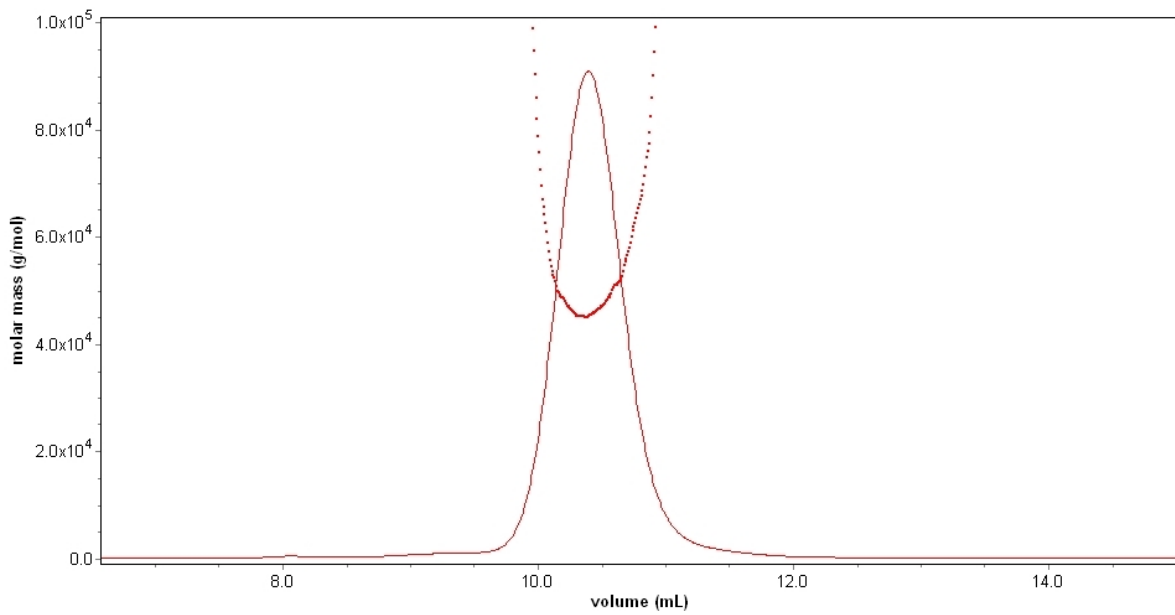


**Figure 27:** SLS experiment with  $1 \frac{mg}{ml}$  pure NwCld in 20 mM HEPES pH 7.4, 2% glycerol. The protein elutes as a single peak and has a molecular mass of approx. 45 kDa, therefore being a dimer also in solution.

## 4 Results



## 5 Discussion

### 5.1 Arginine 173 Mutations have Severe Effects on the Enzymatic Activity

We investigated the structure of one single and one double catalytic arginine mutant of NdCld (R173E, W146Y R173Q) and determined the steady-state kinetics of four arginine single and double mutants (R173Q, R173E, W146Y R173Q and R173Q E210A), extending the study done by Kostan et al. [29] on the R173K and the R173A single mutants, which were characterized functionally and structurally. Our results underline that Arg 173 is a critical residue for the reaction mechanism of chlorite degradation. The catalytic efficiency is in all single arginine mutants reduced by one order of magnitude compared to the wild-type. The value for the double mutant R173Q E210A decreases by two orders of magnitude to a value of  $4.6 \times 10^3 \text{ M}^{-1}\text{s}^{-1}$  and is therefore the mutant with the lowest activity.

Our data confirm that the catalytic arginine in chlorite dismutases is not required for substrate binding to the heme iron, yielding the Michaelis complex, but that the presence of arginine is involved in the various stages of the reaction, especially in positioning and stabilizing the intermediate hypochlorite.

The R173K mutant, described by Kostan et al. [29] is the only arginine mutant until now where substrate binding is severely impaired and therefore the formation of the Michaelis complex is hindered. The structure of this mutant illustrated that the lysine forms a hydrogen bond to a sulfate molecule which is located close to the active site. The lysine is therefore stabilized in this conformation and hinders substrate accessibility to the site of the reaction [29]. Due to its positive charge it is able to understudy for the catalytic arginine in stabilization of the substrate.

The R173E mutant, which was produced and functionally and structurally characterized in this thesis, does hardly interfere with initial formation of the Michaelis complex, exhibiting a  $K_M$  value ( $82 \pm 4 \text{ }\mu\text{M}$ ) closely resembling the wild-type NdCld. It can be suggested that the opposite charge of this mutant therefore does not repulse the substrate, which carries a negative charge as well.

In the structure of the wild-type, the side chain of the catalytic arginine points away from the iron in the direction of the Leu 168 residue (see Figure 8). This orientation is conserved for the different side chains in the other arginine mutant structures, except for R173A and the previously described R173K mutant. A negative charge, as present in the sidechain of the R173E mutant is therefore unlikely to lead to initial substrate repulsion.

## 5 Discussion

The glutamine side chain of the R173Q mutant is also not able to rescue the reaction. It might not be able to stabilize the intermediate  $\text{ClO}^-$  to the extent of lysine due to the missing charge of the amide group and the shorter length of the glutamine compared to arginine or lysine. The carbonyl group of glutamine could additionally disturb stabilization of the intermediate due to sterical hindrance.

All arginine mutants - except for R173K - have significantly reduced turnover rates 15, as much as fifty times lower compared to the wild-type. This supports the model that the positive charge is indispensable for correct positioning and orientation of the reaction intermediate, as suggested by Mlynek et al. [34]. Our data confirm this hypothesis. The mutants with negatively charged side chains are not able to stabilize or even repulse intermediate  $\text{ClO}^-$  during the reaction.

Taken together data underline the importance of the catalytic arginine for the chlorite dismutase reaction [29]; they confirm that the nature of this residue is one of the most important parameters when looking for active chlorite dismutases on a sequence basis. All hitherto validated chlorite dismutases of both Lineage I and II have the arginine in the active site [17, 34]; the R173Q mutant mimicks the "glutamine" cluster in CFPs (see Section 1.3). The reduced activity of this mutant suggests that these proteins are likely to be "bad chlorite degraders" - if at all. They might have a different, yet unknown function, which is likely to be more ancient. The lack of structural informations about the reaction mechanism leaves the exact process, how the catalytic arginine performs its essential task, yet unanswered. Due to the contribution of the catalytic arginine in stabilizing reaction intermediates with its charge, the side chain needs to possess an innate flexibility enabling it during the reaction cycle to adopt a conformation similar to the R173K mutant [29] or to the corresponding residue in AoCld [12].

### 5.2 Investigation of Additional Signature Residues

Several NdCld mutants were designed to address the subject of the signature residues for active chlorite dismutases proposed by Mlynek et al. [34] and Goblirsch et al. [17] besides the already confirmed Arg 173.

The proximal His-Glu-Lys triad, consisting in NdCld of His 160, Glu 210 and Lys 141 was proposed to increase the imidazolic character of the proximal histidine, which coordinates the heme iron (His 160), therefore influencing its redox potential [29]. Based on the structure of wild-type NdCld, Glu 210 forms a hydrogen bond from Lys 141. This positions its carboxyl group of adequately to accept another hydrogen

bond from the N $\delta$  of His 160, which in turn renders Ne of His 160 more able to coordinate Fe<sup>3+</sup>. We produced the mutants K141E and E210A with the goal to disturb this hydrogen bonding network and measured steady-state kinetics of them to see the contribution of these residues to substrate binding and turnover rate. Both mutants had a relatively mild effect on substrate binding, especially the K141E having approximately the same  $K_M$  as the wild-type. Turnover rates were reduced to 25% of the wild-type  $k_{cat}$  in case of E210A and to 5% for K141E. The proposed role of Lys 141 is the stabilization of the H-bonded glutamate side chain in its unusual rotamer conformation in order to facilitate its H-bonding to the proximal histidine. Reversing the charge of Lys 141 is likely to lead to charge repulsion of the adjacent glutamate, which in turn affects the orientation of the juxtaposed proximal histidine more than exchanging Glu 210 to the small, nonpolar alanine.

The structural data (see Figure 14) support the measured steady-state parameters. While the W146Y mutant is structurally unobtrusive, the W145V mutant shows alterations in both the positioning of the neighbouring Trp 146 and the proximal triad. Hence, the W145V mutant shows similar effects to mutants E210A and K141E, possibly through affecting the hydrogen bonding network visible in the structure, stabilizing the His-Glu-Lys triad. Furthermore, the H-bond between Trp 145 and the propionate group of the heme is interrupted in the W145V mutant. Comparison of NdCld wild-type and of this mutant structures shows that Trp 145 stabilizes the orientation of the adjacent Trp 146.

Mutations of the two vicinal tryptophan residues Trp 145 and Trp 146 did not yield information about the formation of a tryptophanyl radical. Measuring steady-state kinetics cannot answer the question whether and how this side path of the chlorite degradation reaction is affected by mutating the two tryptophans and which tryptophan is involved, because heme bleaching and enzyme inactivation is not captured in this experiments. Further studies on this mutants and the double mutant W145V W146Y and the new single mutant W145F will address this question.

It can be concluded that the mechanism of chlorite dismutation depends on many active site residues which are involved in a complex interplay. Our mutational studies suggest immediate effects of Glu 210 and Lys 141, the residues of the proximal triad on the reaction mechanism. While the latter is conserved in all CFPs, Glu 210 is variable in Cld-like CFPs [17, 34].

### 5.3 Mimicking the Active Site of Cld-like Proteins

The double mutants W146Y R173Q and R173Q E210A and the single mutant R173Q of NdCld were designed to mimic Cld-like CFPs, especially LmCld, which exhibits Tyr, Gln and Ala at the corresponding positions in its active site cavity. The structure of heterologously expressed LmCld was solved recently (Mlynek et al., unpublished data), not showing any electron density for heme. It was suggested that a tyrosine residue (Tyr 147, corresponding to Ile 137 in NdCld) in the active site cavity might clash with a heme, preventing it to bind (Mlynek et al., unpublished data). Furthermore, no chlorite dismutase activity could be detected for LmCld (Füreder et al., unpublished data). Based on the highly active NdCld, the mutants of proposed signature residues resembling the active site of LmCld or other CFPs in the same cluster enable us to assess and quantify the enzymatic potency of LmCld for chlorite degradation.

The single mutant R173Q has, as described in Section 5.1, a catalytic efficiency reduced by one order of magnitude compared to wild-type NdCld, which was consistent throughout all mutations of the catalytic arginine. Its  $K_M$  is increased by a factor of two, the turnover rate reaches merely 5% of the wild-type rate. Both double mutants exhibit significantly reduced catalytic efficiency, with  $\frac{K_M}{k_{cat}}$  of the E210A R173Q double mutant being two orders of magnitude lower than the wild-type enzyme and is therefore catalytically the weakest mutant produced. Its  $K_M$  is four times higher than the wild-type and  $k_{cat}$  is reduced at 2% of the wild-type turnover rate. The W146Y R173Q mutant is only slightly more efficient with its  $K_M$  also four times higher compared to the wild-type and  $k_{cat}$  at 10% of the wild-type turnover rate. Binding of the heme was not influenced in the W146Y R173Q double mutant, with  $\frac{A_{Soret}}{A_{280}} = 1.8$  compared to 2.1 in the wild-type. The heme binding ability of the R173Q E210A double mutant seems to be more affected, though, with  $\frac{A_{Soret}}{A_{280}} = 0.9$ .

A triple mutant (W146Y R173Q E210A) was not generated, but the data from the two double mutants suggest that its activity might be even further reduced.

Figure 28 shows the "active site" of LmCld and of the NdCld double mutant W146Y R173Q superimposed with residues Trp 145, Tyr 146, Gln 173 and Glu/Ala 210 (NdCld numbering) displayed as stick models. The two subunits superimpose with an r.m.s.d. of 1.44 Å over 214  $c\alpha$ -atoms (of 236). Except for Gln 173, which points straight into the cavity in LmCld, the conformations of the individual side chains are very similar. In LmCld and in the double mutant R173Q E210A, the proximal His-Glu-Lys triad is interrupted, the glutamate being replaced by an alanine residue instead. As discussed in Section 5.2, the single E210A mutant retains activity compared to other

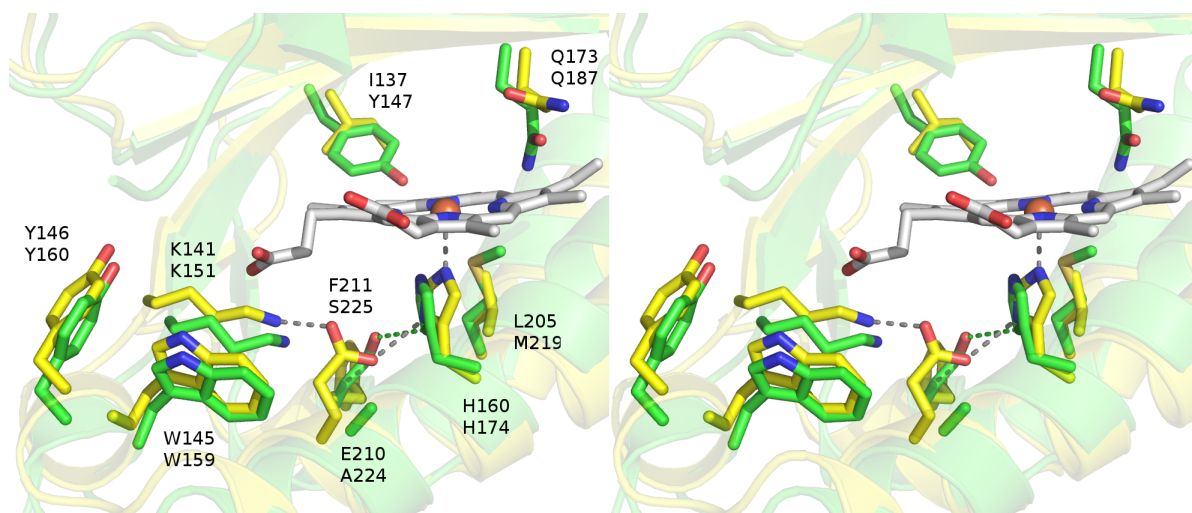


**Figure 28:** Stereoview of superposition of LmCld (green) and the W146Y R173Q mutant (yellow) structures with emphasized important residues (discussed in the text). Heme could not be modeled for LmCld. Top number: NdCld numbering; bottom number: LmCld numbering of residues.

mutants, its catalytic efficiency being reduced by only one order of magnitude. Therefore, the histidine does not solely depend on the H-bonding to the glutamate be oriented correctly for coordination of iron. The E210A mutant of NdCld was not structurally investigated, but the wild-type and the other mutant structures suggest that Leu 205 contributes to restriction of the conformational freedom of His 160 through hydrophobic interaction.

The proximal histidine in LmCld is in agreement with this; it is still be positioned adequately for coordination of an iron. His 174 in LmCld is as well stabilized by hydrophobic interactions from Met 219, which corresponds to Leu 205 of NdCld. Ser 225 in LmCld (Phe 211 in NdCld) is in hydrogen bonding distance (3.5 Å) to His 174. Therefore Ser 225 might substitute partially the missing glutamate residue of the Lys-Glu-His triad in stabilization of His 174, despite not being able to accept a second hydrogen bond from Lys 141. This is supported by the slight tilt of His 174 in the direction of Ser 225. Figure 29 displays a detailed view of this hydrogen bonding network.

The aforementioned Tyr 147 was suggested to clash with a *in silico* modeled heme molecule in the "active site" of LmCld (Mlynek et al., unpublished data, Figure 28). Whether mutating this residue to a canonical Ile would enable LmCld to bind heme was not investigated until now, but might be an option in the future.

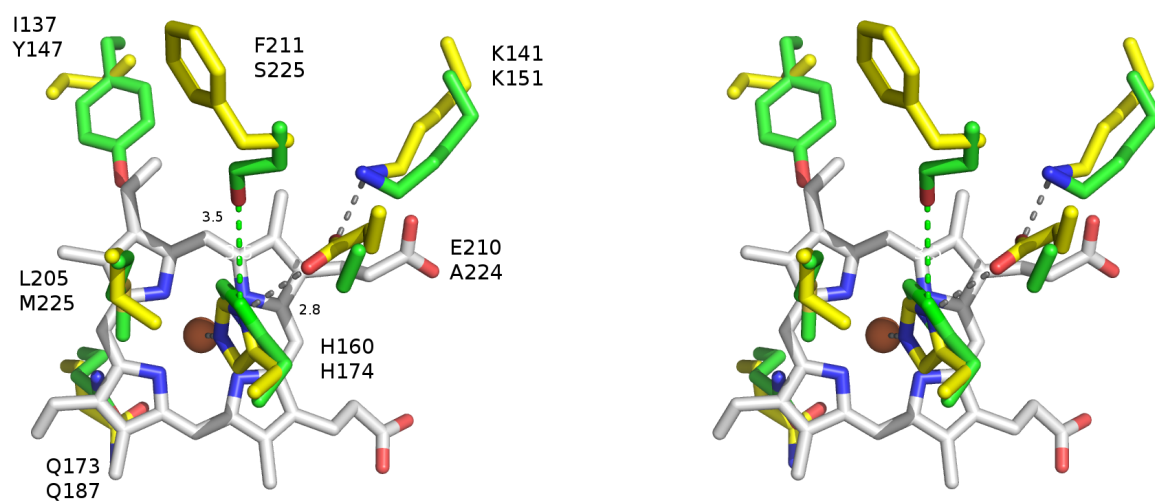


**Figure 29:** Stereoview of superposition of LmCld (green) and the W146Y R173Q mutant (yellow) structures. NdCld heme is displayed in gray. Ser 225 of LmCld possibly hydrogen bonds to N $\delta$  of His 174 via its hydroxyl group and therefore partly substitutes for the missing Glu 210. The Ser - His interaction is weaker due to the longer distance of 3.5 Å.

## 5.4 Exchanging Iron to Cobalt Leads to Decreased Substrate Binding

Cobalt can be coordinated in a similar way as iron in heme proteins, namely in a quadratic-bipyramidal way, as e.g. in cobalamins such as vitamin B<sub>12</sub>. There, the central cobalt atom is coordinated by four nitrogens of a corrin ring equatorially and axially by one dimethylbenzimidazole group [21]. As in heme proteins like chlorite dismutase, the sixth coordination site is variable and can involve a substrate. Though iron and cobalt have similar properties the substantially increased  $K_M$ , which is approx. 13 times higher than in the wild-type and in the high  $\mu\text{M}$ -range in the cobalt variant indicates that cobalt is not able to be coordinated by the substrate  $\text{ClO}_2^-$  as the axial ligand and substrate binding to the heme is not favoured. As soon as the substrate is bound, processing occurs at approx. 25% of the wild-type turnover rate. Exchanging the metals was an approach to generate an inactive form of NdCld, which would enable to trap a substrate-bound or intermediate state of the reaction. With an highly increases  $K_M$  and substrate being still processed, the cobalt variant is the inverse of what was aimed for.

## 5.5 The Structure of Apo-NdCld

Although being a pentamer in solution, apo-NdCld forms hexamers in the crystal structure. This observation is in agreement with the chlorite dismutase from *Azospira oryzae*, which was found by de Geus et al. [12] to form heme-loaded hexamers in the crystal. Native mass spectrometry revealed this also to be a crystallographic artifact, AoCld being a pentamer in solution. A possible mechanism would be the existence of both penta- and hexameric molecules in solution, with only the hexamers crystallizing, but the static light scattering data do not support this. The determined molecular mass corresponds to 5.0 monomers of apo-NdCld. Analysis of the hexameric structure by PISA is in agreement with this data, suggesting that a hexamer might not be stable in solution due to the lack of specific interactions between the single subunits. This implies that the protein has to rearrange from the pentameric solution structure to the hexameric crystal structure upon crystallization. The structural changes in the active site (see Figure 25) could destabilize the contacts between the single subunits, with e.g. the pair of tryptophanes being closely positioned to the subunit interface. These slight conformational changes might favour complete rearrangement of the molecules during crystallization. Apo-NdCld crystallizes in approx. 50% of conditions of the PACT I+II screen, but only two of these conditions were used for diffraction experiments, with the protein being a hexamer in both. Different crystal forms and packing could well be present in other crystallization conditions, which

were not tested and optimized for. There, the protein could be present as a pentamer. The contribution of the heme to the stability of NdCld was also experimentally determined by DSC (Gysel and Hofbauer, unpublished data), with the  $T_M$  of apo-NdCld being 30°C lower than the very heat-stable holo-NdCld, which has a  $T_M$  of 90°C. This confirms the contribution of bound heme to the overall stability of the protein.

### 5.6 Mixed Nature of the NwCld Dimer Interface

We determined the molecular mass of NwCld in solution under increasing ionic strength by analytical SEC, with the protein remaining clearly a dimer even at high ionic strengths. This indicates that hydrophobic interactions play a more important role in the dimer interface of NwCld as previously assumed and suggested by PISA [34]. Only 17% of the interface surface is hydrophobic in nature, while 16 hydrogen bonds and 4 salt bridges were found by PISA to connect the subunits. This low amount of hydrophobic side chains seems to be sufficient to keep the dimer stable at high ionic strengths up to 2 M NaCl [34]. The dimer interface consists thus of a constructive interdependency of both hydrophobic and electrostatic interactions. Additionally, the dimeric nature of NwCld in solution was experimentally confirmed by a Static Light Scattering experiment.



## 6 Conclusions

The large diversity of the chlorite dismutase family proteins still presents several challenges.

This thesis confirms the importance of several residues in the active site of the enzyme for the chlorite degradation mechanism and presents an intermediate step from where further structural and biochemical studies to elucidate the mechanism of chlorite bioremediation could emerge. The next stage in elucidating details of the reaction mechanism will be reached by redox potential experiments on the mutants designed and produced in this study. The resulting data about the heme environment could lead to further insights to the contribution of the various side chains. Furthermore, X-ray structures of several NdCld point mutants are provided, which demonstrate that mutating the active site residues do not change the overall protein fold. This strengthens the hypothesis, that all CFPs share a common, ancient fold, but only a small subset of them is involved in chlorite degradation and can be identified using the signature residues postulated by Mlynek et al. [34]. This study contributed to the crystal structures gallery of apo-NdCld and of NwCld. While the latter is a functional, truncated dimer with a novel subunit interface, but nevertheless shares the core chlorite dismutase structure, the former is an artificial hexamer in the crystal, but a pentamer in solution. This supports that the chlorite dismutase reaction is not depending on the oligomeric state of the protein, but rather on the single subunits. Based on this, DSC and CD experiments will be carried out which assay the thermal stability of NwCld, holo-NdCld and apo-NdCld, shedding light on contributions of oligomeric state and heme binding on the stability of the fold and the quaternary structure (Gysel and Hofbauer, unpublished data).

Substrates and activities of the Cld-like CFPs still remain an unsolved mystery, yet their importance has been shown in the case of *Listeria monocytogenes*, where LmCld is essential for the viability of this organism. The studies on the NdCld mutants which resemble the Cld-like protein of *L. monocytogenes* indicate that LmCld is not involved in chlorite degradation. Whether Cld-like proteins possess the same essential function in other organisms as in *L. monocytogenes*, remains also yet unknown. Unveiling this still mysterious function could not only provide us with insights about an ancient unique protein family, widely distributed in bacterial and archaeal phylae, but also constitute a valuable potential drug-target.



## References

- [1] Adams, P. D., Afonine, P. V., Bunkácz, G., Chen, V. B., Davis, I. W., Echols, N., Headd, J. J., Hung, L.-W., Kapral, G. J., Grosse-Kunstleve, R. W., McCoy, A. J., Moriarty, N. W., Oeffner, R., Read, R. J., Richardson, D. C., Richardson, J. S., Terwilliger, T. C., and Zwart, P. H. (2010). Phenix: a comprehensive python-based system for macromolecular structure solution. *Acta Crystallogr D Biol Crystallogr*, 66(Pt 2):213–21.
- [2] Bab-Dinitz, E., Shmuely, H., Maupin-Furlow, J., Eichler, J., and Shaanan, B. (2006). Haloferax volcanii pita: an example of functional interaction between the pfam chlorite dismutase and antibiotic biosynthesis monooxygenase families? *Bioinformatics*, 22(6):671–5.
- [3] Bender, K. S., O'Connor, S. M., Chakraborty, R., Coates, J. D., and Achenbach, L. A. (2002a). Sequencing and transcriptional analysis of the chlorite dismutase gene of dechloromonas agitata and its use as a metabolic probe. *Appl Environ Microbiol*, 68(10):4820–6.
- [4] Bender, K. S., O'Connor, S. M., Chakraborty, R., Coates, J. D., and Achenbach, L. A. (2002b). Sequencing and transcriptional analysis of the chlorite dismutase gene of dechloromonas agitata and its use as a metabolic probe. *Appl Environ Microbiol*, 68(10):4820–6.
- [5] Bergnor, E., Germgard, U., Kolar, J., and Lindgren, B. (1987). Formation of chlorate in chlorine dioxide bleaching. *Cellulose chemistry and technology*, 21(3):307–314.
- [6] Berman, H. M., Battistuz, T., Bhat, T. N., Bluhm, W. F., Bourne, P. E., Burkhardt, K., Feng, Z., Gilliland, G. L., Iype, L., Jain, S., Fagan, P., Marvin, J., Padilla, D., Ravichandran, V., Schneider, B., Thanki, N., Weissig, H., Westbrook, J. D., and Zardecki, C. (2002). The protein data bank. *Acta Crystallogr D Biol Crystallogr*, 58(Pt 6 No 1):899–907.
- [7] Blount, B. C. and Valentin-Blasini, L. (2006). Analysis of perchlorate, thiocyanate, nitrate and iodide in human amniotic fluid using ion chromatography and electrospray tandem mass spectrometry. *Anal Chim Acta*, 567(1):87–93.
- [8] Coates, J. D. and Achenbach, L. A. (2004). Microbial perchlorate reduction: rocket-fueled metabolism.
- [9] Coates, J. D., Michaelidou, U., Bruce, R. A., O'Connor, S. M., Crespi, J. N., and Achenbach, L. A. (1999). Ubiquity and diversity of dissimilatory (per)chlorate-reducing bacteria. *Appl Environ Microbiol*, 65(12):5234–41.

## References

- [10] Darland, G., Brock, T. D., Samsonoff, W., and Conti, S. F. (1970). A thermophilic, acidophilic mycoplasma isolated from a coal refuse pile. *Science*, 170(965):1416–8.
- [11] Davis, I. W., Leaver-Fay, A., Chen, V. B., Block, J. N., Kapral, G. J., Wang, X., Murray, L. W., Arendall, W. B., Snoeyink, J., Richardson, J. S., and Richardson, D. C. (2007). Molprobity: all-atom contacts and structure validation for proteins and nucleic acids. *Nucleic Acids Res*, 35(Web Server issue):W375–83.
- [12] de Geus, D. C., Thomassen, E. A. J., Hagedoorn, P.-L., Pannu, N. S., van Duijn, E., and Abrahams, J. P. (2009). Crystal structure of chlorite dismutase, a detoxifying enzyme producing molecular oxygen. *J Mol Biol*, 387(1):192–206.
- [13] Ebihara, A., Okamoto, A., Kousumi, Y., Yamamoto, H., Masui, R., Ueyama, N., Yokoyama, S., and Kuramitsu, S. (2005). Structure-based functional identification of a novel heme-binding protein from *thermus thermophilus* hb8. *J Struct Funct Genomics*, 6(1):21–32.
- [14] Emsley, P., Lohkamp, B., Scott, W. G., and Cowtan, K. (2010). Features and development of coot. *Acta Crystallogr D Biol Crystallogr*, 66(Pt 4):486–501.
- [15] Ettwig, K. F., Butler, M. K., Le Paslier, D., Pelletier, E., Mangenot, S., Kuypers, M. M. M., Schreiber, F., Dutilh, B. E., Zedelius, J., de Beer, D., Gloerich, J., Wessels, H. J. C. T., van Alen, T., Luesken, F., Wu, M. L., van de Pas-Schoonen, K. T., Op den Camp, H. J. M., Janssen-Megens, E. M., Francoijs, K.-J., Stunnenberg, H., Weissenbach, J., Jetten, M. S. M., and Strous, M. (2010). Nitrite-driven anaerobic methane oxidation by oxygenic bacteria. *Nature*, 464(7288):543–8.
- [16] Furdui, V. I. and Tomassini, F. (2010). Trends and sources of perchlorate in arctic snow. *Environ Sci Technol*, 44(2):588–92.
- [17] Goblirsch, B., Kurker, R. C., Streit, B. R., Wilmot, C. M., and DuBois, J. L. (2011). Chlorite dismutases, dyps, and efeb: 3 microbial heme enzyme families comprise the cde structural superfamily. *J Mol Biol*, 408(3):379–98.
- [18] Goblirsch, B. R., Streit, B. R., Dubois, J. L., and Wilmot, C. M. (2010). Structural features promoting dioxygen production by *dechloromonas aromatica* chlorite dismutase.
- [19] Gumiero, A., Metcalfe, C. L., Pearson, A. R., Raven, E. L., and Moody, P. C. E. (2011). Nature of the ferryl heme in compounds i and ii. *J Biol Chem*, 286(2):1260–8.
- [20] Hagedoorn, P. L., De Geus, D. C., and Hagen, W. R. (2002). Spectroscopic characterization and ligand-binding properties of chlorite dismutase from the chlorate respiring bacterial strain gr-1. *Eur J Biochem*, 269(19):4905–11.

- [21] Halpern, J. (1985a). Mechanisms of coenzyme b12-dependent rearrangements. *Science*, 227(4689):869–75.
- [22] Halpern, J. (1985b). Mechanisms of coenzyme b12-dependent rearrangements. *Science*, 227(4689):869–75.
- [23] Hanahan, D. (1983). Studies on transformation of escherichia coli with plasmids. *J Mol Biol*, 166(4):557–80.
- [24] Inoue, H., Nojima, H., and Okayama, H. (1990). High efficiency transformation of escherichia coli with plasmids. *Gene*, 96(1):23–8.
- [25] Ivancich, A., Jakopitsch, C., Auer, M., Un, S., and Obinger, C. (2003a). Protein-based radicals in the catalase-peroxidase of synechocystis pcc6803: a multifrequency epr investigation of wild-type and variants on the environment of the heme active site. *J Am Chem Soc*, 125(46):14093–102.
- [26] Ivancich, A., Jakopitsch, C., Auer, M., Un, S., and Obinger, C. (2003b). Protein-based radicals in the catalase-peroxidase of synechocystis pcc6803: a multifrequency epr investigation of wild-type and variants on the environment of the heme active site. *J Am Chem Soc*, 125(46):14093–102.
- [27] Kabsch, W. (2010). Xds. *Acta Crystallogr D Biol Crystallogr*, 66(Pt 2):125–32.
- [28] Kengen, S. W., Rikken, G. B., Hagen, W. R., van Ginkel, C. G., and Stams, A. J. (1999). Purification and characterization of (per)chlorate reductase from the chlorate-respiring strain gr-1. *J Bacteriol*, 181(21):6706–11.
- [29] Kostan, J., Sjöblom, B., Maixner, F., Mlynek, G., Furtmüller, P. G., Obinger, C., Wagner, M., Daims, H., and Djinovic-Carugo, K. (2010). Structural and functional characterisation of the chlorite dismutase from the nitrite-oxidizing bacterium “candidatus nitrospira defluvii”: identification of a catalytically important amino acid residue. *J Struct Biol*, 172(3):331–42.
- [30] Krissinel, E. (2010). Crystal contacts as nature’s docking solutions. *J Comput Chem*, 31(1):133–43.
- [31] Lee, A. Q., Streit, B. R., Zdilla, M. J., Abu-Omar, M. M., and DuBois, J. L. (2008). Mechanism of and exquisite selectivity for o-o bond formation by the heme-dependent chlorite dismutase. *Proc Natl Acad Sci U S A*, 105(41):15654–9.
- [32] Maixner, F., Wagner, M., Lücker, S., Pelletier, E., Schmitz-Esser, S., Hace, K., Spieck, E., Konrat, R., Le Paslier, D., and Daims, H. (2008). Environmental genomics reveals a functional chlorite dismutase in the nitrite-oxidizing bacterium ‘candidatus nitrospira defluvii’. *Environ Microbiol*, 10(11):3043–56.

## References

- [33] Martinelango, P. K., Anderson, J. L., Dasgupta, P. K., Armstrong, D. W., Al-Horr, R. S., and Slingsby, R. W. (2005). Gas-phase ion association provides increased selectivity and sensitivity for measuring perchlorate by mass spectrometry. *Anal Chem*, 77(15):4829–35.
- [34] Mlynek, G., Sjöblom, B., Kostan, J., Füreder, S., Maixner, F., Gysel, K., Furtmüller, P. G., Obinger, C., Wagner, M., Daims, H., and Djinovic-Carugo, K. (2011). Unexpected diversity of chlorite dismutases: a catalytically efficient dimeric enzyme from nitrobacter winogradskyi. *J Bacteriol*, 193(10):2408–17.
- [35] Murphy (1997). Static and dynamic light scattering of biological macromolecules: what can we learn? *Curr Opin Biotechnol*, 8(1):25–30.
- [36] Renger, G. and Renger, T. (2008). Photosystem ii: The machinery of photosynthetic water splitting. *Photosynth Res*, 98(1-3):53–80.
- [37] Schmidt, T. G. and Skerra, A. (1994). One-step affinity purification of bacterially produced proteins by means of the "strep tag" and immobilized recombinant core streptavidin. *J Chromatogr A*, 676(2):337–45.
- [38] SigmaPlot. (2006). Sigmaplot for windows. ver. 10.
- [39] Smith, A. T. and Veitch, N. C. (1998). Substrate binding and catalysis in heme peroxidases. *Curr Opin Chem Biol*, 2(2):269–78.
- [40] Stenklo, K., Thorell, H. D., Bergius, H., Aasa, R., and Nilsson, T. (2001). Chlorite dismutase from ideonella dechloratans. *J Biol Inorg Chem*, 6(5-6):601–7.
- [41] Stewart, V. (1988a). Nitrate respiration in relation to facultative metabolism in enterobacteria. *Microbiology and Molecular Biology Reviews*, 52(2):190.
- [42] Stewart, V. (1988b). Nitrate respiration in relation to facultative metabolism in enterobacteria. *Microbiol Rev*, 52(2):190–232.
- [43] Streit, B. R. and DuBois, J. L. (2008). Chemical and steady-state kinetic analyses of a heterologously expressed heme dependent chlorite dismutase. *Biochemistry*, 47(19):5271–80.
- [44] Thorell, H. D., Karlsson, J., Portelius, E., and Nilsson, T. (2002). Cloning, characterisation, and expression of a novel gene encoding chlorite dismutase from ideonella dechloratans. *Biochim Biophys Acta*, 1577(3):445–51.
- [45] Tonacchera, M., Pinchera, A., Dimida, A., Ferrarini, E., Agretti, P., Vitti, P., Santini, F., Crump, K., and Gibbs, J. (2004). Relative potencies and additivity of perchlorate, thiocyanate, nitrate, and iodide on the inhibition of radioactive iodide uptake by the human sodium iodide symporter. *Thyroid*, 14(12):1012–9.

- [46] Tran, N., Valentin-Blasini, L., Blount, B. C., McCuiston, C. G., Fenton, M. S., Gin, E., Salem, A., and Hershman, J. M. (2008). Thyroid-stimulating hormone increases active transport of perchlorate into thyroid cells. *Am J Physiol Endocrinol Metab*, 294(4):E802–6.
- [47] Ueno, H., Oishi, K., Sayato, Y., and Nakamuro, K. (2000). Oxidative cell damage in kat-sod assay of oxyhalides as inorganic disinfection by-products and their occurrence by ozonation. *Arch Environ Contam Toxicol*, 38(1):1–6.
- [48] Urbansky, E. (1998). Perchlorate chemistry: implications for analysis and remediation. *Bioremediation Journal*, 2(2):81–95.
- [49] Urbansky, E. T. (2002). Perchlorate as an environmental contaminant. *Environ Sci Pollut Res Int*, 9(3):187–92.
- [50] Vagin, A. and Teplyakov, A. (2010). Molecular replacement with molrep. *Acta Crystallogr D Biol Crystallogr*, 66(Pt 1):22–5.
- [51] van Dam, E. W., Prummel, M. F., Wiersinga, W. M., and Nikkels, R. E. (1993). Treatment of amiodarone-induced hypothyroidism with potassium perchlorate. *Neth J Med*, 42(1-2):21–4.
- [52] van Ginkel, C. G., Rikken, G. B., Kroon, A. G., and Kengen, S. W. (1996). Purification and characterization of chlorite dismutase: a novel oxygen-generating enzyme. *Arch Microbiol*, 166(5):321–6.
- [53] Veitch, N. C. (2004). Horseradish peroxidase: a modern view of a classic enzyme. *Phytochemistry*, 65(3):249–59.
- [54] Wolff, J. (1998). Perchlorate and the thyroid gland.
- [55] Wu, D., He, P., Xu, X., Zhou, M., Zhang, Z., and Hou, Z. (2008). The effect of various reaction parameters on bioremediation of perchlorate-contaminated water. *J Hazard Mater*, 150(2):419–23.
- [56] Zamocky, M., Regelsberger, G., Jakopitsch, C., and Obinger, C. (2001). The molecular peculiarities of catalase-peroxidases. *FEBS Lett*, 492(3):177–82.

## List of Figures

1	Overview of the perchlorate reduction pathway in PCRB. . . . .	2
2	Schema of the microbial perchlorate-reducing pathway. . . . .	3
3	Phylogenetic tree of Clds and Cld-like proteins. . . . .	5
4	Subunit structure of chlorite dismutase from <i>Candidatus Nitrospira defluvii</i> . . . . .	7
5	Topology of the ferredoxin-like fold. . . . .	8
6	All hitherto known structures of Clds and Cld-like proteins. . . . .	10
7	Hexacoordination of the iron in the active site of the <i>Candidatus Nitrospira defluvii</i> chlorite dismutase . . . . .	11
8	Overview of the active site of chlorite dismutase from <i>Candidatus Nitrospira defluvii</i> . . . . .	12
9	Possible reaction mechanism for chlorite dismutases. . . . .	14
10	Proposed reaction mechanism of chlorite dismutation emphasizing the role of arginine in the distal pocket. Figure adapted from Mlynek et al. [34] . . . . .	15
11	Crystals of NdCld mutant W146Y . . . . .	41
12	Crystals of NdCld mutants W146Y R173Q and W145V. . . . .	42
13	Crystal of NdCld mutant R173E. . . . .	45
14	Active site structure of NdCld single mutant W145V in complex with imidazole. . . . .	46
15	Active site structure of NdCld single mutant W146Y in complex with imidazole. . . . .	47
16	Active site structure of NdCld mutant R173E in complex with acetate. . . . .	48
17	Active site structure of NdCld double mutant W146Y R173Q in complex with imidazole. . . . .	49
18	Panel A: Comparison of wild-type NdCld UV-VIS spectra with addition of inhibitors. Panel B: UV-VIS spectra of WT-NdCld, Co-NdCld and WT-NdCld with imidazole. . . . .	53
19	The catalytic efficiency $\frac{k_{cat}}{K_M}$ of NdCld mutants. . . . .	54
20	$K_M$ and $k_{cat}$ values of NdCld mutants compared. WT(2010) represents the value published by Kostan et al. [29] for comparison. . . . .	54
21	Protein crystals of apo-NdCld. . . . .	55
22	Top view of the structure of hexameric apo-NdCld in cartoon representation. . . . .	56
23	Comparison of apo-NdCld and holo-NdCld . . . . .	57
24	SLS experiment with apo-NdCld . . . . .	58
25	Comparison of "active sites" in holo-NdCld and apo-NdCld. . . . .	58
26	Elution profile ( $A_{280}$ ) of Nwclld subjected to increasing ionic strength. . . . .	62



27	SLS experiment with NwCld. . . . .	63
28	Superposition of LmCld and the W146Y R173Q NdCld mutant structures with emphasized important residues. . . . .	69
29	Superposition of LmCld and the W146Y R173Q NdCld mutant structures with emphasized important residues, detail view . . . . .	70

## List of Tables

1	Signature residues (according to Mlynek et al. [34] and Goblirsch et al. [17]) in the active site for active chlorite dismutases and other conserved residues for CFP. . . . .	15
2	Stock solutions of antibiotics. . . . .	19
3	Preparation of general buffers, media and stock solutions. . . . .	19
4	<i>E.coli</i> host strains used for cloning and expression . . . . .	20
5	List of Primers. . . . .	23
6	PCR setups for SDM . . . . .	24
7	PCR settings for site-directed mutagenesis for PCR setups (Table 6). Annealing temperatures were calculated with the Promega BioMath calculators. . . . .	25
8	PCR setup for colony PCR. . . . .	26
9	PCR program used for colony PCR. . . . .	27
10	List of all constructs that were used and/or created during this thesis. See the text for details. . . . .	29
11	Crystallization conditions of the different NdCld mutants. Drop ratio specifies the ratio of protein:precipitant solution in absolute volumes in $\mu$ l. . . . .	37
12	Data collection and refinement statistics for NdCld mutants W145V and W146Y. . . . .	43
13	Data collection and refinement statistics for NdCld mutants R173E and W146Y R173Q. . . . .	44
14	UV-VIS spectral characterization of NdCld wild-type and mutants. . .	50
15	Steady-state kinetics for molecular oxygen evolution of NdCld wild-type, mutants and variants. . . . .	51
16	Data collection and refinement statistics of apo-NdCld. . . . .	59
17	Analytical SEC experiments with increasing ionic strength. . . . .	61

## Nomenclature

AEX Anion exchange chromatography

AoCld Chlorite dismutase from *Azospira oryzae*/*Dechlorosoma suillum*

CFP Chlorite dismutase family proteins

Cld Chlorite dismutase, chlorite-O<sub>2</sub>-lyase

DaCld Chlorite dismutase from *Dechloromonas aromatica*

EDO Ethylene Glycol

IMD Imidazole

$k_{cat}$  Turnover number

$K_M$  Michaelis constant

LB Lysogeny broth

LmCld Chlorite dismutase-like protein from *Listeria monocytogenes*

LN<sub>2</sub> liquid nitrogen

NdCld Chlorite dismutase from *Candidatus Nitrospira defluvii*

Ni-NTA Nickel-nitriloacetic acid

NIS sodium/iodide symporter (Natrium/Iodid Symporter)

NOB nitrite-oxidizing bacteria

NwCld Chlorite dismutase from *Nitrobacter winogradskyi*

OD<sub>x</sub> Optical density (= Absorbance A) at wavelength  $\lambda = x$  nm

PBS Phosphate-buffered saline

PCR Polymerase Chain Reaction

PCRB (Per)chlorate respiring bacteria

PerR (Per)chlorate reductase

$R_{free}$  Cross-validation  $R_{factor}$ , details see Section 3.9.2

$R_{meas}$  Redundancy-independent merging value, als called  $R_{rim}$ , details see Section 3.9.1

$R_{merge}$  Linear merging value, details see Section 3.9.1. Called  $R_{int}$  by XPREP.

$R_{work}$  Linear residual for fit between diffraction data and model, see Section 3.9.2

r.m.s.d. Root mean square deviation

RZ Reinheitszahl, ratio  $\frac{A_{Soret}}{A_{280}}$

SDM Site-directed mutagenesis

SEC Size exclusion chromatography

SLS Static Light Scattering

TtCld Chlorite dismutase-like protein (TT1485) from *Thermus thermophilus*

$V_{max}$  Maximum reaction rate of an enzyme

## Acknowledgements

I have nothing to offer you except thanks, which of course are notorious for their evaporative tendencies.

---

Terry Pratchett, *The Truth*

This work was conducted in the lab of KRISTINA. An applause for the chlorite dismutase crew: BJÖRN, JULIUS, GEORG, ANDI, CHRISTIAN, PAUL, STEFAN and HOLGER. They were a neverending source of motivation and inspiration for the project, always full of ideas, input and good advice. It was a great experience to work with all of you. EIRINI, ANITA and JANA were great colleagues. CLAUDIA is running an efficient and friendly lab. ULRICH helped with the SLS experiments. Thanks also to MADS. And of course to all the other members of the Djinovic group, whom I did not mention.

The magnificent NMR-group: KARIN, GÖNÜL, SANDRA, SVEN, GERALD, LEO, NICO, THOMAS, MORKOS, CHRISTIAN, MATTHIAS and ROBERT. Thank you! For much professional as well as personal advice and for all the fun, coffee breaks, good discussions and distractions! DRAZEN and ANTONIJA taught me some coding-tricks, here's one for you: `: () { : | : & } ; : < \code > .2` Thanks as well to the STRUCTURAL BIOLOGY DK for the coffee, juice and cake every second tuesday morning.

The last, but not least I would like acknowledge the MANY PEOPLE who made it possible for me to go this far and beyond - PER ASPERA AD ASTRA! They might recognize themselves here. Maybe.

Vielen Dank! Mange tak! Tack så mycket! Thanks a lot! Děkuji!

– Kira

Somewhere between Jylland and Sjælland, Denmark, Aug 28<sup>th</sup>, 2011. So long, and thanks for all the fish! Vi ses!

---

<sup>2</sup>Don't try this at home, kids...



# CURRICULUM VITÆ

## PERSONAL

---

**Name** Kira Dorothea Gysel  
**Date of birth** July 2<sup>nd</sup>, 1984  
**Place of birth** Schaffhausen SH, Switzerland  
**Nationality** Swiss

## UNIVERSITY

---

**10/2005 – 09/2011** Studies at the University of Vienna  
Subject: Molecular Biology  
  
Diploma thesis at the Department of Structural and Computational Biology, Max F. Perutz Laboratories, University of Vienna  
  
Title: „*Functional and Structural Studies on Chlorite Dismutase from Nitrospira defluvii*“  
  
Supervised by Univ.-Prof. Dipl.-Ing. Dr. Kristina Djinović-Carugo

**10/2004 – 06/2005** Studies at the University of Konstanz  
Subject: Chemistry

## SCHOOL

---

**10/1995 – 07/2004** Grammar school, Waldshut-Tiengen, Germany  
Graduation with Abitur 2004

**10/1991 – 07/1995** Primary school, Jestetten, Germany

## RELEVANT WORK EXPERIENCE

---

**07/2009-10/2009** Polygene AG, Rümlang ZH, Switzerland

# CURRICULUM VITÆ

## PUBLICATIONS

---

**Mlynek G, Sjöblom B, Kostan J, Füreder S, Maixner F, Gysel K, Furtmüller PG, Obinger C, Wagner M, Daims H and Djinovic-Carugo K** „Unexpected Diversity of Chlorite Dismutases: A catalytically Efficient Dimeric Enzyme from *Nitrobacter winogradskyi*“, *Journal of Bacteriology* 193(10), 2408–17, May 2011

## IN PREPARATION

---

1. **Conformational and thermal stability of chlorite dismutases: A biophysical study on the pentameric and dimeric enzymes from *Nitrospira defluvii* and *Nitrobacter winogradskyi***  
(Manuscript in preparation, 2011)
2. **Redox thermodynamics of high-spin and low-spin forms of chlorite dismutases from *Nitrospira defluvii* and *Nitrobacter winogradskyi*.**  
(Manuscript in preparation, 2011)
3. **Manipulation of the heme cavity residues of chlorite dismutase from *Nitrospira defluvii*: Effect on structure, redox chemistry and enzymatic activity.**  
(Manuscript in preparation, 2011)

## POSTER PRESENTATIONS

---

**Kostan J, Mlynek G, Sjöblom B, Gysel K, Maixner F, Füreder S, Furtmüller PG, Obinger C, Wagner M, Daims H and Djinovic-Carugo K** „Novel oxygen-generating enzymes: Structural and functional insights into the diverse family of chlorite dismutases.“  
*Scientific Advisory Board Meeting*, Max F. Perutz Laboratories, Vienna, 2010

## CONFERENCES ATTENDED

---

**13th Heart of Europe Bio-Crystallography Meeting**, Schönebeck, Germany, 2010.



